Nuclear Physics B359 (1991) 343–405
North-Holland

A COMPLETE CALCULATION OF THE ORDER α_s^2 CORRECTION TO THE DRELL–YAN K-FACTOR

R. HAMBERG and W.L. van NEERVEN*

Instituut–Lorentz, University of Leiden, P.O.B. 9506, 2300 RA Leiden, The Netherlands

T. MATSUURA**

II. Institut für Theoretische Physik, Universität Hamburg, D-2000 Hamburg 50, Germany

Received 16 November 1990
(Revised 13 February 1991)

In this paper we present the complete calculation of the order α_s^2 correction in the $\overline{\text{MS}}$ scheme to the Drell–Yan K-factor. All channels represented by the $q\bar{q}$, qg, gg and qq subprocesses have been included now. One of our conclusions is that the $O(\alpha_s^2)$ part of the K-factor is dominated by the $q\bar{q}$ as well as the qg reaction. The latter leads to a negative contribution over the whole energy range under investigation (0.5 TeV $< \sqrt{S} <$ 50 TeV). It even overwhelms the positive $q\bar{q}$ contribution at large collider energies characteristic for LHC and SSC. It turns out that the order α_s^2 corrected K-factor is quite insensitive to variations of the factorization scale M over the region 10 GeV $< M <$ 1000 GeV. We also compare our results with the data obtained by UA1, UA2 and CDF.

1. Introduction

The theoretical justification for perturbative strong interaction corrections to the parton model [1] and their summation by renormalization group techniques in the framework of QCD lead to a wealth of radiative corrections to numerous processes (for a review see ref. [2]). The most interesting outcome of these calculations was that some of the corrections turned out to be rather large. This can mainly be attributed to the considerable size of the running coupling constants $\alpha_s(R^2)$ which decreases slowly as R^2 grows. Because of these large corrections one can question the predictive power of perturbative QCD. However, experiments show that there is a considerable discrepancy between the predictions of the Born approximation and the experimental data. Nowadays it is commonly accepted that the ratio between the measured cross section and the Born approximation, generally called

* Bitnet address: NEERVEN@HLERUL59
** Supported by LAA, CERN, Geneva.

0550-3213/91/$03.50

the K-factor, can be explained by including the higher-order corrections. For most processes only first-order corrections have been calculated. They give a reasonable agreement with the experimental data. Nevertheless, corrections beyond the order of α_s are needed for practical as well as for theoretical reasons.

The practical reason is that the statistics in the ongoing and future experiments will improve so that the higher-order corrections might become noticeable. This is expected because the size of the various K- and R-factors can become rather large. It is also interesting to see how the K-factors will behave at very large energies, which are characteristic for future accelerators like LHC and SSC. Here we expect processes with gluons in the initial state to play a very important role. From the theoretical point of view higher-order corrections are interesting because we can learn something about the behaviour of the perturbation series, in particular about its convergence. One also wants to know by which terms the series is dominated. An example of such a striking term is the soft-gluon part of the K-factor, which is present in reactions with one or more gluons in the final state. Knowledge about these dominant parts can provide us with useful information about which techniques are needed for their resummation. Another possibility to improve the perturbation series is the choice of a suitable mass factorization and renormalization scale. These scales can for instance be determined in optimized perturbation theory. Examples are the principle of minimal sensitivity (PMS) [3] and the method of fastest asymptotic convergence (FAC) [4]. The drawback of these approaches is that they are based on extrapolations of the lowest-order terms, ignoring the effects coming from higher-order corrections. Moreover, we expect that cross sections, calculated in higher order of α_s, will be less sensitive to variations in the factorization and renormalization scales than the lowest-order ones.

In this paper we will present the full order α_s^2 correction to inclusive massive lepton pair production (Drell–Yan process). The first experiment to study this reaction was carried out by the Columbia-BNL group [5] in 1970. From that time onwards this process attracted the attention of many experimentalists as well as theorists in elementary particle physics. Before the $p\bar{p}$ collider at CERN became operational in the beginning of the eighties all experiments were of the fixed target type. One of the aims was to study the structure of hadrons. When the Drell–Yan reaction takes place at relatively low energies ($\sqrt{S} < 20$ GeV), the hadrons are probed by a highly virtual timelike photon which is experimentally observed through its decay into a massive lepton pair. Therefore this process is complementary to deep inelastic lepton–proton scattering where the exchanged photon is spacelike. An advantage of massive lepton pair production is that it allows us to study the structure of unstable particles like pions or kaons. This is not possible in deep inelastic lepton–hadron scattering where the target particles (like the proton or the bound neutron) have to be stable. On the other hand the latter process provides us with much better statistics. Both reactions belong to the class of hard

processes which means that at increasing energies all kinematical variables get large while their ratios stay fixed. In such a case one can apply the methods of perturbative QCD.

The first successful description of massive lepton pair production in the context of the parton model (lowest order QCD) was given by S.D. Drell and T.M. Yan [6]. Later on, this production mechanism, called Drell–Yan (DY) after their inventors, was supplemented by perturbative QCD. Using renormalization group methods and the mass factorization theorem, for which an all order proof exists [7], one can compute QCD corrections to this process. Between 1978 and 1980 the first order α_s corrections were performed by many groups [8–13]. At the same time (1979) the NA3 group [14] found a discrepancy between the data and the zeroth-order parton model, a result which was confirmed by other fixed target experiments (for a review see ref. [15]). Later on a second confirmation came from the $p\bar{p}$ colliders at CERN and FERMILAB [16]. At the energies of these machines, exceeding those of fixed target experiments by two orders of magnitude, the lepton pair is produced through the W- and Z-bosons. Comparison of the data with the theory revealed that the discrepancy, generally represented by the experimental K-factor, could be rather well explained by the existing order α_s corrections. In spite of this success one might question the reliability of perturbation theory, as the corrections turned out to be rather large ($\sim 70\%$ at fixed target energies and $\sim 30\%$ for the Sp$\bar{p}$pS). Therefore higher-order corrections are necessary to put the order α_s predictions on a firmer ground. Unlike other QCD processes the DY reaction seems to be one of the few cases where the calculation of the order α_s^2 corrections is feasible, a property it shares with deep inelastic lepton–hadron scattering. This is because the maximum number of particles appearing in the final state of the parton subprocesses which contribute to these two reactions does not exceed three. Notice that the most complicated parts of these calculations are the many body phase space integrals. If there are more than three particles in the final state the number of these integrals as well as their complexity get completely out of control. In the case of collinear finite processes like R, defined in the reaction $e^+ + e^- \rightarrow$ "X", the situation is a little better. The optical theorem, which relates this quantity to the absorptive part of a two-point function, makes it even possible to calculate its radiative corrections up to order α_s^3 [17]. Another example is the order α_s^2 correction to the two-jet cross section of the same process [18] although here the used methods resemble those used in the DY calculation. However, note that in the last two cases no mass factorization is involved, hence, these quantities only depend on the chosen scheme for the strong coupling constant. Therefore one can study their dependence on the renormalization scale only. In deep inelastic lepton–hadron scattering and the DY process we also have to perform mass factorization rendering the Wilson coefficient dependent on two separate scales. In this way the DY K-factor provides us with a beautiful opportunity to investigate the dependence on the mass factorization as well as on the renormalization scale.

Finally notice that in order to obtain the order α_s^2 correction to the K-factor, we need the two loop corrected splitting functions to remove the collinear divergences from the parton cross sections. This is the first time that the higher-order splitting functions show up in a perturbative calculation.

This paper will be organized as follows. In sect. 2 we present the results of the complete order α_s^2 correction to the DY K-factor, which is calculated in the $\overline{\text{MS}}$ scheme. The latter refers to coupling constant renormalization as well as mass factorization. In particular we have included the contribution of the hard gluon radiation to the $q\bar{q}$ process and the order α_s correction to the qg reaction which were not presented previously. In sect. 3 we discuss the effect of the higher-order corrections on heavy vector boson production at current and future accelerators. The long expressions for the hadronic structure function and the DY correction terms, not presented in sect. 2, can be found in appendices A and B respectively.

2. The α_s^2 correction to the DY process

Massive lepton pair production in hadronic collisions proceeds through the following reaction:

$$\begin{array}{l} H_1 + H_2 \rightarrow V + \text{"X"} \\ \qquad\qquad\quad \hookrightarrow \ell_1 + \ell_2 \end{array} \tag{2.1}$$

where V is one of the vector bosons of the standard model (γ, Z or W) which subsequently decays into a lepton pair (ℓ_1, ℓ_2). The symbol "X" denotes any inclusive final hadronic state allowed by conservation of quantum numbers. The colour-averaged inclusive cross section is given by

$$\frac{d\sigma^V}{dQ^2} = \tau \sigma_V(Q^2, M_V^2) W_V(\tau, Q^2), \qquad \tau = \frac{Q^2}{S}. \tag{2.2}$$

The quantity σ_V is the pointlike cross section (see eqs. (A.1)–(A.3)). The variables $\sqrt{S}$ and $\sqrt{Q^2}$ stand for the c.m. energy of the incoming hadrons H_1, H_2 and the invariant mass of the dilepton pair respectively. The hadronic structure function is represented by $W_V(\tau, Q^2)$. According to the DY mechanism it can be written as

$$W_V(\tau, Q^2) = \sum_{i,j} \int_0^1 dx_1 \int_0^1 dx_2 \int_0^1 dx\, \delta(\tau - x x_1 x_2) \mathrm{PD}_{ij}^V(x_1, x_2, M^2) \Delta_{ij}(x, Q^2, M^2). \tag{2.3}$$

The functions $\mathrm{PD}_{ij}^V(x_1, x_2, M^2)$ stand for the usual combination of parton distribution functions, which depend on the mass factorization scale M. The indices i and j refer to the type of incoming partons. Furthermore the PD_{ij}^V contain all the

information on the coupling of the quarks to the vector bosons, such as the quark charges, the Weinberg angle θ_W and the Cabibbo angle θ_C (the other angles and phases of the Kobayashi–Maskawa (KM) matrix are neglected). The explicit way in which the functions PD_{ij}^{V} combine with the correction terms Δ_{ij} is given in eq. (A.20). Notice that the parton distribution functions not only depend on the mass factorization scale M, but also on the renormalization scale R, because the calculation of their scale dependence originates from operator renormalization (= mass factorization) as well as from coupling constant renormalization. However, in the existing parametrizations of the parton distribution functions the two scales M and R are always set to be equal. Also the DY correction term $\Delta_{ij}(x, Q^2, M^2)$ (Wilson coefficient) depends on both scales. This can be seen by expanding the DY correction term in a power series in the running coupling constant $\alpha_s(R^2)$

$$\Delta_{ij}(x, Q^2, M^2) = \sum_{n=0}^{\infty} \alpha_s^n(R^2) \Delta_{ij}^{(n)}(x, Q^2, M^2, R^2). \tag{2.4}$$

When $\alpha_s(R^2)$ is expanded in a power series in $\alpha_s(M^2)$, the explicit R-dependence in eq. (2.4) drops out.

The DY correction term Δ_{ij} can be obtained from the DY partonic structure function $\hat{W}_{ij}$ through mass factorization

$$\hat{W}_{ij}(z, Q^2, M^2, \varepsilon) = \sum_{k,l} \int_0^1 \mathrm{d}x_1 \int_0^1 \mathrm{d}x_2 \int_0^1 \mathrm{d}x \, \delta(z - x x_1 x_2) \times \Gamma_{ki}(x_1, M^2, \varepsilon) \Gamma_{lj}(x_2, M^2, \varepsilon) \Delta_{kl}(x, Q^2, M^2) \tag{2.5}$$

where $\hat{W}_{ij}$ is determined by the parton subprocess

$$i + j \to \mathrm{V} + \text{“X”} \tag{2.6}$$

and Γ_{ki} represents the transition function (parton $i \to$ parton k). In eq. (2.5) we assume that coupling constant renormalization has already been performed. Like the DY correction term presented in eq. (2.4) the quantities $\hat{W}$ and Γ can be expanded in a power series in the renormalized coupling constant $\alpha_s(R^2)$ and therefore implicitly depend on the chosen renormalization scale R. The collinear divergences present in $\hat{W}$ and Γ are handled using n-dimensional regularization and manifest themselves as pole terms of the type $1/\varepsilon$ ($\varepsilon \equiv n - 4$).

The parton subprocesses contributing to the DY cross section up to second order in α_s are listed in table 1.

TABLE 1
List of Drell–Yan processes up to $O(\alpha_s^2)$

Figure		Drell–Yan subprocesses	
1	α_s^0:	$q + \bar{q} \to V$	
2	α_s^1:	$q + \bar{q} \to V$	(one-loop correction)
3		$q + \bar{q} \to V + g$	
3		$q(\bar{q}) + g \to V + q(\bar{q})$	
4	α_s^2:	$q + \bar{q} \to V$	(two-loop correction)
5		$q + \bar{q} \to V + g$	(one-loop correction)
6		$q + \bar{q} \to V + g + g$	
5		$q(\bar{q}) + g \to V + q(\bar{q})$	(one-loop correction)
6		$q(\bar{q}) + g \to V + q(\bar{q}) + g$	
7,8		$q + \bar{q} \to V + q + \bar{q}$	
8,9		$q(\bar{q}) + q(\bar{q}) \to V + q(\bar{q}) + q(\bar{q})$	
6		$g + g \to V + q + \bar{q}$	

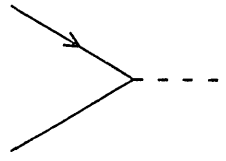

Fig. 1. The Born contribution to the subprocess $q + \bar{q} \to V$.

In zeroth order in α_s the only parton subprocess is given by quark–antiquark ($q\bar{q}$) annihilation (see fig. 1) and the resulting expression for $\hat{W}$ is given by

$$\hat{W}_{q\bar{q}}^{(0)} = \delta(1 - x) . \tag{2.7}$$

The first-order corrections, calculated using n-dimensional regularization, can be found in refs. [8, 12]. The order α_s correction to the $q\bar{q}$ process receives contributions from virtual (fig. 2) as well as real gluon (fig. 3) graphs. Furthermore, the qg subprocess (fig. 3), showing up for the first time in this order, has to be computed

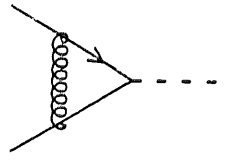

Fig. 2. The one-loop correction to the process $q + \bar{q} \to V$.

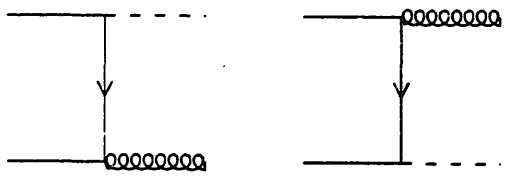

Fig. 3. Diagrams contributing to the subprocess $q + \bar{q} \to V + g$. The graphs corresponding to the subprocess $q(\bar{q}) + g \to V + q(\bar{q})$ can be obtained from those presented in this figure via crossing.

too. The partonic structure functions can be expressed in the following form:

$$\hat{W}^{(1)}_{q\bar{q}} = \frac{\alpha_s^u}{4\pi} S_\varepsilon \left(\frac{Q^2}{\mu^2}\right)^{\varepsilon/2} \left\{\frac{2}{\varepsilon} P^0_{qq} + w^0_{q\bar{q}} + \varepsilon \bar{w}^0_{q\bar{q}}\right\} \tag{2.8}$$

$$\hat{W}^{(1)}_{qg} = \hat{W}^{(1)}_{\bar{q}g} = \frac{\alpha_s^u}{4\pi} S_\varepsilon \left(\frac{Q^2}{\mu^2}\right)^{\varepsilon/2} \left\{\frac{1}{2\varepsilon} P^0_{qg} + w^0_{qg} + \varepsilon \bar{w}^0_{qg}\right\}, \tag{2.9}$$

where S_ε is defined by

$$S_\varepsilon = e^{\varepsilon(\gamma_E - \ln 4\pi)/2}. \tag{2.10}$$

Here α_s^u stands for the unrenormalized strong coupling constant. It is related to the renormalized running coupling constant $\alpha_s(R^2)$ in the following way:

$$\frac{\alpha_s^u}{4\pi} = \frac{\alpha_s(R^2)}{4\pi}\left(1 + \frac{\alpha_s(R^2)}{4\pi}\frac{2\beta_0}{\varepsilon} S_\varepsilon \left(\frac{R^2}{\mu^2}\right)^{\varepsilon/2}\right). \tag{2.11}$$

The constant β_0 is the lowest-order coefficient of the β-function, equal to

$$\beta_0 = \tfrac{11}{3} C_A - \tfrac{2}{3} n_f. \tag{2.12}$$

In the following we will denote $\alpha_s(R^2)$ by α_s and refer to R as the renormalization scale. The residues of the collinear divergences are given by the Altarelli–Parisi splitting functions P^n_{ij} [19]. In lowest order they are

$$P^0_{qq} = 4C_F\left[2\mathscr{D}_0(x) - 1 - x + \tfrac{3}{2}\delta(1-x)\right], \tag{2.13}$$

$$P^0_{qg} = 8T_f\left[(1-x)^2 + x^2\right], \tag{2.14}$$

$$P^0_{gq} = 4C_F\frac{(1-x)^2 + 1}{x}, \tag{2.15}$$

$$P^0_{gg} = 8C_A\left[\mathscr{D}_0(x) + \frac{1}{x} - 2 + x - x^2 + \tfrac{11}{12}\delta(1-x)\right] - \tfrac{4}{3} n_f \delta(1-x). \tag{2.16}$$

The definition of the distribution $\mathscr{D}_i(x)$ can be found in appendix B [eq. (B.5)].

The SU(N) Casimir operators are given by

$$C_A = N, \qquad C_F = \frac{N^2-1}{2N}, \tag{2.17}$$

where N is the number of colours. The number of flavours is indicated by n_f and T_f ($=\frac{1}{2}$) is the normalization corresponding to the fundamental representation. For completeness we have also presented P^0_{gq} and P^0_{gg} since they will be needed later on. The calculation of the non-pole terms in eqs. (2.8) and (2.9) yields the expressions

$$\frac{\alpha_s}{4\pi} w^0_{q\bar{q}} = \Delta^{(1)}_{q\bar{q}}(M^2 = Q^2), \tag{2.18}$$

$$\frac{\alpha_s}{4\pi} w^0_{qg} = \Delta^{(1)}_{qg}(M^2 = Q^2), \tag{2.19}$$

$$\begin{aligned} \bar{w}^0_{q\bar{q}} = C_F \Big\{ & 8\mathscr{D}_2(x) - 6\zeta(2)\mathscr{D}_0(x) + (1+x)\left[-4\ln^2(1-x) + 3\zeta(2)\right] \\ & + \frac{1+x^2}{1-x}\left[-4\ln x \ln(1-x) + \ln^2 x\right] + 4(1-x) \\ & + \delta(1-x)\left[16 - \tfrac{21}{2}\zeta(2)\right] \Big\}, \end{aligned} \tag{2.20}$$

$$\begin{aligned} \bar{w}^0_{qg} = T_f \Big\{ & \tfrac{1}{2}(1 + 2x^2 - 2x)\left[\ln^2\left(\frac{(1-x)^2}{x}\right) - 3\zeta(2)\right] \\ & + \tfrac{1}{2}(1 - 7x^2 + 6x)\ln\left(\frac{(1-x)^2}{x}\right) - 3 + 7x^2 - 4x \Big\}. \end{aligned} \tag{2.21}$$

The functions $w^0_{q\bar{q}}$ and w^0_{qg} are equal to the DY correction terms $\Delta^{(1)}_{q\bar{q}}$ and $\Delta^{(1)}_{qg}$ (see eqs. (B.2) and (B.17) respectively) provided the latter are calculated in the $\overline{\text{MS}}$ mass factorization scheme. The ε-parts $\bar{w}^0_{q\bar{q}}$ and $\bar{w}^0_{qg}$ are also given, as we will need them for the order α_s^2 calculations.

In second order of α_s the set of possible parton–parton reactions is completed by the qq and gg subprocesses. This exhausts all possible combinations of i and j in $\hat{W}_{ij}$. A part of them has already been presented in the literature. The first calculation was done for the qq process [20] (see figs. 8 and 9). Its results also hold for the $q\bar{q}$ scattering subprocess where a gluon is exchanged between the quark and the antiquark line. Thereafter the soft and virtual gluon contributions from the $q\bar{q}$ process with two gluons or a quark pair in the final state were determined [21–24] (see figs. 4–7). Finally, we recently finished the computation of the gg subprocess [25] (see fig. 6). All calculations mentioned above have been performed in the DIS mass factorization scheme. However, the results can easily be transformed to the $\overline{\text{MS}}$ scheme. The latter procedure only requires the knowledge of

the DY partonic cross sections, whereas in the DIS scheme one also has to calculate the deep inelastic partonic structure functions. In both schemes the following reactions were missing until now:
(a) the hard gluon contribution to the $q\bar{q}$ subprocess (figs. 5–7);
(b) the order α_s correction to the qg subprocess (figs. 5 and 6), and
(c) all possible interference terms between the various $q\bar{q} \to q\bar{q}V$ subprocesses (figs. 7–9).

In order to complete the α_s^2 correction to the DY process we include these missing pieces, which is the main goal of this paper. The calculation of the subprocesses listed in table 1 can be outlined as follows. While computing the cross sections corresponding to the graphs in figs. 1–9 one encounters three types of singularities, namely ultraviolet (UV), infrared (IR) and collinear/mass singularities. They are all dealt with using the technique of n-dimensional regularization. According to the Bloch–Nordsieck theorem [26], which holds for massless quarks only [27], the IR divergences are cancelled in the sum of virtual and radiative gluon graphs. The UV divergences are removed by the renormalization of the strong coupling constant, which is performed in the $\overline{\text{MS}}$ scheme. Since we consider an inclusive reaction only, there are no final-state collinear divergences left as stated by the KLN theorem [28]. The initial state collinear divergences are extracted from the cross section by absorbing them into the parton distribution functions, for which we choose the $\overline{\text{MS}}$ scheme, too. The mass factorization in the DIS scheme requires the computation of the partonic deep inelastic structure functions for the Vq and Vg subprocesses. The calculation of these structure functions is of the same level of complexity as the one encountered in the DY process and will therefore be postponed to the future.

The calculation of the squared amplitudes was performed in n dimensions using the algebraic manipulation programs REDUCE [29], SCHOONSCHIP* and FORM**. Since we also compute W- and Z-production we had to deal with the γ_5 matrix which cannot be trivially extended to n dimensions. Following the procedure discussed in ref. [31] we can distinguish the following types of trace structures. Defining the general electroweak vector boson quark coupling $Vq\bar{q}$ by

$$Vq_i\bar{q}_j\colon\ ig_V\gamma_\mu\left(v_i^V + a_i^V\gamma_5\right) \tag{2.22}$$

we distinguish three types of matrix elements:

(1) One fermion trace matrix elements, where the fermion trace contains two vertices of the form given in eq. (2.22). Matrix elements of this type appear in the computation of the graphs in figs. 1–6 and in the interference terms AC, AD, BC, BD, CE, CF, DE and DF in figs. 7–9;

* SCHOONSCHIP is an algebraic manipulation program written by M. Veltman, see ref. [30].
** FORM (version 1.0) is a symbolic manipulation program written by J.A.M. Vermaseren (NIKHEF-H, Amsterdam).

(2) Two fermion trace matrix elements, where one of the traces contains both vertices of the form (2.22). They appear in the terms A^2, B^2, C^2, D^2, E^2 and F^2 in figs. 7–9;

(3) Two fermion trace matrix elements, in which each trace contains one vertex of the type given above. Contributions of these type originate from the combinations AB, CD and EF in figs. 7–9.

Traces of types (1) and (2) can be performed by anticommuting the γ_5 with all Dirac matrices γ_μ so that the matrix element is proportional to the one obtained for a virtual photon ($V = \gamma$) multiplied by $v_i^2 + a_i^2$. Traces of type (3) have to be dealt with more care. However, since the partonic structure functions $\hat{W}$ corresponding to the combinations mentioned in (3) are manifestly collinearly finite, the trace can be calculated in four dimensions. In this case the vector–vector ($v_i v_j$) and the axial–axial ($a_i a_j$) parts of the matrix element are in general not equal to each other.

After having computed the traces we have to integrate the matrix elements over all internal-loop and final-state momenta which is the most difficult part of the calculation. In this paper we take all partons to be massless. The case of massive quarks (e.g. when heavy flavours are produced in the final state) will be discussed at the end of this section. Even if the partons are massless the integrals are very numerous and far from trivial. This in particular holds for the two-loop integrals appearing in the quark form factor (fig. 4) and the three-body phase-space integrals showing up in the calculation of the graphs in figs. 5–9. Some of them even have to be expanded up to order ε^4.

Starting with the two-loop graphs in fig. 4 we had to evaluate 107 different types of scalar integrals [32]. Note that they are not linearly independent. The irreducible set contains 36 elements only and can be found in ref. [33]. Apart from one misprint in the scalar integral corresponding to diagram 4C in the appendix of ref. [33], we agree with their result. The final result for the quark form factor is presented in eq. (2.49) of ref. [21] (see also appendix A of ref. [23]). This result agrees with the one quoted in ref. [18]. Finally we would like to comment on the

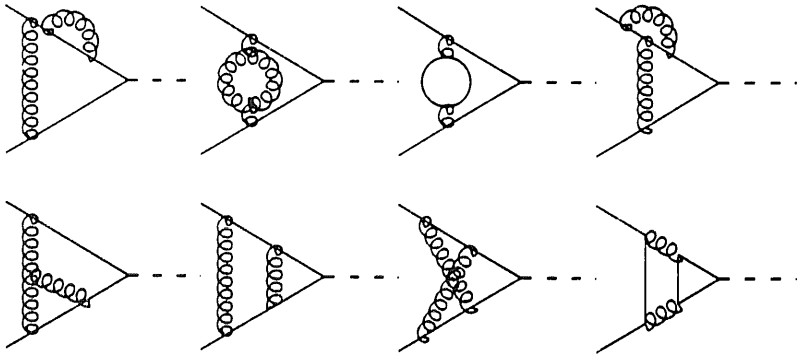

Fig. 4. The two-loop corrections to the process $q + \bar{q} \to V$.

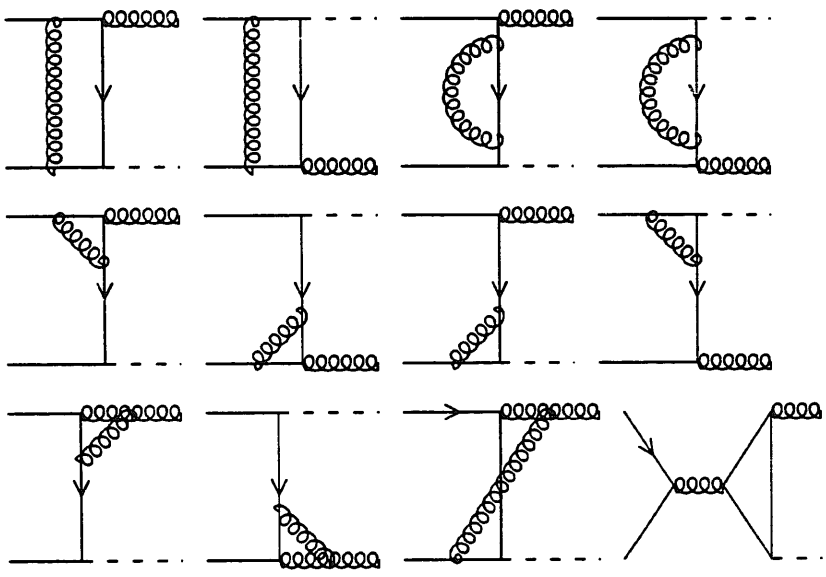

Fig. 5. The one-loop corrections to the process $q + \bar{q} \to V + g$. The diagrams corresponding to the one-loop correction to the subprocess $q(\bar{q}) + g \to V + q(\bar{q})$ can be obtained via crossing.

vertex graphs in fig. 4 containing the triangle fermion loop. These graphs only contribute in the case of Z-production with massive quarks in the loop. Notice that one always has to sum over all flavours in a quark family in order to cancel the anomaly arising from this type of graphs.

The two-body phase-space integrals emerging from fig. 5 constitute the easiest part of the calculation. They can be expressed in the following way:

$$\int \mathrm{dPS}^{(2)} |\mathscr{M}|^2 = 2^{4-2n} \frac{\pi^{1-n/2}}{\Gamma(\frac{1}{2}n-1)} \left(\frac{s-Q^2}{s}\right)^{n-3} s^{\frac{1}{2}n-2} \int_0^{\pi} \mathrm{d}\theta \, (\sin\theta)^{n-3} |\mathscr{M}|^2, \quad (2.23)$$

where s is the c.m. energy of the incoming partons and θ is the angle between one of the incoming and the outgoing parton. The amplitude $|\mathscr{M}|^2$ contains all one-loop integrals. The scalar loop integrals can be found in appendix F of ref. [24]. It turned out that we had to evaluate 89 integrals of the kind in eq. (2.23), which however do not form an independent set. Distinguishing them in soft (singular at $s = Q^2$) and hard (regular at $s = Q^2$) gluon integrals we count 8 and 81 respectively. Again the graph containing the fermion loop in fig. 5 only contributes in the case of Z-production with a massive quark loop. As for the two-loop diagram of fig. 4 one has to sum over the members of a quark family in order to cancel the anomaly.

The most difficult and laborious part of the calculation is due to the purely radiative subprocesses given in figs. 6–9 which contain three particles in the final state. They involve the calculation of the three-body phase-space integrals of the

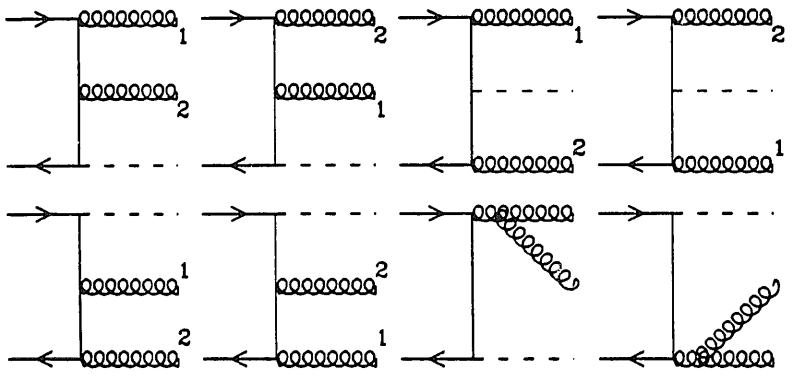

Fig. 6. Diagrams contributing to the subprocess $q + \bar{q} \to V + g + g$. The graphs corresponding to the subprocess $q(\bar{q}) + g \to V + q(\bar{q}) + g$ can be obtained from those presented in this figure via crossing. By crossing two pairs of lines one can obtain the diagrams corresponding to the subprocess $g + g \to V + q + \bar{q}$.

form

$$\int \mathrm{dPS}^{(3)} = \frac{1}{(4\pi)^n} \frac{s^{1-n/2}}{\Gamma(n-3)} \int_0^\pi \mathrm{d}\theta \int_0^\pi \mathrm{d}\phi (\sin\theta)^{n-3} (\sin\phi)^{n-4} \int_{Q^2}^s \mathrm{d}s_1$$

$$\times \int_{sQ^2/s_1}^{s+Q^2-s_1} \mathrm{d}s_2 \left((s_1 s_2 - sQ^2)(s + Q^2 - s_1 - s_2) \right)^{\frac{1}{2}n-2}. \qquad (2.24)$$

This expression has been derived in the c.m. frame of the incoming partons, where s_i denotes the invariant mass of the vector boson combined with one of the final state partons i. In many cases it is more convenient to evaluate the three-particle phase-space integrals in other Lorentz frames like the c.m. frame of the two outgoing partons [21, 23, 24, 34] or the c.m. frame of the vector boson and one of the outgoing partons [35]. In order to perform the angular integrations the matrix element $|\mathscr{M}|^2$ has to be decomposed in such a way that only two factors contain

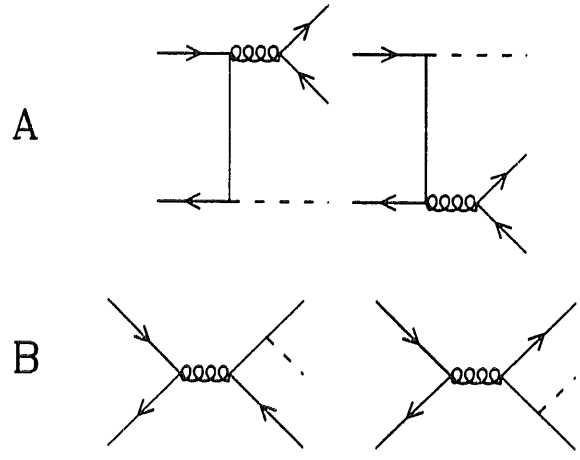

Fig. 7. Annihilation graphs contributing to the subprocess $q + \bar{q} \to V + q + \bar{q}$.

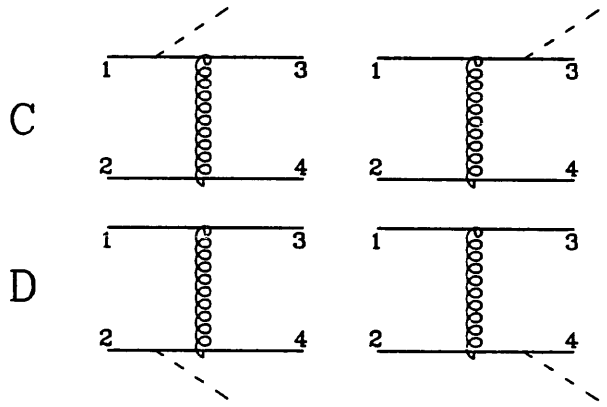

Fig. 8. Gluon exchange graphs contributing to the subprocesses $q + \bar{q} \to V + q + \bar{q}$ and $q(\bar{q}) + q(\bar{q}) \to V + q(\bar{q}) + q(\bar{q})$.

the angular variables θ and ϕ. The angular integrals are of the form

$$I_n^{(i,j)} = \int_0^\pi d\theta \int_0^\pi d\phi \frac{(\sin\theta)^{n-3}(\sin\phi)^{n-4}}{(a + b\cos\theta)^i (A + B\cos\theta + C\sin\theta\cos\phi)^j}, \quad (2.25)$$

where a, b, A, B and C are functions of the kinematical invariants s, Q^2, s_1 and s_2. These integrals can be found in appendix C of ref. [36]. For $n = 4 + \varepsilon$ and either $a^2 \neq b^2$ or $A^2 \neq B^2 + C^2$ the expressions are very cumbersome, let alone when both $a^2 \neq b^2$ and $A^2 \neq B^2 + C^2$. Fortunately the latter case can be avoided by choosing an appropriate frame. The partial fractioning of $|\mathcal{M}|^2$ leads to 217 three-body phase-space integrals, each of them containing four integration variables. We did not bother to see how they could be reduced to a linearly independent set. Due to the vast amount of integrals we are not able to publish them. Among these integrals only 10 were of the soft gluon type (singular at $s = Q^2$); they can be found in appendix G of ref. [24]. Some other three-body

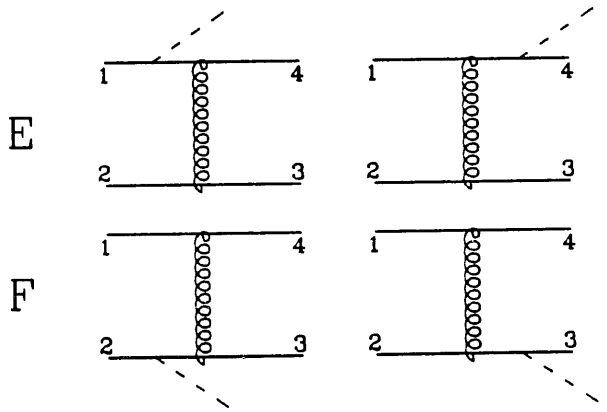

Fig. 9. Gluon exchange graphs contributing to the subprocess $q(\bar{q}) + q(\bar{q}) \to V + q(\bar{q}) + q(\bar{q})$ with identical quarks in the initial and/or final state.

phase-space integrals are listed in appendix A of ref. [25]. All scalar integrals can be obtained from us on request.

The partonic structure functions $\hat{W}_{ij}$ calculated up to second order in α_s can be divided into two classes. The first class originates from the matrix elements corresponding to types (1) and (2) mentioned below eq. (2.22). It contains all $\hat{W}_{ij}$ which have collinear divergences. To the second class belong all partonic structure functions which are collinearly finite (type (3) and some of type (1)). In order to perform the mass factorization according to eq. (2.5) for the $\hat{W}_{ij}$ (class I) we need the transition functions Γ_{ij}. These functions describe the transition of a parton j into a parton i. The qq and $q\bar{q}$ transition functions are divided into a non-singlet (NS) and a singlet (S) part in the following way:

$$\Gamma_{q_i q_j} = \delta_{ij}\Gamma_{qq}^{NS} + \Gamma_{q_i q_j}^{S}, \qquad \Gamma_{q_i \bar{q}_j} = \delta_{ij}\Gamma_{q\bar{q}}^{NS} + \Gamma_{q_i \bar{q}_j}^{S}, \qquad (2.26),(2.27)$$

where the indices i and j refer to the flavour of the (anti)quark. As the expressions for the transition functions do not explicitly depend on the flavours, we will suppress the flavour indices from now on. In the $\overline{\text{MS}}$ mass factorization scheme the Γ_{ij} can be expressed in terms of the Altarelli–Parisi splitting functions as

$$\Gamma_{qq}^{NS} = \Gamma_{\bar{q}\bar{q}}^{NS} = 1 + \frac{\alpha_s^u}{4\pi}\left(\frac{M^2}{\mu^2}\right)^{\varepsilon/2}\left[\frac{1}{\varepsilon}P_{qq}^0\right] + \left(\frac{\alpha_s^u}{4\pi}\right)^2\left(\frac{M^2}{\mu^2}\right)^{\varepsilon}\left[\frac{1}{\varepsilon^2}\left(\frac{1}{2}P_{qq}^0 \otimes P_{qq}^0 - \beta_0 P_{qq}^0\right) + \frac{1}{2\varepsilon}P_{qq}^{1,NS}\right], \qquad (2.28)$$

$$\Gamma_{q\bar{q}}^{NS} = \Gamma_{\bar{q}q}^{NS} = \left(\frac{\alpha_s^u}{4\pi}\right)^2\left(\frac{M^2}{\mu^2}\right)^{\varepsilon}\left[\frac{1}{2\varepsilon}P_{qq}^{1,-}\right], \qquad (2.29)$$

$$\Gamma_{qq}^{S} = \Gamma_{\bar{q}\bar{q}}^{S} = \left(\frac{\alpha_s^u}{4\pi}\right)^2\left(\frac{M^2}{\mu^2}\right)^{\varepsilon}\left[\frac{1}{\varepsilon^2}\left(\frac{1}{4}P_{qg}^0 \otimes P_{gq}^0\right) + \frac{1}{4\varepsilon}P_{qq}^{1,S}\right], \qquad (2.30)$$

$$\Gamma_{q\bar{q}}^{S} = \Gamma_{\bar{q}q}^{S} = \left(\frac{\alpha_s^u}{4\pi}\right)^2\left(\frac{M^2}{\mu^2}\right)^{\varepsilon}\left[\frac{1}{\varepsilon^2}\left(\frac{1}{4}P_{qg}^0 \otimes P_{gq}^0\right) + \frac{1}{4\varepsilon}P_{qq}^{1,S}\right], \qquad (2.31)$$

$$\Gamma_{qg} = \Gamma_{\bar{q}g} = \frac{\alpha_s^u}{4\pi}\left(\frac{M^2}{\mu^2}\right)^{\varepsilon/2}\left[\frac{1}{2\varepsilon}P_{qg}^0\right] + \left(\frac{\alpha_s^u}{4\pi}\right)^2\left(\frac{M^2}{\mu^2}\right)^{\varepsilon} \times\left[\frac{1}{\varepsilon^2}\left(\tfrac{1}{4}P_{qg}^0 \otimes P_{gg}^0 + \tfrac{1}{4}P_{qq}^0 \otimes P_{qg}^0 - \tfrac{1}{2}\beta_0 P_{qg}^0\right) + \frac{1}{4\varepsilon}P_{qg}^1\right], \qquad (2.32)$$

$$\Gamma_{gq} = \Gamma_{g\bar{q}} = \left(\frac{\alpha_s^u}{4\pi}\right)\left(\frac{M^2}{\mu^2}\right)^{\varepsilon/2}\left[\frac{1}{\varepsilon}P_{gq}^0\right], \qquad (2.33)$$

$$\Gamma_{gg} = 1 + \left(\frac{\alpha_s^u}{4\pi}\right)\left(\frac{M^2}{\mu^2}\right)^{\varepsilon/2}\left[\frac{1}{\varepsilon}P_{gg}^0\right], \qquad (2.34)$$

where M is the mass factorization scale. To obtain the above expressions in terms of the renormalized coupling constant $\alpha_s(R^2)$, one has to perform coupling constant renormalization (see eq. (2.11)). Notice that at $O(\alpha_s^2)$ the transition functions Γ_{qq}^S and $\Gamma_{q\bar{q}}^S$ are equal, which is not necessarily true at higher orders. The convolution symbol $\otimes$ is defined by

$$(f\otimes g)(x)=\int_0^1 dx_1\int_0^1 dx_2\,\delta(x-x_1x_2)f(x_1)g(x_2). \tag{2.35}$$

The lowest-order Altarelli–Parisi splitting functions have already been listed in eqs. (2.13)–(2.16) and the expression for β_0 can be found in eq. (2.12). In the next-to-leading order we need P_{qg}^1 and the singlet (S) as well as the non-singlet (NS) part of P_{qq}^1. They can be obtained from eqs. (16) and (17) in ref. [37] (see also refs. [38–41]). Since we use a little different notation we will list them here below,

$$\begin{aligned}P_{qq}^{1,NS}=n_fC_f\Big\{&\delta(1-x)\big[-\tfrac{2}{3}-\tfrac{16}{3}\zeta(2)\big]-\tfrac{80}{9}\mathscr{D}_0(x)-\frac{8}{3}\frac{1+x^2}{1-x}\ln x-\tfrac{8}{9}+\tfrac{88}{9}x\Big\}\\
&+C_F^2\Big\{\delta(1-x)[3-24\zeta(2)+48\zeta(3)]-16\frac{1+x^2}{1-x}\ln x\ln(1-x)\\
&-4(1+x)\ln^2x-8\Big(2x+\frac{3}{1-x}\Big)\ln x-40(1-x)\Big\}\\
&+C_AC_F\Big\{\delta(1-x)\big[\tfrac{17}{3}+\tfrac{88}{3}\zeta(2)-24\zeta(3)\big]+\big(\tfrac{536}{9}-16\zeta(2)\big)\mathscr{D}_0(x)\\
&+4\frac{1+x^2}{1-x}\ln^2x+8(1+x)\zeta(2)\\
&-\tfrac{4}{3}\Big(5+5x-\frac{22}{1-x}\Big)\ln x+\tfrac{4}{9}(53-187x)\Big\},\end{aligned} \tag{2.36}$$

$$\begin{aligned}P_{qq}^{1,S}=8C_FT_f\Big\{&-2(1+x)\ln^2x+\big(2+10x+\tfrac{16}{3}x^2\big)\ln x\\
&+\frac{40}{9}\frac{1}{x}-4+12x-\tfrac{112}{9}x^2\Big\},\end{aligned} \tag{2.37}$$

$$\begin{aligned}P_{qq}^{1,-}=8C_F\big(C_F-\tfrac{1}{2}C_A\big)\Big\{&\frac{1+x^2}{1+x}\big[\ln^2x-4\ln x\ln(1+x)-4\,\mathrm{Li}_2(-x)-2\zeta(2)\big]\\
&+2(1+x)\ln x+4(1-x)\Big\},\end{aligned} \tag{2.38}$$

$$P_{qg}^{1} = -8C_F T_f\{2(1-2x+2x^2)[2\ln x \ln(1-x) + 2\zeta(2) - \ln^2(1-x)]$$

$$-(1-2x+4x^2)\ln^2 x - 8x(1-x)\ln(1-x) - (3-4x+8x^2)\ln x$$

$$-14+29x-20x^2\} - 8C_A T_f\Big\{-(1+2x+2x^2)[\ln^2 x - 4\ln x \ln(1-x)$$

$$-4\,\mathrm{Li}_2(-x) - 2\zeta(2)] + (1-2x+2x^2)[2\ln^2(1-x) - 2\zeta(2)]$$

$$+(3+6x+2x^2)\ln^2 x + 8x(1-x)\ln(1-x) - \tfrac{2}{3}(3+24x+44x^2)\ln x$$

$$-\frac{2}{9}\left(\frac{20}{x} - 18 + 225x - 218x^2\right)\Big\}. \tag{2.39}$$

The relation between the anomalous dimension of the composite operators denoted by $\gamma_{ij}^{(n)}$ and the splitting functions P_{ij} is given through a Mellin transformation

$$\gamma_{ij}^{k}(n) = -\int_0^1 \mathrm{d}x x^{n-1} P_{ij}^{k}(x). \tag{2.40}$$

In the literature the expressions $\gamma_{qq}^{1,NS} + (-1)^n \gamma_{qq}^{1,-}$ stand for the non-singlet anomalous dimension. The singlet anomalous dimensions we need for our calculation are given by $\gamma_{qq}^{1,NS} + (-1)^n \gamma_{qq}^{1,-} + \gamma_{qq}^{1,S}$ and γ_{qg}^{1} respectively. The reason that the splitting functions P_{qg}^{k} in eqs. (2.30)–(2.32) are multiplied by an extra factor $\frac{1}{2}$ can be attributed to the fact that the corresponding anomalous dimensions γ_{qg}^{k} receive contributions from the quark as well as the antiquark. The same applies to $P_{qq}^{1,S}$ in eqs. (2.30) and (2.31). Notice that the splitting functions P_{gq}^{k} and P_{gg}^{k} are only needed up to first order in α_s since the vector boson V does not couple directly to the gluon.

For the mass factorization of $\hat{W}_{ij}$ it is convenient to split $\hat{W}_{qq}$, $\hat{W}_{q\bar{q}}$, Δ_{qq} and $\Delta_{q\bar{q}}$ into non-singlet and singlet parts as has been done for the transition functions (see eqs. (2.26) and (2.27)). Then the mass singular partonic structure functions can be classified as

(i) $\hat{W}_{q\bar{q}}^{(2),NS}$, which gets contributions from the graphs in figs. 4–6 and A^2, AC and AD in figs. 7 and 8.

(ii) $\hat{W}_{q\bar{q}}^{(2),S}$. It receives contributions from C^2 and D^2 in fig. 8. Likewise $\hat{W}_{qq}^{(2),S}$ which is determined by C^2, D^2, E^2 and F^2 in figs. 8 and 9.

(iii) $\hat{W}_{qq}^{(2),NS}$, which receives its contributions from CE and DF (see figs. 8 and 9).

(iv) $\hat{W}_{qg}^{(2)}$. It gets contributions from the graphs in figs. 5 and 6.

(v) $\hat{W}_{gg}^{(2)}$, which receives contributions from the graphs in fig. 6.

Since the partonic structure functions $\hat{W}_{ij}$, calculated in this paper, satisfy the mass factorization theorem, the unrenormalized and mass singular expressions can

be written as follows (where S_ε is defined in eq. (2.10))

$$\hat{W}_{q\bar{q}}^{(2),NS} = \Gamma_{qq}^{NS}\Gamma_{\bar{q}\bar{q}}^{NS}\Delta_{q\bar{q}}^{NS} = \left(\frac{\alpha_s^u}{4\pi}\right)^2 S_\varepsilon^2\left(\frac{Q^2}{\mu^2}\right)^\varepsilon \left\{\frac{1}{\varepsilon^2}\left[2P_{qq}^0 \otimes P_{qq}^0 - 2\beta_0 P_{qq}^0\right]\right.$$

$$\left. + \frac{1}{\varepsilon}\left[P_{qq}^{1,NS} + 2P_{qq}^0 \otimes w_{q\bar{q}}^0 - 2\beta_0 w_{q\bar{q}}^0\right] + 2P_{qq}^0 \otimes \bar{w}_{q\bar{q}}^0 - 2\beta_0 \bar{w}_{q\bar{q}}^0 + w_{q\bar{q}}^{1,NS}\right\}, \quad (2.41)$$

$$\hat{W}_{q\bar{q}}^{(2),S} = \hat{W}_{qq}^{(2),S}$$

$$= \Gamma_{qq}^{NS}\Gamma_{\bar{q}\bar{q}}^{NS}\Delta_{q\bar{q}}^{S} + \Gamma_{qq}^{NS}\Gamma_{\bar{q}\bar{q}}^{S}\Delta_{q\bar{q}}^{NS} + \Gamma_{qq}^{S}\Gamma_{\bar{q}\bar{q}}^{NS}\Delta_{q\bar{q}}^{NS} + \Gamma_{gq}\Gamma_{\bar{q}\bar{q}}^{NS}\Delta_{\bar{q}g} + \Gamma_{g\bar{q}}\Gamma_{qq}^{NS}\Delta_{qg}$$

$$= \left(\frac{\alpha_s^u}{4\pi}\right)^2 S_\varepsilon^2\left(\frac{Q^2}{\mu^2}\right)^\varepsilon \left\{\frac{1}{2\varepsilon^2}P_{q\bar{g}}^0 \otimes P_{gq}^0 + \frac{1}{\varepsilon}\left[\tfrac{1}{2}P_{qq}^{1,S} + 2P_{gq}^0 \otimes w_{qg}^0\right]\right.$$

$$\left. + 2P_{gq}^0 \otimes \bar{w}_{qg}^0 + w_{q\bar{q}}^{1,S}\right\}, \quad (2.42)$$

$$\hat{W}_{qq}^{(2),NS} = \Gamma_{qq}^{NS}\Gamma_{qq}^{NS}\Delta_{qq}^{NS} + \Gamma_{qq}^{NS}\Gamma_{\bar{q}q}\Delta_{q\bar{q}}^{NS} + \Gamma_{\bar{q}q}\Gamma_{qq}^{NS}\Delta_{\bar{q}q}^{NS}$$

$$= \left(\frac{\alpha_s^u}{4\pi}\right)^2 S_\varepsilon^2\left(\frac{Q^2}{\mu^2}\right)^\varepsilon \left\{\frac{1}{\varepsilon}P_{qq}^{1,-} + w_{qq}^{1,NS}\right\}, \quad (2.43)$$

$$\hat{W}_{qg}^{(2)} = \Gamma_{qq}^{NS}\Gamma_{\bar{q}g}\Delta_{q\bar{q}}^{NS} + \Gamma_{qq}^{NS}\Gamma_{gg}\Delta_{qg}$$

$$= \left(\frac{\alpha_s^u}{4\pi}\right)^2 S_\varepsilon^2\left(\frac{Q^2}{\mu^2}\right)^\varepsilon \left\{\frac{1}{\varepsilon^2}\left[\tfrac{3}{4}P_{qq}^0 \otimes P_{qg}^0 + \tfrac{1}{4}P_{gg}^0 \otimes P_{qg}^0 - \tfrac{1}{2}\beta_0 P_{qg}^0\right]\right.$$

$$+ \frac{1}{\varepsilon}\left[\tfrac{1}{4}P_{qg}^1 - 2\beta_0 w_{qg}^0 + \tfrac{1}{2}P_{qg}^0 \otimes w_{q\bar{q}}^0 + \left(P_{qq}^0 + \bar{P}_{gg}^0\right) \otimes w_{qg}^0\right]$$

$$\left. - 2\beta_0 \bar{w}_{qg}^0 + \tfrac{1}{2}P_{qg}^0 \otimes \bar{w}_{q\bar{q}}^0 + \left(P_{qq}^0 + P_{gg}^0\right) \otimes \bar{w}_{qg}^0 + w_{qg}^1\right\}, \quad (2.44)$$

$$\hat{W}_{gg}^{(2)} = 2\Gamma_{qg}\Gamma_{\bar{q}g}\Delta_{q\bar{q}}^{NS} + 2\Gamma_{qg}\Gamma_{gg}\Delta_{qg} + 2\Gamma_{\bar{q}g}\Gamma_{gg}\Delta_{\bar{q}g} + \Gamma_{gg}\Gamma_{gg}\Delta_{gg}$$

$$= \left(\frac{\alpha_s^u}{4\pi}\right)^2 S_\varepsilon^2\left(\frac{Q^2}{\mu^2}\right)^\varepsilon \left\{\frac{1}{2\varepsilon^2}P_{qg}^0 \otimes P_{qg}^0 + \frac{2}{\varepsilon}P_{qg}^0 \otimes w_{qg}^0 + 2P_{qg}^0 \otimes \bar{w}_{qg}^0 + w_{gg}^1\right\}. \quad (2.45)$$

In the above equations α_s^u is the unrenormalized strong coupling constant, which

has to be renormalized using the relation in eq. (2.11). The UV divergencies are due to the loop diagrams appearing in the calculation of $\hat{W}^{(2),\mathrm{NS}}_{q\bar{q}}$ and $\hat{W}^{(2)}_{qg}$. Notice that the gg subprocess can be made finite by using the lowest-order splitting function P^0_{qg} only. The various non-pole terms w^1_{ij} are equal to

$$\left(\frac{\alpha_s}{4\pi}\right)^2 w^{1,\mathrm{NS}}_{q\bar{q}} = \Delta^{(2)}_{q\bar{q}}(M^2 = Q^2, R^2 = Q^2), \tag{2.46}$$

$$\left(\frac{\alpha_s}{4\pi}\right)^2 w^{1,\mathrm{S}}_{q\bar{q}} = 2\Delta^{(2)}_{q\bar{q},C^2}(M^2 = Q^2), \tag{2.47}$$

$$\left(\frac{\alpha_s}{4\pi}\right)^2 w^{1,\mathrm{NS}}_{qq} = 2\Delta^{(2)}_{qq,CE}(M^2 = Q^2), \tag{2.48}$$

$$\left(\frac{\alpha_s}{4\pi}\right)^2 w^{1}_{qg} = \Delta^{(2)}_{qg}(M^2 = Q^2, R^2 = Q^2), \tag{2.49}$$

$$\left(\frac{\alpha_s}{4\pi}\right)^2 w^{1}_{gg} = \Delta^{(2)}_{gg}(M^2 = Q^2). \tag{2.50}$$

The expressions for the DY correction terms $\Delta^{(2)}_{ij}$, calculated in the $\overline{\mathrm{MS}}$ scheme, can be found in appendix B (see eqs. (B.7), (B.21), (B.24), (B.18) and (B.28) respectively).

The remaining contributions to $\hat{W}_{ij}$ (class II) which are not collinearly divergent do not need mass factorization. They originate from the combinations of the graphs B^2, BC, BD, CD, CF, DE and FE in figs. 7–9. In the case of Z-production also the combination AB contributes. It vanishes if one sums over all flavours in one family unless the final-state quarks are massive. This situation is akin to the virtual graphs in figs. 4 and 5 except that here no anomaly term appears. The class II partonic structure functions $\hat{W}_{ij}$ are equal to the DY correction terms Δ_{ij} (see appendix B) which implies that they are scheme independent at least up to order α_s^2.

Summarizing the content of this section we conclude that the calculation of the order α_s^2 correction to the inclusive DY cross section has been completed now in the $\overline{\mathrm{MS}}$ scheme. As already mentioned in this section there is another popular scheme to present the correction terms to various QCD processes, namely the DIS scheme. In our case this requires the calculation of the deep inelastic partonic structure functions $\hat{\mathscr{F}}_{2q}$ and $\hat{\mathscr{F}}_{2g}$, which is as laborious as the calculation of the DY structure functions $\hat{W}_{ij}$. A part of this work has already been published in the literature. The soft plus virtual gluon part of $\hat{\mathscr{F}}_{2q}$ is given in ref. [23]. The part of $\hat{\mathscr{F}}_{2q}$ due to the DIS counterparts of the diagrams A in fig. 7 can be found in ref. [24]. Ten years ago the contribution to $\hat{\mathscr{F}}_{2q}$ corresponding to the graphs obtained

by crossing the diagrams in figs. 8 and 9 were calculated in ref. [20]. Left over are the hard gluon part of $\hat{\mathscr{F}}_{2q}$ coming from the diagrams found by crossing the vector boson and a quark in figs. 5 and 6 and the full order α_s^2 contribution to $\hat{\mathscr{F}}_{2g}$. The graphs for the latter can be found by appropriate crossings in figs. 5 and 6. Their calculation will be presented in the near future. In principle we also need the three-loop contribution to the anomalous dimensions γ_{ij} in eq. (2.40). The coefficients of the perturbative expansion in the running coupling constant $\alpha_s(Q^2)$ of the renormalization group improved Wilson coefficient are only scheme independent if Δ_{ij}^k as well as γ_{ij}^{k+1} are known (see refs. [38,42]).

Finally we want to comment on heavy flavour production in the DY process. In this paper we assume all heavy flavours to be massless. This in particular is a crude assumption for top-quark production. A part of this problem is investigated in ref. [43] where the contributions due to triangle graphs of figs. 4 and 5 have been calculated in the case of heavy quarks. The calculation reveals a correction of 0.025% for $q\bar{q} \to Zg$ and 0.005% for $qg \to Zq$ at CERN collider energies coming from the last graph of fig. 5. The contribution of the two-loop triangle graph in fig. 4 is larger and amounts to 0.73% at most. These corrections become even smaller at larger energies. They never exceed the contributions coming from the smallest subprocess calculated above (qq scattering) and can therefore be completely neglected. Still missing are the production mechanisms $q + \bar{q} \to Q + \overline{Q} + V$ due to graphs A and B in fig. 7 and $g + g \to Q + \overline{Q} + V$ in fig. 6. Their contributions will have to be calculated, but we expect that they are small.

3. Total cross sections for W- and Z-production

In this section we will show results for vector boson production and compare them with the most recent data from the UA2 and CDF experiments. The total inclusive cross section is given by (see eq. (2.2))

$$\sigma_{\text{tot}}(S) = \int \mathrm{d}Q^2\, \sigma_V(Q^2, M_V^2) W_V(\tau, Q^2). \tag{3.1}$$

The pointlike cross section $\sigma_V(Q^2, M_V^2)$ for $V = \gamma, Z, W$ is explicitly given in eqs. (A.1)–(A.3). The hadronic structure function $W_V(\tau, Q^2)$ can be obtained from eq. (2.3) by combining the various combinations of the parton distribution functions indicated by PD_{ij}^V with the DY correction terms Δ_{ij} discussed in sect. 2. The explicit expression can be found in eq. (A.20). For our subsequent discussions it is convenient to rewrite W_V in the following way:

$$W_V(\tau, Q^2) = \sum_{i,j} \int_\tau^1 \frac{\mathrm{d}x}{x} \Phi_{ij}(x, M^2)\, \Delta_{ij}\left(\frac{\tau}{x}, Q^2, M^2\right), \tag{3.2}$$

where Φ_{ij} denotes the parton flux which is defined by

$$\Phi_{ij}(x, M^2) = \int_x^1 \frac{dy}{y} \mathrm{PD}_{ij}^{\mathrm{V}}\left(y, \frac{x}{y}, M^2\right). \tag{3.3}$$

At high energies the total cross section is dominated by W- and Z-production. Since the widths of these vector bosons are small compared to their masses, the integral in eq. (3.1) can be performed using the narrow-width approximation. The integration becomes trivial and its result for σ_{tot} is given by the expressions in eqs. (A.10) and (A.11).

We will now present the DY cross section and its K-factor for both $p\bar{p}$ and pp collisions at the current and future high-energy colliders. The c.m. energies under consideration are $\sqrt{S} = 0.63$ TeV (Sp$\bar{p}$S), $\sqrt{S} = 1.8$ TeV (Tevatron), $\sqrt{S} = 16$ TeV (LHC) and $\sqrt{S} = 40$ TeV (SSC). For the electroweak parameters we take the following values: $M_{\mathrm{Z}} = 91$ GeV, $M_{\mathrm{W}} = 80$ GeV, $G_{\mathrm{F}} = 1.166 \times 10^{-5}$ GeV^{-2} (Fermi constant), $\sin^2\theta_{\mathrm{W}} = 0.227$ and $\sin^2\theta_{\mathrm{C}} = 0.05$. Further we assume the top quark to be heavier than the W. For the running coupling constant, determined in the $\overline{\mathrm{MS}}$ scheme, we adopt the expression in eq. (10) of ref. [44] which is corrected up to two loops with the heavy-flavour thresholds included. The number of flavours n_{f} is chosen to be five and the QCD scale parameter Λ is given below. Since the DY correction terms are calculated in the $\overline{\mathrm{MS}}$ scheme we need the parton distribution functions in the same scheme. Here we have taken the HMRS parametrizations [45, 46], which are indicated by HMRSE$_+$, HMRSE, HMRSE$_-$ ($\Lambda = 100$ MeV) and HMRSB ($\Lambda = 190$ MeV). Furthermore, to make a comparison of the various independent parametrization sets we also used the parton distribution functions given in tables I2 and I4 of ref. [47], which we will refer to as MTE ($\Lambda = 155$ MeV) and MTB ($\Lambda = 194$ MeV) respectively. Unless stated otherwise, all results are obtained using the HMRSB parametrization. The renormalization scale R is always taken to be equal to the mass factorization scale M (see the comment above eq. (2.4)), for which we have chosen the canonical value $\sqrt{Q^2}$. Since the total cross section is calculated in the narrow width approximation this implies that $M = M_{\mathrm{V}}$ (vector boson mass). The dependence of the cross section on the chosen mass factorization scale will be discussed at the end of this section. All numerical results in this paper are produced by our Fortran program ZWPROD, which can be obtained on request.

For the discussion of various contributions to the Drell–Yan correction term it is convenient to introduce the K-factor. In this paper the theoretical K-factor is defined as follows

$$K_{\mathrm{th}} = \sum_{n=0}^{\infty} K^{(n)}, \tag{3.4}$$

where $K^{(n)}$ is the $O(\alpha_s^n)$ contribution to the K-factor, which is given by

$$K^{(n)} = \frac{W^{(n)}(\tau, Q^2)}{W^{(0)}(\tau, Q^2)} = \frac{\sigma^{(n)}}{\sigma^{(0)}} . \tag{3.5}$$

The functions $W^{(n)}(\tau, Q^2)$ and $\sigma^{(n)}$ are the $O(\alpha_s^n)$ correction to the hadronic structure function $W_V(\tau, Q^2)$ and cross section respectively. They originate from the $O(\alpha_s^n)$ contribution to Δ_{ij} in eq. (2.4). The order α_s^i corrected K-factor is defined by

$$K_i = \sum_{n=0}^{i} K^{(n)} = \frac{\sigma_i}{\sigma_0} , \tag{3.6}$$

where σ_i is the $O(\alpha_s^i)$ corrected DY cross section and σ_0 the Born contribution.

In the discussion of the results we will try to answer the following questions:
(1) How large is the $O(\alpha_s^2)$ contribution to the K-factor ($K^{(2)}$) compared with the $O(\alpha_s)$ one ($K^{(1)}$)?
(2) What is the relative contribution of the four different subprocesses $q\bar{q}$, qg, qq and gg to the $O(\alpha_s^2)$ part of the DY cross section?
(3) How does the cross section depend on the various parametrizations chosen for the parton distribution functions?
(4) How does the cross section depend on the different choices made for the factorization scale M and the renormalization scale R?

The same type of questions can also be raised in the case of the other processes like heavy flavour production [36,48,49], direct photon production [50] or jet production [51]. Note that the answers to the first question and to a lesser extent to the second and third one very heavily depend on the chosen renormalization and mass factorization schemes (we use $\overline{\text{MS}}$) and the scales R and M. A change of schemes at a fixed value for M and R alters the coefficients in the perturbation series of the Wilson coefficient. The same happens if in a given scheme M or R is varied. This leads to an increase or decrease of the higher-order corrections with respect to the lower-order ones. It also entails a redistribution of the contributions, coming from the various production mechanisms, to the Wilson coefficient. Therefore an investigation of the problems (1), (2) and (3) only makes sense if the schemes and scales are specified. In this paper we have chosen the $\overline{\text{MS}}$ scheme and have taken $R = M = M_V$, unless mentioned otherwise.

Starting with W-production at $p\bar{p}$ colliders we show in fig. 10 the $O(\alpha_s)$ and $O(\alpha_s^2)$ corrections to the DY K-factor for $0.5 \text{ TeV} < \sqrt{S} < 50 \text{ TeV}$. Here the K-factor originates from eqs. (3.5) and (3.6) where the total cross section stands for the sum of W^+ and W^- production. The figure reveals that the $O(\alpha_s^2)$ contribution to the K-factor, i.e. $K^{(2)}$, gets negative for $\sqrt{S} > 2.7$ TeV which implies $K_2 < K_1$ at high energies. Moreover, $K^{(2)}$ is much smaller than $K^{(1)}$ so that the

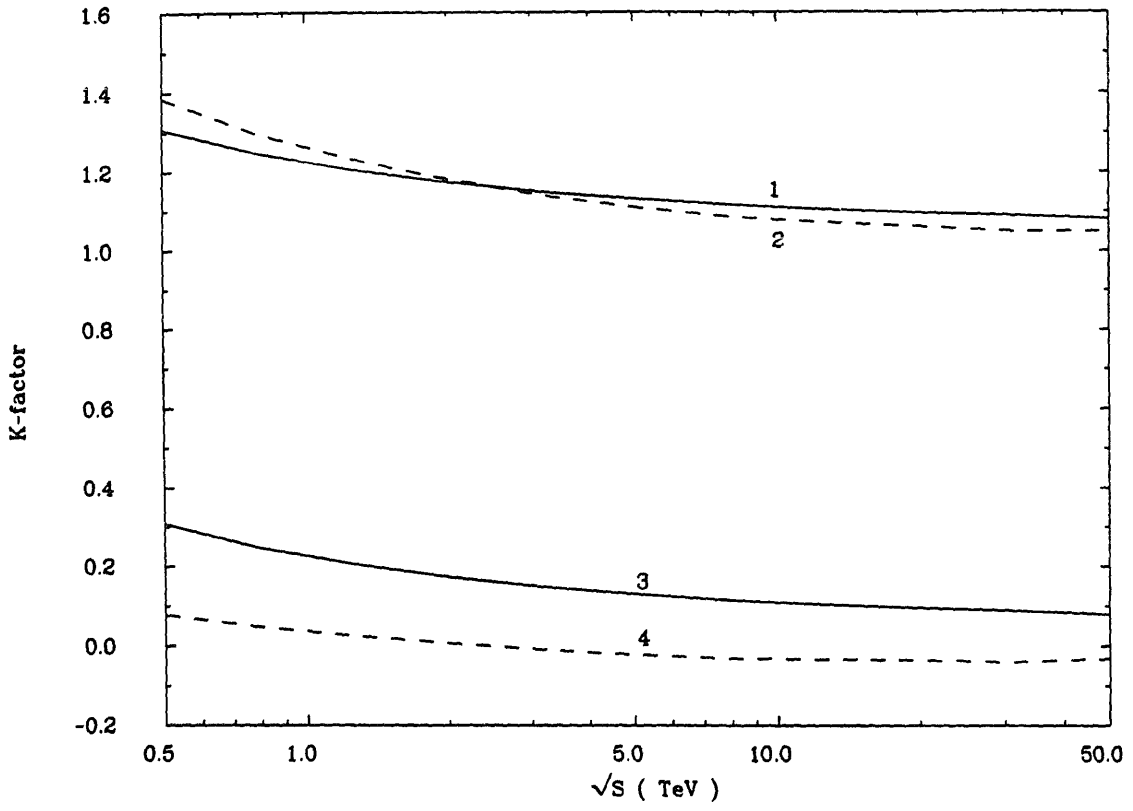

Fig. 10. The K-factor for $W^+ + W^-$ production at a $p\bar{p}$ collider (see eqs. (3.5) and (3.6)). (1) K_1; (2) K_2; (3) $K^{(1)}$; (4) $K^{(2)}$.

first-order corrected cross section σ_1 is hardly modified over the whole energy range. The same phenomenon is also observed for pp collisions where $K^{(2)} < 0$ at $\sqrt{S} > 2.0$ TeV (see fig. 11). The same behaviour of the K-factor is also observed when other parametrizations of the parton distribution functions are used like HMRSE, MTE or MTB. The property that $K^{(2)}$ gets negative at very large energies can be wholly attributed to the qg subprocess. Notice that the latter leads to a negative correction over the whole energy range, hence, the positive contribution of the $q\bar{q}$ subprocess is always compensated (see figs. 12 and 13). Remember that the $O(\alpha_s)$ part of the qg subprocess is negative too, but in this case its absolute value is always smaller than the one computed for the $q\bar{q}$ reaction at the same order of α_s.

The separate contributions to the K-factor coming from the four subprocesses are shown in figs. 12 and 13. From these figures we infer that the K-factor is dominated by the $q\bar{q}$ and qg subprocesses. A striking result of our calculations is the small contribution of gg fusion to the K-factor, in particular when we compare it to the qg process. At first sight this might be unexpected since the numerical evaluation of both reactions involves the gluon distribution function which steeply rises at small x. As has been shown in a previous paper [25] the relative size of the

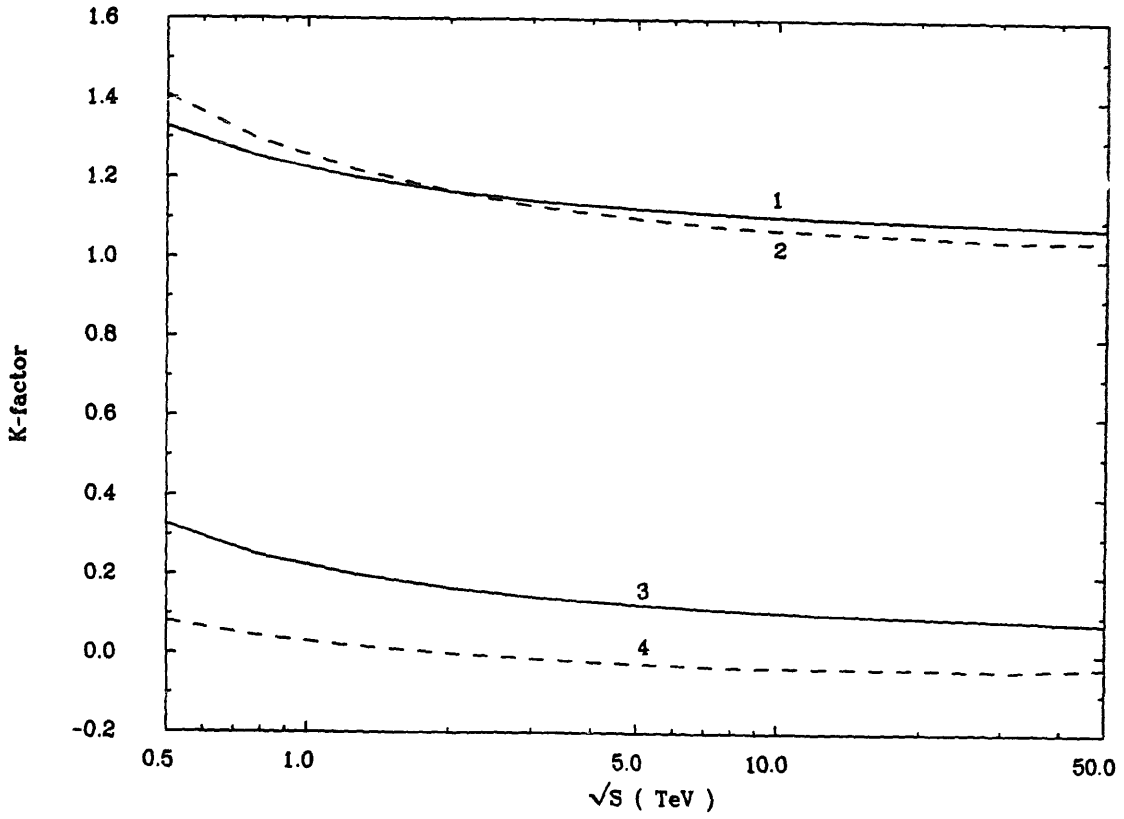

Fig. 11. The same as in fig. 10 but now for a pp collider.

contributions coming from the four subprocesses can be understood as follows. The parton flux Φ_{ij} (see eq. (3.3)) steeply rises as $x \to 0$ whereas it sharply decreases for $x \to 1$. This implies that $x \sim \tau$ is the relevant integration region in eq. (3.2). Therefore the cross section will heavily depend on the behaviour of $\Delta_{ij}(\tau/x, Q^2, M^2)$ near $x = \tau$. The functional form of $\Delta_{ij}(x, Q^2, M^2)$ near $x = 1$ for the various subprocesses is given in appendix B. Qualitatively they behave like (see eqs. (B.29)–(B.46))

$$\Delta_{q\bar{q}} \overset{x\to 1}{\sim} a_i \mathscr{D}_i(x) + b_i \ln^i(1-x) + c\delta(1-x) + d, \tag{3.7}$$

$$\Delta_{qg} \overset{x\to 1}{\sim} a_i \ln^i(1-x) + b, \tag{3.8}$$

$$\Delta_{qq} \overset{x\to 1}{\sim} (1-x)^a \ln^2(1-x) \qquad (a>0), \tag{3.9}$$

$$\Delta_{gg} \overset{x\to 1}{\sim} (1-x)^b \ln^2(1-x) \qquad (b>0). \tag{3.10}$$

The vanishing of the last two correction terms near $x = 1$ is caused by the absence

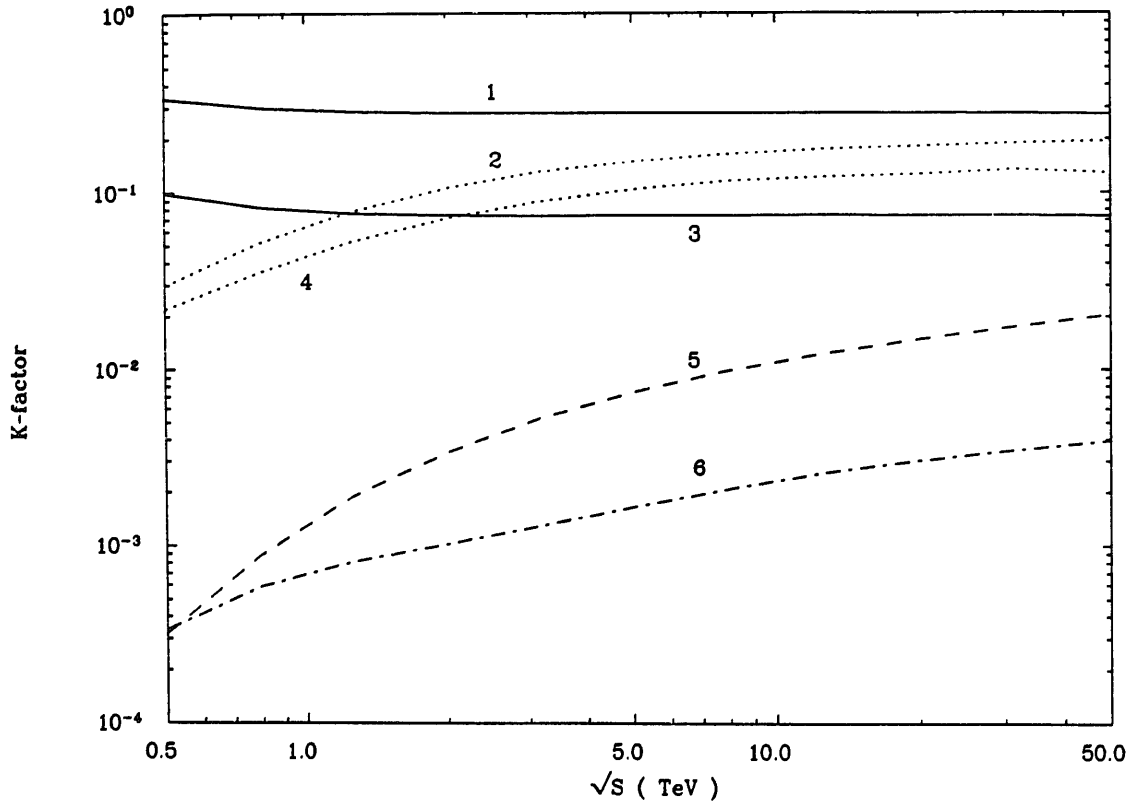

Fig. 12. The various contributions to the K-factor for $W^+ + W^-$ production at a $p\bar{p}$ collider (see eq. (3.5)). (1) $K_{q\bar{q}}^{(1)}$; (2) $-K_{qg}^{(1)}$; (3) $K_{q\bar{q}}^{(2)}$; (4) $-K_{qg}^{(2)}$; (5) $K_{gg}^{(2)}$; (6) $K_{qq}^{(2)}$.

of gluons in the final state. In that case the three-body phase-space integrals do not contribute at the boundary of phase space. Now one can understand why the contributions from qq and gg are small compared to those from $q\bar{q}$ and qg. The Drell–Yan correction term Δ_{gg} tends to suppress the fast rise of the gg flux, whereas Δ_{qg} enhances the behaviour of the qg flux. However, notice that the suppression of the DY correction term near $x = 1$ is more and more compensated at higher energies, due to the faster growth of the gg flux relative to the other fluxes, as can be seen in figs. 12 and 13.

We also want to comment on the contributions coming from the distributions $\mathscr{D}_i(x)$ and $\delta(1-x)$ in eq. (3.7). The coefficients of these functions can be determined by a soft gluon approximation, which means that only the contributions coming from soft and virtual gluons are taken into account. As is known from the literature, in the DIS scheme (with $M = R = M_V$) the dominant part of the K-factor can be attributed to the soft/virtual piece of the Drell–Yan correction terms (see tables 2 and 3). However, in the $\overline{\text{MS}}$ scheme (also with $M = R = M_V$) this is no longer true. This can be seen in figs. 14 and 15, where we have split the contribution to $K_{q\bar{q},NS}^{(i)}$ into a soft/virtual ($K_{q\bar{q}}^{(i),S+V}$) and a hard ($K_{q\bar{q}}^{(i),H}$) part, as

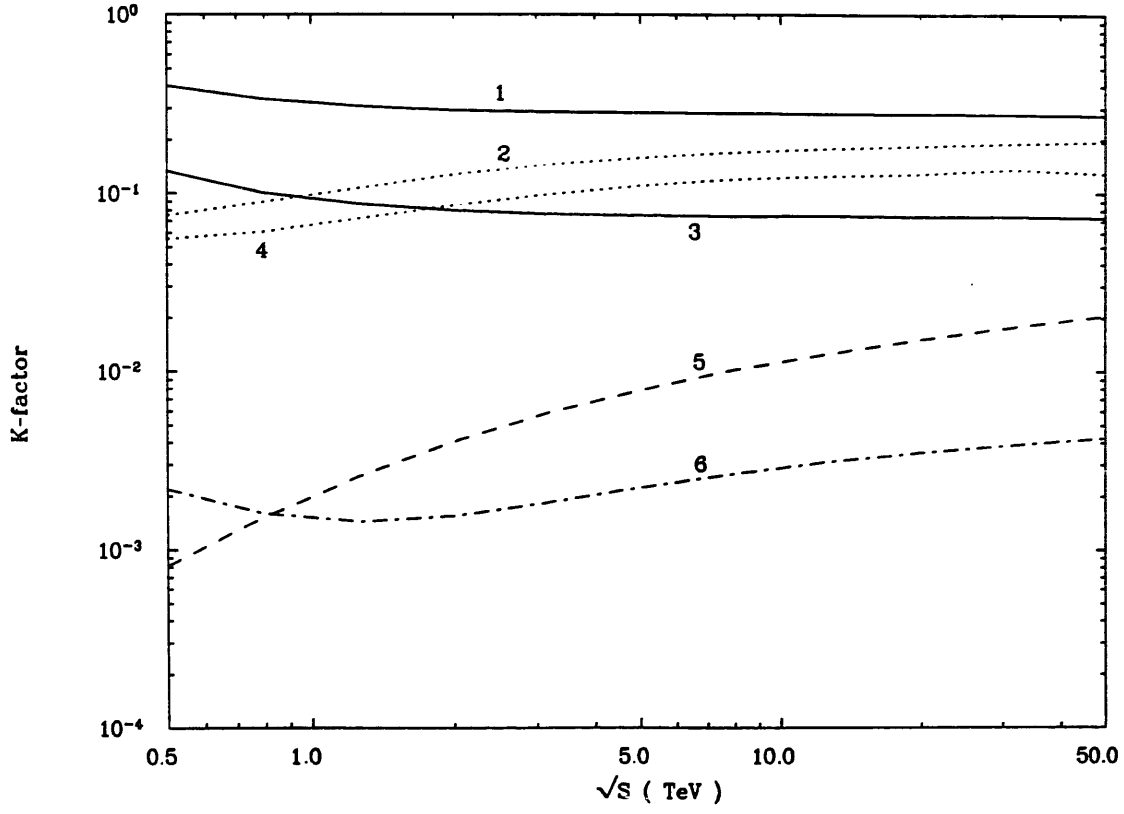

Fig. 13. The same as in fig. 12 but now for a pp collider.

described in appendix B (see below eq. (B.7). From these figures we infer that in $\overline{\text{MS}}$ the hard part is much larger than the soft/virtual piece. Moreover, in the DIS scheme the main contribution to $K_{q\bar{q}}^{(i),S+V}$ can be traced back to the $\delta(1-x)$ function. In the $\overline{\text{MS}}$ scheme, however, the $\mathscr{D}_i(x)$ dominate the S + V part. The above discussion implies that the exponentiation of the soft/virtual gluon contribution only makes sense in the DIS scheme. These observations illustrate very nicely that the answer to the question, which reaction or production mechanism is dominant, depends very much on the chosen schemes and scales. As a further illustration of this fact we have made a comparison between the $\overline{\text{MS}}$ and DIS scheme results in tables 2 and 3. For the DIS parton distribution function we have chosen the one given in table I3 of ref. [47] ($\Lambda = 194$ MeV), which is the DIS scheme counterpart of MTB. Notice that the Born cross section for $\overline{\text{MS}}$ is always slightly larger than the one obtained in the DIS scheme. Although the $O(\alpha_s)$ contributions to the soft/virtual and hard gluon parts depend heavily on the chosen scheme, the total $q\bar{q}$ result is hardly affected by this choice. For the $O(\alpha_s)$ qg subprocess this dependence is stronger and we find that the $\overline{\text{MS}}$ result is always more negative than the one obtained for DIS. Contrary to the Born cross section we find that the $O(\alpha_s)$ corrected cross section in DIS is slightly larger than in MS.

TABLE 2
Comparison of $\overline{\text{MS}}$ and DIS scheme results at Sp$\bar{\text{p}}$S and Tevatron

	$W^+ + W^-$ production (nb)			
	Sp$\bar{\text{p}}$S		Tevatron	
	MTB, $\overline{\text{MS}}$	MTB, DIS	MTB, $\overline{\text{MS}}$	MTB, DIS
	Born		Born	
$q\bar{q}$	4.93	4.90	16.0	15.7
	$O(\alpha_s)$		$O(\alpha_s)$	
$q\bar{q}$, S + V	0.61	1.79	1.16	5.66
$q\bar{q}$, H	0.93	−0.21	3.41	−0.97
$q\bar{q}$, total	1.54	1.58	4.57	4.69
qg	−0.18	−0.10	−1.57	−0.98
$\sigma^{(1)}$	1.36	1.48	3.00	3.71
σ_1	6.29	6.38	19.0	19.4
	$O(\alpha_s^2)$		$O(\alpha_s^2)$	
$q\bar{q}$, S + V	−0.05	0.59	−0.12	1.87
$q\bar{q}$, H	0.49	?	1.35	?
$q\bar{q}$, total	0.44	?	1.23	?
qg	−0.13	?	−1.06	?
gg	2.2×10^{-3}	0.6×10^{-3}	4.3×10^{-2}	2.0×10^{-2}
$qq + \bar{q}\bar{q}$	2.1×10^{-3}	1.3×10^{-3}	1.6×10^{-2}	2.5×10^{-2}
$\sigma^{(2)}$	0.31	?	0.23	?

From tables 2 and 3 we infer that the difference is about 5%. In the DIS scheme the second order contribution to the K-factor from the hard gluon part of the $q\bar{q}$ subprocess is only partially known and no $O(\alpha_s^2)$ result exists for the qg process. Therefore we have put in tables 2 and 3 a question mark in the entries corresponding to these subprocesses. At second order we find that the numerical results for those DY correction terms, which are known for both the DIS and the $\overline{\text{MS}}$ scheme, depend considerably on the chosen mass factorization procedure. Furthermore, assuming that the scheme dependence of $\sigma^{(2)}$ is comparable to that of $\sigma^{(1)}$, we find that in the DIS scheme only for the Sp$\bar{\text{p}}$S ($\sqrt{S} = 0.63$ TeV) one can approximate the second-order contribution to the cross section by the soft/virtual part of the $q\bar{q}$ subprocess. At higher energies this approximation seems to become very bad. In order to make a full comparison between both schemes the calculation of the still missing contributions in DIS (i.e. the hard gluon part of $q\bar{q}$ and qg) will be necessary.

The same discussion applies for Z-production at $p\bar{p}$ as well as at pp colliders, therefore we will not give separate figures or tables for this case.

TABLE 3
Comparison of $\overline{\text{MS}}$ and DIS scheme results at LHC and SSC

	$W^+ + W^-$ production (nb)			
	LHC		SSC	
	MTB, $\overline{\text{MS}}$	MTB, DIS	MTB, $\overline{\text{MS}}$	MTB, DIS
	Born		Born	
$q\bar{q}$	120.0	119.0	262.0	260.0
	$O(\alpha_s)$		$O(\alpha_s)$	
$q\bar{q}$, S + V	7.5	42.7	14.8	93.3
$q\bar{q}$, H	26.2	−7.8	58.3	−17.8
$q\bar{q}$, total	33.7	34.9	73.1	75.5
qg	−21.0	−15.5	−48.3	−37.8
$\sigma^{(1)}$	12.7	19.4	24.8	37.7
σ_1	132.0	138.0	287.0	298.0
	$O(\alpha_s^2)$		$O(\alpha_s^2)$	
$q\bar{q}$, S + V	−0.8	14.1	−1.8	30.8
$q\bar{q}$, H	9.9	?	21.5	?
$q\bar{q}$, total	9.1	?	19.7	?
qg	−14.9	?	−33.5	?
gg	1.5	1.1	4.4	3.6
$qq + \bar{q}\bar{q}$	0.4	1.0	1.0	2.6
$\sigma^{(2)}$	−3.9	?	−8.4	?

The size of the various contributions to the DY cross section depends very heavily on the specific set of parton distribution functions. These functions are mainly extracted from the data in deep inelastic lepton hadron scattering which have been taken for $x \geqslant 0.01$. However, vector boson production at future high-energy colliders require the knowledge of the parton densities at $x \sim M_V/\sqrt{S}$. For LHC and SSC this implies $x \sim 6 \times 10^{-3}$ and $x \sim 3 \times 10^{-3}$ respectively. A recent analysis [52] has shown that W- and Z-production at these future colliders even probes sea quarks at $x \sim 10 M_V^2/S$, which is about 5×10^{-5} for SSC. Therefore one has to extrapolate these densities to x-regions which were not accessible to the deep inelastic experiments carried out up to now. In the future this situation will probably improve, when the HERA machine is put into operation. Moreover, there is some theoretical uncertainty how to parametrize the gluon distribution function at $Q^2 = Q_0^2$. One often assumes that $xG(x, Q_0^2) \to$ constant for $x \to 0$. However, there are some theoretical reasons to believe that a more correct behaviour for small x would be $xG(x, Q_0^2) \to 1/\sqrt{x}$ [53]. Notice that such a change of the parametrization of the gluon at Q_0^2 will also strongly influence the

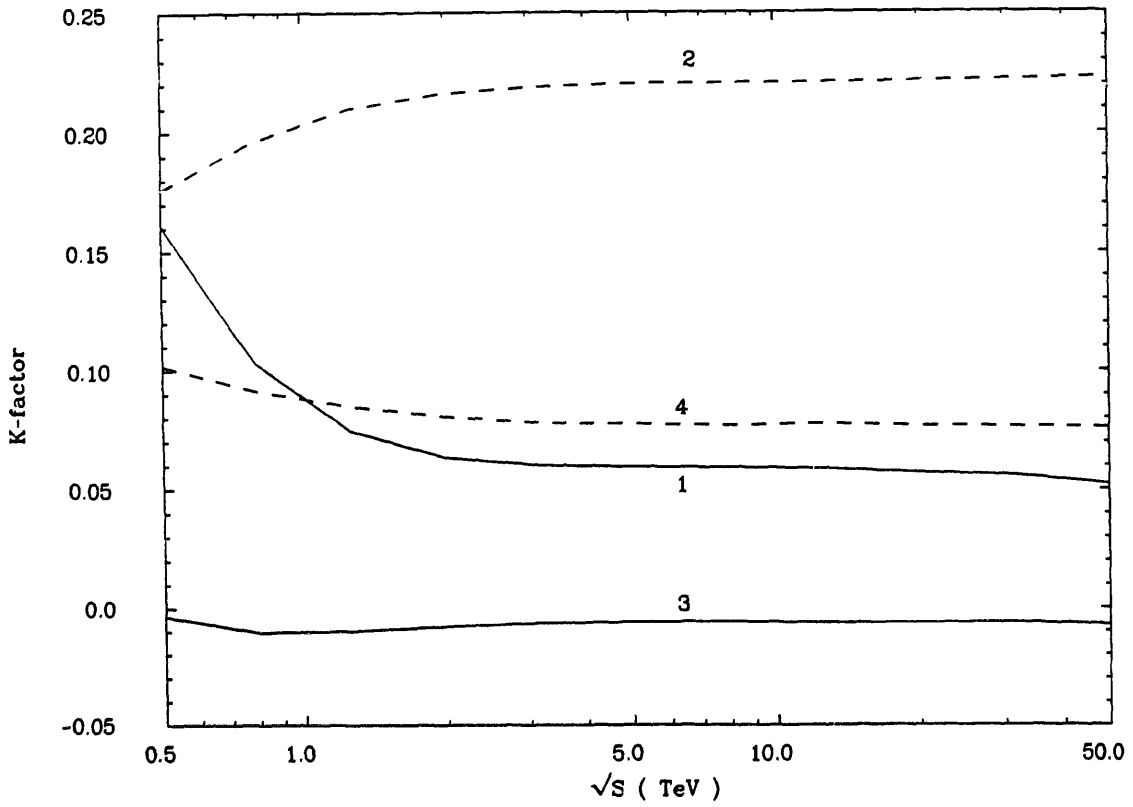

Fig. 14. The soft + virtual (S + V) and hard (H) gluon part of $K_{q\bar{q}}^{(i)}$ for $W^+ + W^-$ production at a $p\bar{p}$ collider (see eq. (3.5)). (1) $K_{q\bar{q}}^{(1),S+V}$; (2) $K_{q\bar{q}}^{(1),H}$; (3) $K_{q\bar{q}}^{(2),S+V}$; (4) $K_{q\bar{q}}^{(2),H}$.

small-x behaviour of the sea quarks at higher Q^2, because the sea quarks are coupled to the gluons through the Altarelli–Parisi evolution equations. This implies that at high energies considerable differences in the size of the DY cross section can be expected, even at the Born level, if one changes the $x \to 0$ behaviour of the gluon at Q_0^2. To incorporate this kind of uncertainties in our predictions for the W- and Z-production rates we have taken a wide range of different parametrizations. The HMRSE and HMRSB parametrizations [45] correspond with a $xG(x, Q_0^2) \to$ constant behaviour for $x \to 0$. The HMRSE_+ and HMRSE_- behave like $\sqrt{x}$ and $1/\sqrt{x}$ for $x \to 0$ and are referred to as the valence-like and singular gluon distribution functions in ref. [52]. For the parametrization of the gluon densities in the case of MTE and MTB one even has included a logarithmic dependence on x, viz. $xG(x, Q_0^2) \to x^{\alpha}(-\ln x)^{\beta}$ for $x \to 0$, with α and β some negative exponents (see tables I2 and I4 of ref. [47]).

The total cross sections for W-production are displayed in table 4 for $\sqrt{S} = 0.63$ TeV ($Sp\bar{p}S$), $\sqrt{S} = 1.8$ TeV (Tevatron), $\sqrt{S} = 16$ TeV (LHC) and $\sqrt{S} = 40$ TeV (SSC). From this table we infer that the $O(\alpha_s^2)$ correction is much smaller than the $O(\alpha_s)$ one. Moreover the cross sections obtained with the different parton densi-

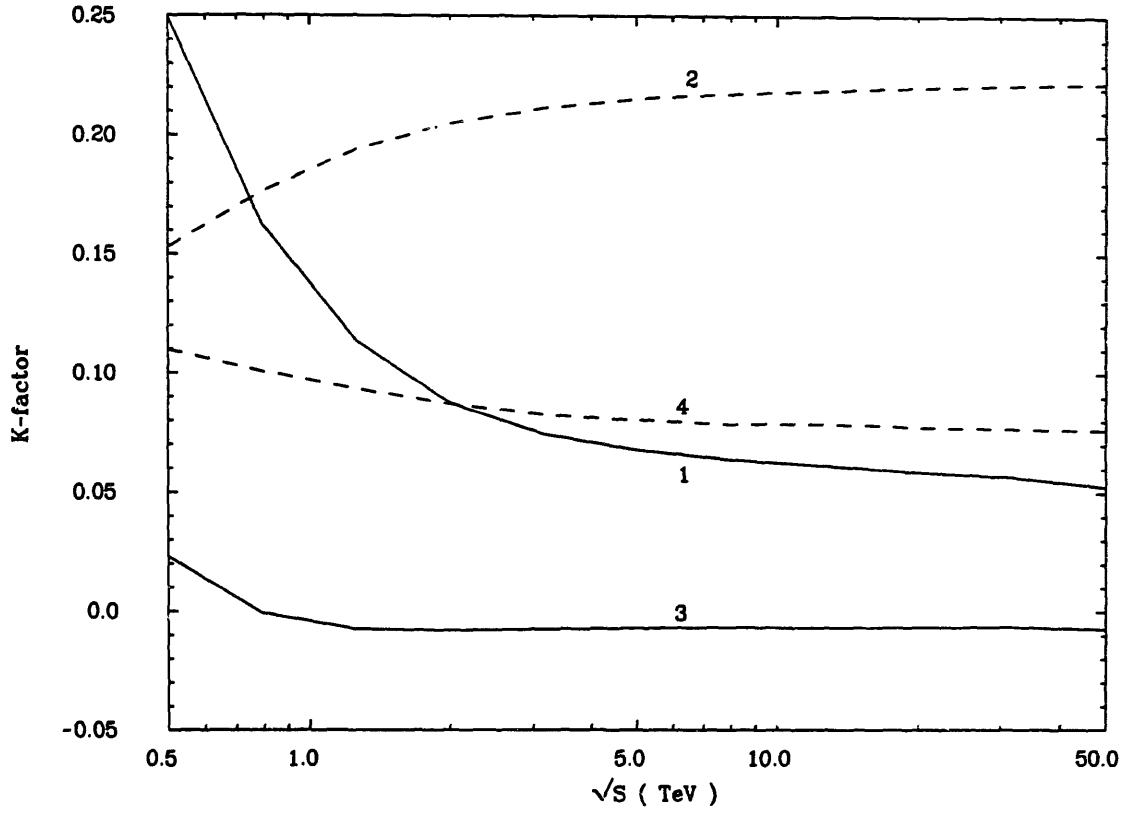

Fig. 15. The same as in fig. 14 but now for a pp collider.

ties differ from each other by at least the same order of magnitude as the second-order correction. Although at Sp$\bar{p}$S and Tevatron the results for the various parton distributions do not differ very much, these discrepancies do not allow to discern clearly the $O(\alpha_s^2)$ corrections. This situation becomes worse at LHC and SSC, where it even might become difficult to identify the first-order corrections. For these colliders this is mainly due to the uncertainties present in the small-x behaviour of the parton distribution functions. Unless these uncertainties are reduced, it will not be possible to learn much about QCD corrections at the future colliders by studying W- and Z-production. In table 5 we have listed our results for Z-production. Roughly the same comments apply here as for W-production. However, note the slightly improved possibility to see $O(\alpha_s^2)$ corrections in the case of Z-production at $\sqrt{S} = 0.63$ TeV. The reason for this improvement can be attributed to the dominant contribution of the $u_V\bar{u}_V$ channel in Z-production, whereas the W cross section is mainly determined by the $u_V\bar{d}_V$ and $\bar{u}_V d_V$ subprocesses. It seems that the mutual agreement of the various parton densities for the u_V-quark is better than for the d_V-quark. Summarizing the above we can state that the uncertainty in the cross sections can be estimated to be about 10% for Sp$\bar{p}$S and Tevatron and 150% and 250% for LHC and SSC, respectively.

TABLE 4
The total cross section for W-production at SpS̄, Tevatron, LHC and SSC

	$W^+ + W^-$ production (nb)					
$\alpha_s(M_W)$	HMRSE$_+$ 0.107	HMRSE 0.107	HMRSE$_-$ 0.107	HMRSB 0.117	MTE 0.114	MTB 0.118
			SpS̄ ($\sqrt{S}$ = 0.63 TeV)			
Born	5.51	5.31	5.20	5.03	4.84	4.93
$O(\alpha_s)$	6.81	6.60	6.48	6.41	6.13	6.29
$O(\alpha_s^2)$	7.06	6.86	6.74	6.72	6.41	6.61
			Tevatron ($\sqrt{S}$ = 1.8 TeV)			
Born	14.7	15.1	14.7	15.8	15.5	16.0
$O(\alpha_s)$	17.0	17.6	17.1	18.7	18.3	19.0
$O(\alpha_s^2)$	17.1	17.7	17.3	18.9	18.5	19.2
			LHC ($\sqrt{S}$ = 16.0 TeV)			
Born	49.3	75.8	112.0	104.0	114.0	120.0
$O(\alpha_s)$	53.7	81.9	122.0	114.0	128.0	132.0
$O(\alpha_s^2)$	52.7	79.5	118.0	110.0	126.0	129.0
			SSC ($\sqrt{S}$ = 40.0 TeV)			
Born	85.1	151.0	303.0	225.0	257.0	262.0
$O(\alpha_s)$	91.7	161.0	324.0	244.0	288.0	287.0
$O(\alpha_s^2)$	90.6	157.0	313.0	236.0	284.0	278.0

To get a better impression of the size of the corrections we give in tables 6 and 7 the first- and second-order K-factors for W- and Z-production. Notice that for the K-factor a large part of the uncertainty due to the various parametrizations of the parton densities drops out. In this case the main reason for the discrepancies can be traced back to the different values for α_s. Only at very high energies the K-factors start depending on the specific choice of the parton distribution function, mainly through the variation of the size of the qg contribution. Therefore while studying radiative corrections it is better to look at the K-factor than at the cross section. From these tables one can also observe that the K-factors are roughly the same for W- and Z-production. This implies that the ratio

$$R = \frac{\sigma_W}{\sigma_Z} \frac{\mathrm{BR}(W \to \ell \nu_\ell)}{\mathrm{BR}(Z \to \ell^+ \ell^-)} \tag{3.11}$$

is hardly affected by QCD corrections.

TABLE 5
The total cross section for Z-production at SpS̄, Tevatron, LHC and SSC

Z-production (nb)						
$\alpha_s(M_Z)$	HMRSE$_+$ 0.105	HMRSE 0.105	HMRSE$_-$ 0.105	MHRSB 0.115	MTE 0.112	MTB 0.115
SpS̄ ($\sqrt{S}$ = 0.63 TeV)						
Born	1.66	1.61	1.58	1.54	1.60	1.55
$O(\alpha_s)$	2.06	2.00	1.97	1.96	2.02	1.98
$O(\alpha_s^2)$	2.14	2.08	2.06	2.06	2.12	2.09
Tevatron ($\sqrt{S}$ = 1.8 TeV)						
Born	4.62	4.66	4.52	4.79	4.74	4.86
$O(\alpha_s)$	5.38	5.45	5.30	5.69	5.64	5.81
$O(\alpha_s^2)$	5.44	5.51	5.37	5.78	5.74	5.92
LHC ($\sqrt{S}$ = 16.0 TeV)						
Born	15.8	23.5	33.1	31.7	34.6	36.2
$O(\alpha_s)$	17.2	25.4	35.8	34.9	38.9	40.1
$O(\alpha_s^2)$	16.9	24.8	34.9	33.9	38.5	39.1
SSC ($\sqrt{S}$ = 40.0 TeV)						
Born	27.5	47.4	89.5	69.8	79.2	80.7
$O(\alpha_s)$	29.6	50.6	95.9	75.7	88.7	88.2
$O(\alpha_s^2)$	29.3	49.4	93.1	73.6	87.9	86.0

For $\sqrt{S} = 0.63$ TeV and 1.8 TeV (CERN and FNAL) we compare our predictions with the measurements by the UA1 [54], UA2 [55] and CDF [56,57] collaborations (see tables 8–10). In particular we are interested in the decay channels $W \to \ell \nu_\ell$ and $Z \to \ell^+ \ell^-$ for $\ell = e$ or $\ell = \mu$. In this case we have to multiply the total cross sections in tables 4 and 5 by the branching ratios $BR(W \to \ell \nu_\ell)$ and $BR(Z \to \ell^+ \ell^-)$ respectively. Starting with the CERN collider we find that the central values of the UA1 results for W- and Z-production [54], which were obtained in the muon channel only, are well below our second-order predictions. However, due to the large statistical and systematic errors all our approximations are compatible with their data. In case of UA2 [55] we find that for Z-production the second-order cross sections are in very good agreement with the experimental values, although the first-order corrected ones can accommodate the data rather well, too. However, for W-production the theoretical predictions at $O(\alpha_s^2)$ lie systematically above the UA2 data but this discrepancy is not dramatic.

TABLE 6
K-factors for W-production at Sp$\bar{p}$S, Tevatron, LHC and SSC

	$W^+ + W^-$ production					
$\alpha_s(M_W)$	HMRSE$_+$ 0.107	HMRSE 0.107	HMRSE$_-$ 0.107	HMRSB 0.117	MTE 0.114	MTB 0.118
	Sp$\bar{p}$S ($\sqrt{S}$ = 0.63 TeV)					
K_1	1.24	1.24	1.25	1.27	1.27	1.28
K_2	1.28	1.29	1.30	1.34	1.32	1.34
	Tevatron ($\sqrt{S}$ = 1.8 TeV)					
K_1	1.16	1.16	1.16	1.18	1.18	1.19
K_2	1.17	1.17	1.17	1.19	1.20	1.20
	LHC ($\sqrt{S}$ = 16.0 TeV)					
K_1	1.09	1.08	1.08	1.10	1.13	1.11
K_2	1.07	1.05	1.05	1.06	1.11	1.07
	SSC ($\sqrt{S}$ = 40.0 TeV)					
K_1	1.08	1.07	1.07	1.08	1.12	1.09
K_2	1.07	1.04	1.03	1.05	1.11	1.06

For the Tevatron collider [56] the Born approximation as well as the higher-order results agree with the data due to the large systematic errors in the CDF experiment. For completeness we give in table 10 the values for the ratio R, defined in eq. (3.11). As mentioned above, the QCD corrections do not change the value of R very much. The theoretical values of R for Sp$\bar{p}$S tend to be larger than the result obtained by UA2 [55]. This was to be expected, because our results for $\sigma_W \cdot$ BR were also larger than the cross section found by the UA2 collaboration. The agreement is better with the UA1 value of R [54], but in this case the experimental errors in R are rather large. For Tevatron we find good agreement with the measurement by CDF [57]. In this case one can observe that by studying the ratio R instead of the separate W- and Z-production rates, as advocated in the literature, the uncertainty due to the choice of the parton distribution functions is reduced. However, this does not apply to the results given for CERN. In this case the spread in the values obtained for the ratio R and the cross sections are of the same order of magnitude.

Summarizing the discussion above we conclude that the current experiments carried out at the Sp$\bar{p}$S and Tevatron do not allow us to distinguish between $O(\alpha_s)$

TABLE 7
K-factors for Z-production at SpS̄, Tevatron, LHC and SSC

Z-production						
$\alpha_s(M_Z)$	HMRSE$_+$ 0.105	HMRSE 0.105	HMRSE$_-$ 0.105	HMRSB 0.115	MTE 0.112	MTB 0.115
SpS̄ ($\sqrt{S}$ = 0.63 TeV)						
K_1	1.24	1.25	1.25	1.28	1.27	1.28
K_2	1.29	1.30	1.30	1.34	1.32	1.35
Tevatron ($\sqrt{S}$ = 1.8 TeV)						
K_1	1.17	1.17	1.17	1.19	1.19	1.20
K_2	1.18	1.18	1.19	1.21	1.21	1.22
LHC ($\sqrt{S}$ = 16.0 TeV)						
K_1	1.09	1.08	1.08	1.10	1.13	1.11
K_2	1.07	1.05	1.05	1.07	1.11	1.08
SSC ($\sqrt{S}$ = 40.0 TeV)						
K_1	1.08	1.07	1.07	1.08	1.12	1.09
K_2	1.07	1.04	1.04	1.05	1.11	1.07

and $O(\alpha_s^2)$ corrected cross sections. This is due to the large systematic errors in the existing data, the uncertainty in the parton distribution functions and the fact that the second-order correction is smaller than has originally been expected from the result obtained by the $O(\alpha_s)$ calculation. Unless the higher-order corrections beyond the $O(\alpha_s^2)$ turn out to be very large, the convergence of the perturbation series does not seem to be a problem for W- and Z-production at the current and future hadron colliders. Therefore we are now able to give a firm prediction for the total cross section; the main limitations to our predictions are set by the uncertainty in the parton distribution functions.

Finally we want to investigate the dependence of the DY cross section on the chosen mass factorization scale M. In a previous paper [25] we studied the variations of the cross sections when the mass factorization scale M is varied independently of the renormalization scale R. This we will not do in this paper as there is no distinction between these two scales in the current parton distribution functions. Moreover, the dependence of the cross section on M is much larger than on R, because the Born approximation does not depend on the coupling

TABLE 8
$\sigma_W \cdot BR$ and $\sigma_Z \cdot BR$ for Sp$\bar{p}$S [55]. We have used $BR(W \to \ell \nu_\ell) = 0.109$ and $BR(Z \to \ell^+\ell^-) = 3.35 \times 10^{-2}$. $\sqrt{S} = 0.63$ TeV

	HMRSE$_+$	HMRSE	HMRSE$_-$	HMRSB	MTE	MTB
			$\sigma_W BR(W \to \ell \nu_\ell)$ (pb)			
UA1			$609 \pm 41 \pm 94$			
UA2			$660 \pm 15 \pm 37$			
$\alpha_s(M_W)$	0.107	0.107	0.107	0.117	0.114	0.118
Born	600.0	579.0	567.0	549.0	528.0	538.0
$O(\alpha_s)$	743.0	720.0	706.0	699.0	668.0	686.0
$O(\alpha_s^2)$	770.0	748.0	735.0	733.0	699.0	720.0
			$\sigma_Z BR(Z \to \ell^+\ell^-)$ (pb)			
UA1			$58.6 \pm 7.8 \pm 8.4$			
UA2			$70.4 \pm 5.5 \pm 4.0$			
$\alpha_s(M_Z)$	0.105	0.105	0.105	0.115	0.112	0.115
Born	55.4	53.8	52.9	51.4	53.4	51.8
$O(\alpha_s)$	68.9	67.0	66.1	65.8	67.8	66.4
$O(\alpha_s^2)$	71.6	69.8	68.9	69.2	71.0	69.9

constant α_s. This is contrary to what one observes in pure hadronic cross sections like heavy flavour production [36, 48, 49] or di-jet production [51] where the Born cross sections do depend on α_s and therefore are much more sensitive to the choice of R. In principle, physical (experimentally observable) quantities like the hadronic structure function $W_V(\tau, Q^2)$ (eq. (2.3)) should be scale independent. However, the theoretical result for $W_V(\tau, Q^2)$ does depend on the chosen scale. This can be attributed to the fact that the logarithmic terms of the type $\ln(Q^2/M^2)$ (see appendix B) in the Wilson coefficient $\Delta_{ij}(x, Q^2, M^2)$ are only calculated up to finite orders of α_s, whereas they are resummed in all orders for the parton densities using renormalization group methods. This introduces the problem of choosing an appropriate scale. There are many discussions in the literature concerning the choice of the right scale. Some groups prefer PMS [3] whereas other physicists advocate FAC [4]. Another possibility is to vary the scale between some canonical values in order to give an estimate for the theoretical error. The best solution to the problem would be to show that the resulting expressions exhibit a very small variation under a wide range of scale choices. This might be

TABLE 9
$\sigma_W \cdot BR$ and $\sigma_Z \cdot BR$ for Tevatron [56]. We have used $BR(W \to e\nu_e) = 0.109$ and $BR(Z \to e^+e^-) = 3.35 \times 10^{-2}$. $\sqrt{S} = 1.8$ TeV

	HMRSE$_+$	HMRSE	HMRSE$_-$	HMRSB	MTE	MTB
			$\sigma_W BR(W \to e\nu_e)$ (nb)			
CDF			$2.06 \pm 0.04 \pm 0.34$			
$\alpha_s(M_W)$	0.107	0.107	0.107	0.117	0.114	0.118
Born	1.60	1.65	1.61	1.73	1.69	1.74
$O(\alpha_s)$	1.86	1.91	1.87	2.04	1.99	2.07
$O(\alpha_s^2)$	1.87	1.93	1.88	2.06	2.02	2.10
			$\sigma_Z BR(Z \to e^+e^-)$ (nb)			
CDF			$0.197 \pm 0.012 \pm 0.032$			
$\alpha_s(M_Z)$	0.105	0.105	0.105	0.115	0.112	0.115
Born	0.155	0.156	0.152	0.160	0.159	0.163
$O(\alpha_s)$	0.180	0.182	0.178	0.191	0.189	0.195
$O(\alpha_s^2)$	0.182	0.185	0.180	0.194	0.192	0.198

TABLE 10
The ratio R (see eq. (3.11)) for $Sp\bar{p}S$ [55] and Tevatron [57]

	HMRSE$_+$	HMRSE	The ratio R HMRSE$_-$	HMRSB	MTE	MTB
			$\sqrt{S} = 0.63$ TeV			
UA1			$10.4^{+1.8}_{-1.5} \pm 0.8$			
UA2			$9.38^{+0.82}_{-0.72} \pm 0.25$			
Born	10.8	10.8	10.7	10.7	9.9	10.4
$O(\alpha_s)$	10.8	10.7	10.7	10.6	9.9	10.3
$O(\alpha_s^2)$	10.8	10.7	10.7	10.6	9.9	10.3
			$\sqrt{S} = 1.8$ TeV			
CDF			$10.2 \pm 0.8 \pm 0.4$			
Born	10.4	10.6	10.6	10.8	10.6	10.7
$O(\alpha_s)$	10.3	10.5	10.5	10.7	10.6	10.6
$O(\alpha_s^2)$	10.3	10.4	10.5	10.6	10.5	10.6

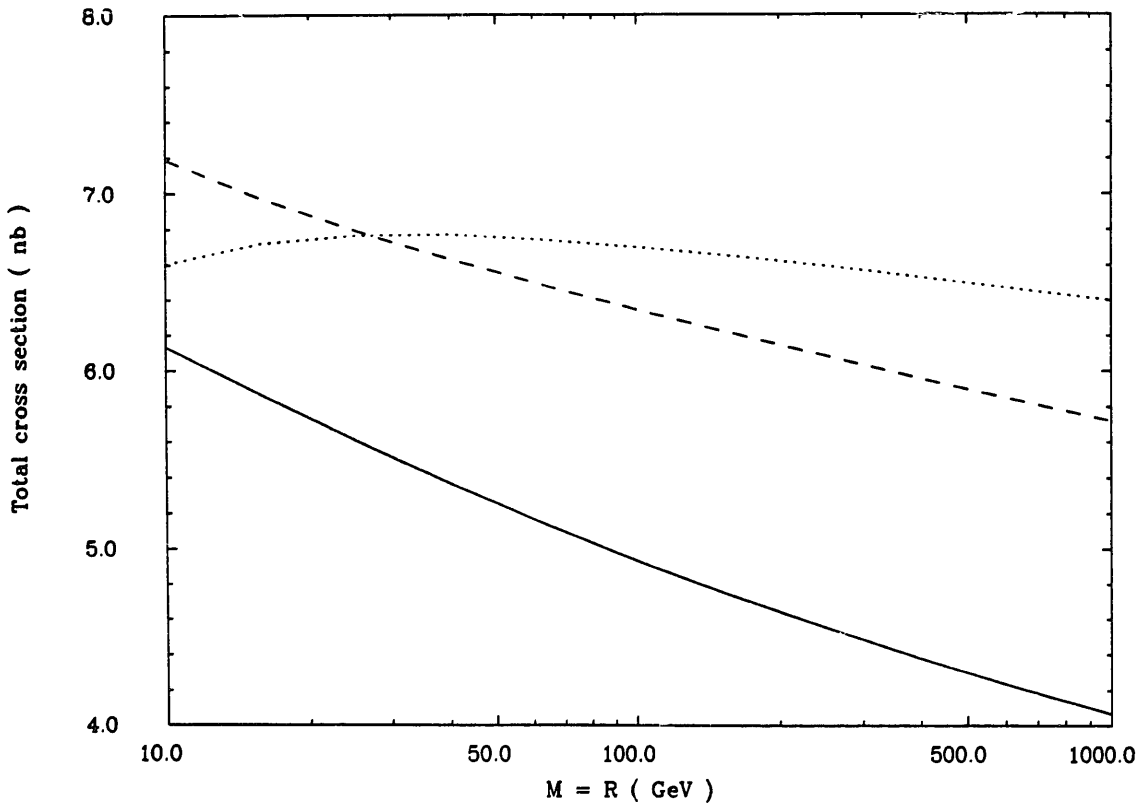

Fig. 16. Mass factorization scale (M) dependence of $\sigma_{W^+ + W^-}$ for Sp$\bar{p}$S, $\sqrt{S} = 0.63$ TeV. Solid line: Born; dashed line: $O(\alpha_s)$; dotted line: $O(\alpha_s^2)$.

achieved provided the QCD corrections can be computed beyond the leading order in α_s. The Drell–Yan and deep inelastic lepton–hadron cross sections are good candidates for satisfying this condition, since their Born cross sections are independent of α_s and the radiative corrections can be computed up to $O(\alpha_s^2)$. Using the HMRSB structure functions we have plotted the DY cross section for W^+ plus W^- production in the range 10 GeV $\leqslant M \leqslant$ 1000 GeV. Starting with the Sp$\bar{p}$S ($\sqrt{S} = 0.63$ TeV, see fig. 16) we observe a considerable improvement in the scale independence of the cross section σ_W when it is computed in higher order in α_s. Note the maximum at $M = 40$ GeV in σ_2 (PMS point) which is not present in the lower-order results σ_0 and σ_1. As has been mentioned before, the difference between σ_1 and σ_2 depends on the chosen scale although it never becomes very large (< 0.6 nb). Finally, the difference $(\sigma_2)_{max} - (\sigma_2)_{min}$ in the range $10 \leqslant M \leqslant$ 1000 GeV is about 0.4 nb which can be considered as a theoretical uncertainty of our calculation due to the uncertainty in the scale. The same features are also observed for W-production at the Tevatron ($\sqrt{S} = 1.8$ TeV, see fig. 17) although here the difference between the σ_1 and σ_2 is extremely small. The PMS point is at

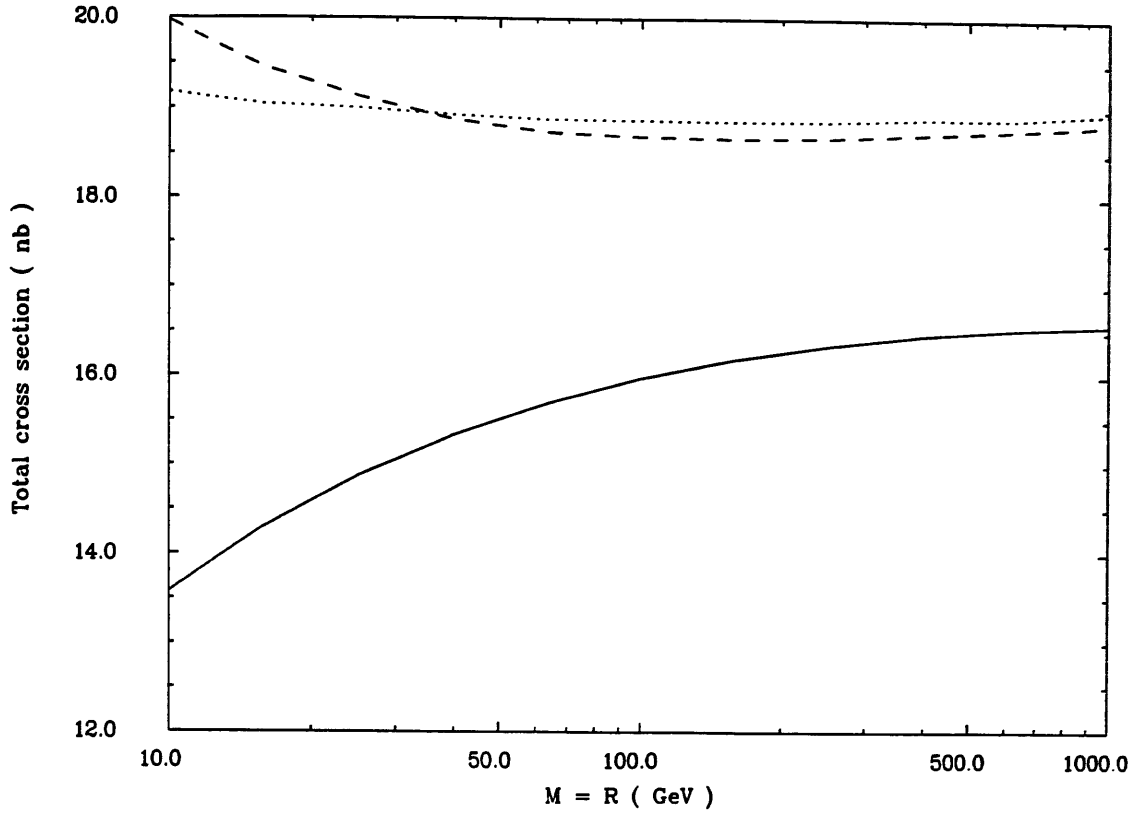

Fig. 17. Mass factorization scale (M) dependence of $\sigma_{W^+ + W^-}$ for Tevatron, $\sqrt{S} = 1.8$ TeV. Solid line: Born; dashed line: $O(\alpha_s)$; dotted line: $O(\alpha_s^2)$.

$M = 200$ GeV, where σ_2 exhibits a minimum and $(\sigma_2)_{max} - (\sigma_2)_{min} \sim 0.3$ nb. Notice that at both energies $\sigma_2 - \sigma_1$ becomes zero at a certain M whereas $\sigma_i - \sigma_0 \neq 0$ $(i = 1, 2)$ over the whole range of scales.

When we study the DY process at higher energies like $\sqrt{S} = 16$ TeV (LHC, fig. 18) or $\sqrt{S} = 40$ TeV (SSC, fig. 19), we find that some of the properties of the higher-order α_s corrected cross sections change when compared to those obtained for $\sqrt{S} < 2$ TeV. First we observe that the scale dependence is much stronger at these energies. Secondly the extremum in σ_2 (PMS point) has disappeared but now there is a value for M where either σ_1 or σ_2 becomes equal to σ_0 (FAC point). Notice that $\sigma_2 = \sigma_0$ near $M = 100$ GeV for LHC as well as SSC energies. The difference between the maximum and minimum value for σ_2 equals 15 nb at $\sqrt{S} = 16$ TeV and 35 nb at $\sqrt{S} = 40$ TeV. The same features discussed for W-production also show up for Z-production, therefore we will not present any figures in this case. In tables 11 and 12 we give the variation of the cross section for the various parton distribution functions when the mass factorization scale is chosen in the range $10 \text{ GeV} \leqslant M \leqslant 1000$ GeV. This variation is expressed by the

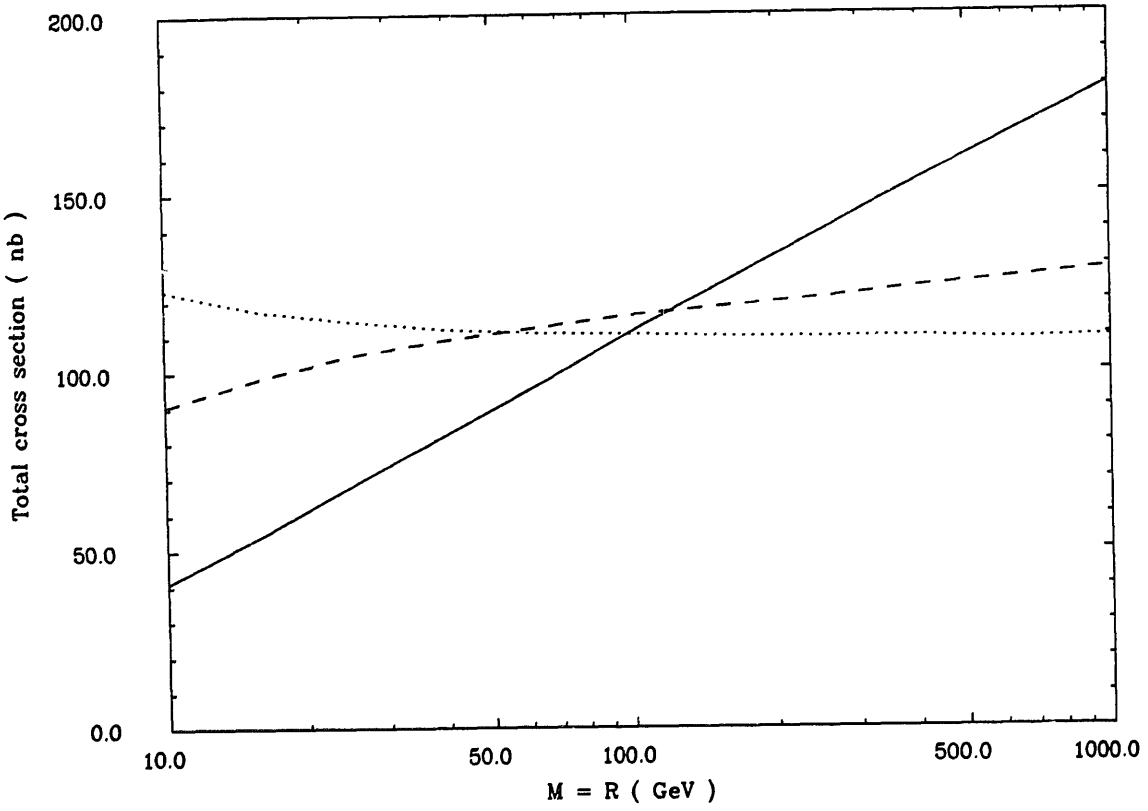

Fig. 18. Mass factorization scale (M) dependence of $\sigma_{W^+ + W^-}$ for LHC, $\sqrt{S} = 16$ TeV. Solid line: Born; dashed line: $O(\alpha_s)$; dotted line: $O(\alpha_s^2)$.

quantity S_i defined by

$$S_i = \frac{(\sigma_i)_{\max} - (\sigma_i)_{\min}}{(\sigma_i)_{\text{av}}}, \tag{3.12}$$

where $(\sigma_i)_{\text{av}}$ is the average value of σ_i. In these tables one can observe that the scale dependence is roughly the same for all parton distribution functions, except for MTE. In the case of MTE we find at LHC and SSC that the inclusion of the higher-order corrections does not improve the scale independence as much as in the case of the other parton densities. Also notice the rather large value of S_2 at Tevatron for MTE. From the values of S_2 one can conclude that the $O(\alpha_s^2)$ corrected DY cross section depends much less on the scale than on the chosen set of parton distribution functions. Therefore an important outcome of the $O(\alpha_s^2)$ computation is that the dependence of the production rates on the scale choice is considerably reduced. The main theoretical uncertainty can now be attributed to the variations in the cross sections when different parametrizations of the parton distribution functions are used. This is especially clear for the future hadron colliders, the LHC and the SSC. At these colliders the parton distribution functions are probed at very small x-values, for which our knowledge of these

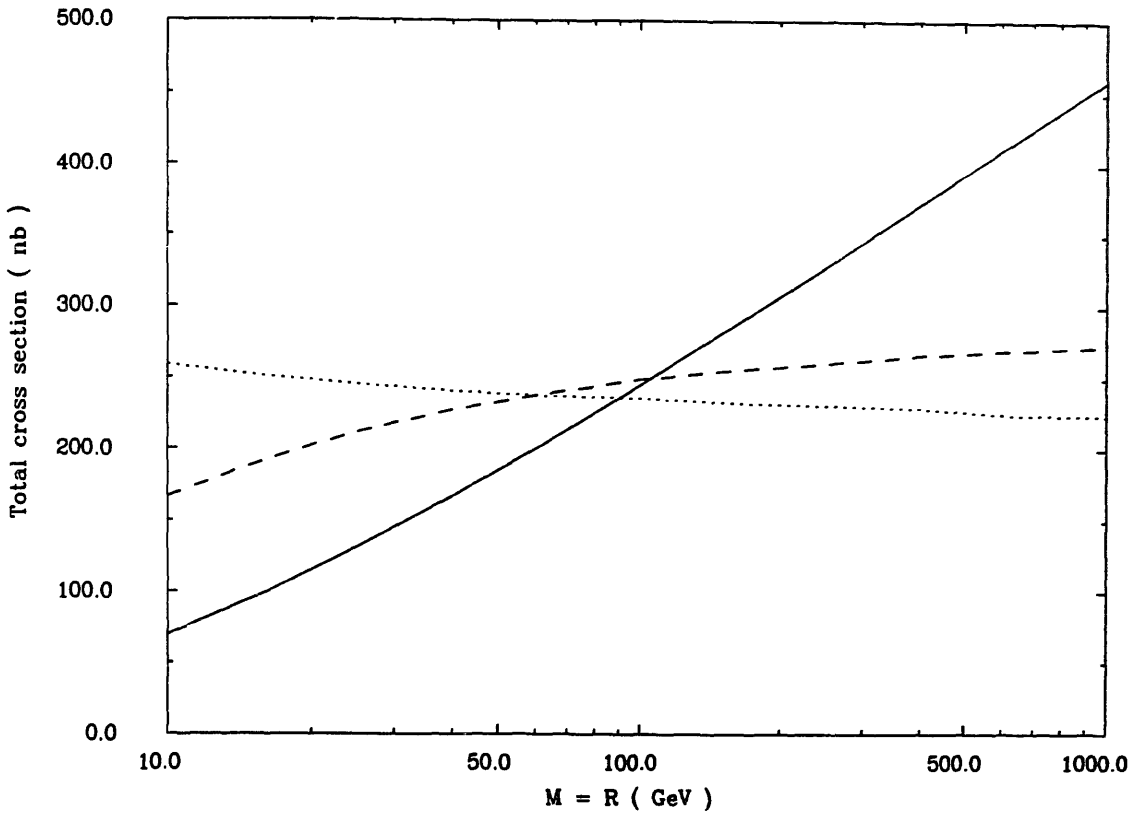

Fig. 19. Mass factorization scale (M) dependence of $\sigma_{W^+ + W^-}$ for SSC, $\sqrt{S} = 40$ TeV. Solid line: Born; dashed line: $O(\alpha_s)$; dotted line: $O(\alpha_s^2)$.

distribution functions is not very good yet. In particular we want to mention once more the sizable, negative contribution of the qg subprocess to both the first- and second-order corrections. At very high energies this subprocess is particularly sensitive to the behaviour of the input gluon distribution function at small x-values.

Summarizing the content of this paper we have presented the full $O(\alpha_s^2)$ correction to the K-factor which is calculated in the $\overline{\text{MS}}$ scheme. To this end the partonic structure functions $\hat{W}_{ij}$ (see eqs. (2.41)–(2.45)) had to be calculated to second order in α_s. One then encounters new collinear divergences which have not appeared in any calculation performed until now. To remove these singularities by mass factorization one, for the first time, needs the $O(\alpha_s^2)$ corrected splitting functions calculated in refs. [37–41]. The calculation reveals that the dominant parton subprocesses are given by the $q\bar{q}$ (non-singlet) and qg reactions. This holds for the $O(\alpha_s)$ as well as for the $O(\alpha_s^2)$ correction provided the results are presented for $M = R = M_V$. Further the qg contribution to $K^{(1)}$ as well as to $K^{(2)}$ (the $O(\alpha_s)$ and $O(\alpha_s^2)$ corrections to the DY K-factor, respectively) is negative. For $K^{(2)}$ it even overwhelms the positive contribution due to the $q\bar{q}$ subprocess when $\sqrt{S} > 3$ TeV. For this reason the $O(\alpha_s^2)$ part of the K-factor is much smaller than

TABLE 11
Scale dependence of the cross section for W-production at SpS̄, Tevatron, LHC and SSC (see eq. (3.12))

	$W^+ + W^-$ production					
	$HMRSE_+$	HMRSE	$HMRSE_-$	HMRSB	MTE	MTB
			SpS̄ ($\sqrt{S}$ = 0.63 TeV)			
S_0	0.31	0.34	0.35	0.41	0.38	0.42
S_1	0.17	0.18	0.18	0.23	0.20	0.23
S_2	0.03	0.04	0.04	0.06	0.03	0.06
			Tevatron ($\sqrt{S}$ = 1.8 TeV)			
S_0	0.26	0.22	0.19	0.19	0.27	0.17
S_1	0.04	0.05	0.05	0.07	0.07	0.06
S_2	0.03	0.02	0.02	0.02	0.12	0.01
			LHC ($\sqrt{S}$ = 16.0 TeV)			
S_0	1.44	1.30	1.08	1.26	1.27	1.12
S_1	0.38	0.32	0.24	0.34	0.60	0.27
S_2	0.16	0.14	0.08	0.13	0.33	0.15
			SSC ($\sqrt{S}$ = 40.0 TeV)			
S_0	1.77	1.60	1.24	1.54	1.53	1.39
S_1	0.50	0.42	0.28	0.45	0.78	0.38
S_2	0.17	0.16	0.10	0.15	0.43	0.19

the $O(\alpha_s)$ contribution, contrary to what we have observed in a previous paper [25] where the K-factor has been calculated in the DIS scheme. However, in the latter scheme the $O(\alpha_s^2)$ corrections due to the qg subprocess and the hard gluon part of the $q\bar{q}$ reaction have not been included yet. Notice that all these comparisons only make sense when the renormalization scale R and the factorization scale M are specified. The factorization scale dependence of the DY cross section has been investigated and we found a considerable improvement by including the $O(\alpha_s^2)$ correction. Finally we have seen that the DY cross section heavily depends on the chosen parametrization for the parton distribution functions. A large part of this dependence can be attributed to our ignorance about their small-x behaviour. The main theoretical uncertainties in our predictions are just due to this phenomenon. To complete the study of the DY process it is still necessary to compute the correction term in the DIS scheme in view of the parton densities given in that scheme. Moreover, one also has to investigate the effect of heavy flavour production (massive quarks in the final state). Both calculations will be presented in the near future.

TABLE 12
Scale dependence of the cross section for Z-production at SpS̄, Tevatron, LHC and SSC (see eq. (3.12))

	Z-production					
	HMRSE$_+$	HMRSE	HMRSE$_-$	HMRSB	MTE	MTB
			SpS̄ ($\sqrt{S}$ = 0.63 TeV)			
S_0	0.36	0.38	0.38	0.46	0.42	0.48
S_1	0.18	0.19	0.19	0.24	0.21	0.25
S_2	0.04	0.04	0.04	0.06	0.04	0.07
			Tevatron ($\sqrt{S}$ = 1.8 TeV)			
S_0	0.17	0.14	0.11	0.11	0.18	0.09
S_1	0.06	0.07	0.07	0.09	0.04	0.11
S_2	0.03	0.01	0.01	0.01	0.10	0.02
			LHC ($\sqrt{S}$ = 16.0 TeV)			
S_0	1.37	1.25	1.04	1.21	1.22	1.06
S_1	0.36	0.30	0.22	0.31	0.56	0.23
S_2	0.13	0.12	0.09	0.13	0.31	0.15
			SSC ($\sqrt{S}$ = 40.0 TeV)			
S_0	1.72	1.56	1.22	1.50	1.49	1.35
S_1	0.49	0.42	0.28	0.44	0.75	0.36
S_2	0.11	0.12	0.09	0.13	0.41	0.17

We thank W.J. Stirling for providing us with the programs to generate the HMRS parton distribution functions.

Appendix A

BASIC FORMULAE FOR THE DRELL–YAN PROCESS

In this appendix we will present the basic notations and some formulae needed for the calculation of the DY cross section. The pointlike cross sections $\sigma_V(Q^2, M_V^2)$ defined in eq. (2.2) are equal to

$$\sigma_\gamma(Q^2) = \frac{4\pi\alpha^2}{3Q^4}\frac{1}{N}, \tag{A.1}$$

$$\sigma_Z(Q^2, M_Z^2) = \frac{\pi\alpha}{4M_Z \sin^2\theta_W \cos^2\theta_W}\frac{1}{N}\cdot\frac{\Gamma_{Z\to \ell\bar{\ell}}}{(Q^2 - M_Z^2)^2 + M_Z^2\Gamma_Z^2}, \tag{A.2}$$

$$\sigma_W(Q^2, M_W^2) = \frac{\pi\alpha}{2M_W \sin^2\theta_W}\frac{1}{N}\frac{\Gamma_{W\to \ell\bar{\nu}_\ell}}{(Q^2 - M_W^2)^2 + M_W^2\Gamma_W^2}. \tag{A.3}$$

For completeness we also give the formula for the γ-Z interference

$$\sigma_{\gamma Z} = \frac{\pi\alpha^2}{6} \frac{1-4\sin^2\theta_W}{\sin^2\theta_W \cos^2\theta_W} \frac{1}{N} \frac{1}{Q^2} \frac{(Q^2 - M_Z^2)}{(Q^2 - M_Z^2)^2 + M_Z^2\Gamma_Z^2}. \tag{A.4}$$

In these formulae Γ_Z and Γ_W denote the total width of the Z- and W-boson respectively (sum over all decay channels) and $N = 3$. The partial widths due to the leptonic decay of the Z and W are given by

$$\Gamma_{Z\to\ell\bar{\ell}} = \frac{\alpha M_Z\left(1 + (1-4\sin^2\theta_W)^2\right)}{48\sin^2\theta_W\cos^2\theta_W}, \tag{A.5}$$

$$\Gamma_{W\to\ell\bar{\nu}_\ell} = \frac{\alpha M_W}{12\sin^2\theta_W}. \tag{A.6}$$

In the case of W- and Z-production the total cross section can be obtained using the narrow width approximation in the integrand of eq. (3.1), i.e.

$$\frac{1}{(Q^2 - M_V^2)^2 + M_V^2\Gamma_V^2} \to \frac{\pi}{M_V\Gamma_V}\delta(Q^2 - M_V^2). \tag{A.7}$$

We then find

$$\sigma_{V\to\ell_1\ell_2} = \sigma_V \mathrm{BR}(V\to\ell_1\ell_2) \tag{A.8}$$

where $\mathrm{BR}(V\to\ell_1\ell_2)$ stands for the branching ratio

$$\mathrm{BR}(V\to\ell_1\ell_2) = \frac{\Gamma_{V\to\ell_1\ell_2}}{\Gamma_V} \tag{A.9}$$

and the total rates σ_V (sum over all leptonic and hadronic decay channels) are given by

$$\sigma_Z = \frac{\pi^2\alpha}{4\sin^2\theta_W\cos^2\theta_W} \frac{1}{N}\frac{1}{S} W_Z\left(\frac{M_Z^2}{S}, M_Z^2\right), \tag{A.10}$$

$$\sigma_W = \frac{\pi^2\alpha}{2\sin^2\theta_W} \frac{1}{N}\frac{1}{S} W_W\left(\frac{M_W^2}{S}, M_W^2\right). \tag{A.11}$$

Notice that all particles into which the vector bosons decay are taken to be massless. Since the electroweak radiative corrections to $\sin^2\theta_W$ are not negligible, it is better to replace $\sin^2\theta_W$ appearing in the denominators of the above expressions by

$$\sin^2\theta_W = \frac{\sqrt{2}M_W^2}{\pi\alpha} G_F, \tag{A.12}$$

where $G_F = 1.166\times 10^{-5}\ \mathrm{GeV}^{-2}$ (Fermi constant). In the numerators we have put $\sin^2\theta_W = 0.227$.

Combining the various parton densities denoted by PD_{ij}^{V} with the corresponding DY correction terms Δ_{ij} in eq. (2.3) we can construct a compact formula for $W_V(\tau,Q^2)$. Before giving its expression let us first fix the notations. The coefficients v_i^V and a_i^V in eq. (A.20) are related to the vector and axial couplings of the vector boson V to the quarks (see eq. (2.22)). For the u- and d-type quarks they are equal to

$$
\begin{aligned}
&v_u^\gamma = \tfrac{2}{3}, && a_u^\gamma = 0,\\
&v_d^\gamma = -\tfrac{1}{3}, && a_d^\gamma = 0,\\
&v_u^Z = 1 - \tfrac{8}{3}\sin^2\theta_W, && a_u^Z = -1,\\
&v_d^Z = -1 + \tfrac{4}{3}\sin^2\theta_W, && a_d^Z = 1,\\
&v_u^W = v_d^W = 1/\sqrt{2}, && a_u^W = a_d^W = -1/\sqrt{2}.
\end{aligned}
\tag{A.13}
$$

For the antiquarks the values for v_i^V and a_i^V are the same as for the quarks. Further we introduce three $2n_f \times 2n_f$ matrices C^{ii}, C^{if} and C^{ff}. These matrices contain the information of the coupling of the respective quark flavours to the vector bosons. The indices i and f stand for initial and final; the combination in which they occur with the C indicate the orientation of the quark line to which the vector boson is coupled. For the γ and the Z they are defined by

$$
C^{ii}(q_k,q_l) = C^{ff}(q_k,q_l) = \begin{cases} 1 & \text{if } q_k = \bar{q}_l \\ 0 & \text{otherwise} \end{cases}, \tag{A.14}
$$

$$
C^{if}(q_k,q_l) = \begin{cases} 1 & \text{if } q_k = q_l \\ 0 & \text{otherwise} \end{cases}. \tag{A.15}
$$

For the $W^{\pm}$ they are

$$
C^{ii}(q_k,q_l) = \begin{cases} |V_{q_k q_l}|^2 & \text{if } e_{q_k} + e_{q_l} = \pm 1 \\ 0 & \text{otherwise} \end{cases}, \tag{A.16}
$$

$$
C^{if}(q_k,q_l) = \begin{cases} |V_{q_k q_l}|^2 & \text{if } e_{q_k} = \pm 1 + e_{q_l} \\ 0 & \text{otherwise} \end{cases}, \tag{A.17}
$$

$$
C^{ff}(q_k,q_l) = \begin{cases} |V_{q_k q_l}| & \text{if } e_{q_k} + e_{q_l} = \mp 1 \\ 0 & \text{otherwise} \end{cases}, \tag{A.18}
$$

where q_k and q_l stand for the (anti)quarks and e_{q_k} is the charge of q_k. The symbol $V_{q_k q_l}$ denotes the KM matrix, which in our calculation is approximated by

$$
V_{ud} = V_{cs} = \cos\theta_C, \qquad V_{us} = -V_{cd} = \sin\theta_C \tag{A.19}
$$

with $\sin^2\theta_C = 0.05$. The remaining matrix elements are put equal to zero. Using the convention that for example $q_u = \bar{q}_{\bar{u}}$ = the up-quark density and $\bar{q}_u = q_{\bar{u}}$ = the anti-up-quark density, the hadronic structure function can be written as

$$
\begin{aligned}
W_V(\tau,Q^2) = \int_0^1 dx_1 \int_0^1 dx_2 \int_0^1 dx\, \delta(\tau - x x_1 x_2)
\\
\times \Bigg\{ \sum_{i,j\in Q,\bar{Q}} \Bigg[& C^{ii}(q_i,\bar{q}_j)\left(v_i^2 + a_i^2\right)\Delta_{q\bar{q}}(x)
\\
& + \delta_{ij} \sum_{k,l\in Q} C^{ff}(q_k,\bar{q}_l)\left(v_k^2 + a_k^2\right)\Delta^{(2)}_{q\bar{q},B^2}(x)
\\
& + \delta_{ij} \sum_{k\in Q,\bar{Q}} \left(C^{if}(q_i,\bar{q}_k) + C^{if}(\bar{q}_i,q_k)\right)\left(v_i^2 + a_i^2\right)\Delta^{(2)}_{q\bar{q},BC}(x)
\\
& + \delta_{ij} \sum_{k\in Q} C^{ff}(q_k,\bar{q}_k)\left(v_i v_k\, \Delta^{(2),V}_{q\bar{q},AB}(x) + a_i a_k\, \Delta^{(2),A}_{q\bar{q},AB}(x)\right)\Bigg] q_i(x_1)\bar{q}_j(x_2)
\\
+ \sum_{i,k\in Q,\bar{Q}} & C^{if}(q_i,q_k)\left(v_i^2 + a_i^2\right)\Delta_{qg}(x)\left(q_i(x_1)g(x_2) + q_i(x_2)g(x_1)\right)
\\
+ \sum_{i,j\in Q,\bar{Q}} \Bigg[& \sum_{k\in Q,\bar{Q}} \left(C^{if}(q_i,q_k)\left(v_i^2 + a_i^2\right) + C^{if}(q_j,q_k)\left(v_j^2 + a_j^2\right)\right)\Delta^{(2)}_{qq,C^2}(x)
\\
& + C^{if}(q_i,q_i)\left(v_i v_j\, \Delta^{(2),V}_{q_i q_j,CD}(x) + a_i a_j\, \Delta^{(2),A}_{qq,CD}(x)\right)\Bigg] q_i(x_1) q_j(x_2)
\\
+ \sum_{i,j\in Q,\bar{Q}} \Bigg[& \left(C^{if}(q_i,q_j)\left(v_i^2 + a_i^2\right) + C^{if}(q_j,q_i)\left(v_j^2 + a_j^2\right)\right)\Delta^{(2)}_{qq,CE}(x)
\\
& + \delta_{ij} \sum_{k\in Q,\bar{Q}} C^{if}(q_i,q_k)\left(v_i^2 + a_i^2\right)\Delta^{(2)}_{qq,CF}(x)\Bigg] q_i(x_1) q_j(x_2)
\\
+ \sum_{k,l\in Q} & C^{ff}(q_k,\bar{q}_l)\left(v_k^2 + a_k^2\right)\Delta^{(2)}_{gg}(x) g(x_1) g(x_2)\Bigg\}, \qquad \text{(A.20)}
\end{aligned}
$$

where

$$\Delta_{q\bar{q}}(x) = \delta(1-x) + \Delta^{(1)}_{q\bar{q}}(x) + \Delta^{(2),NS}_{q\bar{q}}(x), \qquad \text{(A.21)}$$

$$\Delta_{qg}(x) = \Delta^{(1)}_{qg}(x) + \Delta^{(2)}_{qg}(x) \qquad \text{(A.22)}$$

and the sets Q and $\bar{Q}$ are given by

$$Q = \{u,d,s,c\}, \qquad \bar{Q} = \{\bar{u},\bar{d},\bar{s},\bar{c}\}. \qquad \text{(A.23)}$$

Furthermore, the scale to be used in the parton distribution functions is the mass factorization scale M. The DY correction terms Δ_{ij} can be found in appendix B.

They are listed in the same order as they appear in eq. (A.20). For the $\gamma - Z$ interference the right combinations of the parton distributions can be found by taking the photon formula and making the following replacements:

$$v_i^2 \to v_i^\gamma v_i^Z, \qquad v_i v_j \to \tfrac{1}{2}\left(v_i^\gamma v_j^Z + v_j^\gamma v_i^Z\right). \tag{A.24}$$

Finally, we want to comment on the treatment of the distributions $\mathscr{D}_i(x)$ when they appear in the convolution integral in eq. (3.2). In that case one should use the relation

$$\begin{aligned}\int_0^1 \mathrm{d}x \int_0^1 \mathrm{d}\xi\, \Phi(\xi, M^2)\mathscr{D}_i(x)\delta(\tau - x\xi) \\ = \Phi(\tau, M^2)\frac{1}{(1+i)}\ln^{i+1}(1-\tau) \\ + \int_\tau^1 \mathrm{d}x \left\{\frac{1}{x}\Phi(\tau/x, M^2) - \Phi(\tau, M^2)\right\}\frac{\ln^i(1-x)}{1-x}.\end{aligned} \tag{A.25}$$

Notice that the convolution integral does not depend on the IR cutoff δ.

Appendix B. Drell–Yan correction terms

In this appendix we will present the explicit expressions for the DY correction terms Δ_{ij} the calculation of which is outlined in sect. 2. In order to make the presentation self-contained we also give the lowest-order contributions already calculated in the literature [8–13]. We distinguish the following contributions to Δ_{ij}:

(i) quark–antiquark (non-singlet);
(ii) (anti)quark–gluon;
(iii) the quark–antiquark (singlet) and non-identical quark–quark;
(iv) the identical quark–quark, and
(v) gluon–gluon.

Before presenting the results of the Drell–Yan correction terms mentioned above, we want to make two remarks. Firstly, in the expressions below the scale in the running coupling constant α_s is always taken to be the renormalization scale R. Secondly, for the interference terms, we use the convention that $AC = AC^\dagger + CA^\dagger$, etc.

B.1. THE QUARK–ANTIQUARK CONTRIBUTIONS (NON-SINGLET)

The lowest-order contribution originating from the Born graph in fig. 1 is given by

$$\Delta_{q\bar{q}}^{(0)} = \delta(1-x). \tag{B.1}$$

The $O(\alpha_s)$ correction to the $q\bar{q}$ subprocess which receives contributions from the graphs in figs. 2 and 3 has been calculated in the literature [8–13]. Choosing the $\overline{\text{MS}}$ scheme the expression for $\Delta_{q\bar{q}}^{(1)}$ can be very easily obtained using n-dimensional

regularization [8, 12]. From the numerical as well as the theoretical point of view it is convenient to divide it into two pieces, viz.

$$\Delta^{(1)}_{q\bar{q}}(x) = \Delta^{(1),S+V}_{q\bar{q}}(x) + \Delta^{(1),H}_{q\bar{q}}(x), \tag{B.2}$$

where the S + V part can be obtained by doing the calculation in a soft gluon approximation ($x \to 1$), which means that one only takes the contributions from the soft and virtual gluons into account. To obtain the remaining piece, denoted by H one has to perform an exact computation. The expressions for $\Delta^{(1),S+V}_{q\bar{q}}$ and $\Delta^{(1),H}_{q\bar{q}}$ are

$$\Delta^{(1),S+V}_{q\bar{q}} = \frac{\alpha_s}{4\pi} C_F \left\{ \delta(1-x)\left[6\ln\left(\frac{Q^2}{M^2}\right) + 8\zeta(2) - 16 \right] + 8\mathscr{D}_0(x)\ln\left(\frac{Q^2}{M^2}\right) + 16\mathscr{D}_1(x) \right\}, \tag{B.3}$$

$$\Delta^{(1),H}_{q\bar{q}} = \frac{\alpha_s}{4\pi} C_F \left\{ -4(1+x)\ln\left(\frac{Q^2}{M^2}\right) - 8(1+x)\ln(1-x) - 4\frac{1+x^2}{1-x}\ln x \right\}. \tag{B.4}$$

The distribution $\mathscr{D}_i(x)$ is defined by

$$\mathscr{D}_i(x) = \delta(1-x)\frac{\ln^{i+1}\delta}{(i+1)} + \theta(1-\delta-x)\frac{\ln^i(1-x)}{1-x}. \tag{B.5}$$

The parameter δ is introduced in order to distinguish between the soft (S) ($x \geqslant 1-\delta$) and hard (H) ($x \leqslant 1-\delta$) gluon regions in the phase space integrals, which have to be performed for the contributions from fig. 3. The $\ln\delta$ terms arise when the factor $(1-x)^{-1+\varepsilon}$ appearing in these integrals is replaced by the distribution

$$(1-x)^{-1+\varepsilon} \to \frac{1}{\varepsilon}\delta^\varepsilon\delta(1-x) + (1-x)^{-1+\varepsilon}\theta(1-x-\delta). \tag{B.6}$$

In the literature the $\ln\delta$ terms are very often omitted and the distributions $\mathscr{D}_i(x)$ are then denoted by $(\ln^i(1-x)/(1-x))_+$, see e.g. ref. [8]. Note that the coefficient of $\delta(1-x)$ in eq. (B.3) also receives contributions from the virtual gluon graph depicted in fig. 2.

The second-order correction to the non-singlet part of $\Delta_{q\bar{q}}$ is determined by the diagrams in figs. 4–7 and the interference between the graphs in figs. 7 and 8. It can be split into two parts. The first piece is related through mass factorization to the collinearly singular part of the partonic structure function $\hat{W}_{q\bar{q}}$ and will be denoted by

$$\Delta^{(2),NS}_{q\bar{q}} = \Delta^{(2),S+V}_{q\bar{q}} + \Delta^{(2),C_A}_{q\bar{q}} + \Delta^{(2),C_F}_{q\bar{q}} + \Delta^{(2)}_{q\bar{q},A^2} + 2\Delta^{(2)}_{q\bar{q},AC} + \frac{\alpha_s}{4\pi}\beta_0\Delta^{(1)}_{q\bar{q}}\ln\left(\frac{R^2}{M^2}\right), \tag{B.7}$$

where β_0 represents the lowest-order coefficient of the β-function (eq. (2.12)) and $\Delta_{q\bar{q}}^{(1)}$ is given in eq. (B.2). The symbols M and R stand for the mass factorization and renormalization scales respectively. The appearance of the β_0 term in eq. (B.7) is a remnant of the fact that the calculation of this part involves coupling constant renormalization to remove the UV divergencies.

The second piece consists of the DY correction terms $\Delta_{q_q,B^2}^{(2)}$, $\Delta_{q\bar{q},BC}^{(2)} = \Delta_{q\bar{q},BD}^{(2)}$, $\Delta_{q\bar{q},AB}^{(2),V}$ and $\Delta_{q\bar{q},AB}^{(2),A}$ originating from those parts of the parton structure function $\hat{W}_{q\bar{q}}$ which are collinearly finite and therefore do not need mass factorization.

First we will discuss the contributions in eq. (B.7). As in the case of the first order calculation a part of $\Delta_{q\bar{q}}^{(2),NS}$ can be obtained by a soft gluon approximation [23]. This piece we have again denoted by S + V. For the remaining Drell–Yan correction terms in eq. (B.7) an exact calculation is necessary. The contributions to $\Delta_{q\bar{q}}^{(2),S+V}$ come from the two-loop virtual graphs in fig. 4, the soft gluon radiative corrections due to figs. 5 and 6 and soft quark pair production due to diagrams A in fig. 7. The expression for this part is equal to

$$
\begin{aligned}
\Delta_{q\bar{q}}^{(2),S+V} = \left(\frac{\alpha_s}{4\pi}\right)^2 \delta(1-x)\Bigg\{ C_A C_F\Bigg[&-11\ln^2\left(\frac{Q^2}{M^2}\right) \\
&+\left[\tfrac{193}{3} - 24\zeta(3)\right]\ln\left(\frac{Q^2}{M^2}\right) - \tfrac{12}{5}\zeta(2)^2 + \tfrac{592}{9}\zeta(2) + 28\zeta(3) - \tfrac{1535}{12}\Bigg] \\
&+C_F^2\Bigg[\left[18 - 32\zeta(2)\right]\ln^2\left(\frac{Q^2}{M^2}\right) + \left[24\zeta(2) + 176\zeta(3) - 93\right]\ln\left(\frac{Q^2}{M^2}\right) + \tfrac{8}{5}\zeta(2)^2 - 70\zeta(2) \\
&-60\zeta(3) + \tfrac{511}{4}\Bigg] + n_f C_F\Bigg[2\ln^2\left(\frac{Q^2}{M^2}\right) - \tfrac{34}{3}\ln\left(\frac{Q^2}{M^2}\right) + 8\zeta(3) - \tfrac{112}{9}\zeta(2) + \tfrac{127}{6}\Bigg]\Bigg\} \\
&+C_A C_F\Bigg[-\tfrac{44}{3}\mathscr{D}_0(x)\ln^2\left(\frac{Q^2}{M^2}\right) + \left[\left(\tfrac{536}{9} - 16\zeta(2)\right)\mathscr{D}_0(x)\right. \\
&\left. -\tfrac{176}{3}\mathscr{D}_1(x)\right]\ln\left(\frac{Q^2}{M^2}\right) - \tfrac{176}{3}\mathscr{D}_2(x) + \left[\tfrac{1072}{9} - 32\zeta(2)\right]\mathscr{D}_1(x) \\
&+\left[56\zeta(3) + \tfrac{176}{3}\zeta(2) - \tfrac{1616}{27}\right]\mathscr{D}_0(x)\Bigg] + C_F^2\Bigg[\left[64\mathscr{D}_1(x) + 48\mathscr{D}_0(x)\right]\ln^2\left(\frac{Q^2}{M^2}\right) \\
&+\left[192\mathscr{D}_2(x) + 96\mathscr{D}_1(x) - (128 + 64\zeta(2))\mathscr{D}_0(x)\right]\ln\left(\frac{Q^2}{M^2}\right) \\
&+128\mathscr{D}_3(x) - (128\zeta(2) + 256)\mathscr{D}_1(x) + 256\zeta(3)\mathscr{D}_0(x)\Bigg] \\
&+n_f C_F\Bigg[\tfrac{8}{3}\mathscr{D}_0(x)\ln^2\left(\frac{Q^2}{M^2}\right) + \left[\tfrac{32}{3}\mathscr{D}_1(x) - \tfrac{80}{9}\mathscr{D}_0(x)\right]\ln\left(\frac{Q^2}{M^2}\right) \\
&+\tfrac{32}{3}\mathscr{D}_2(x) - \tfrac{160}{9}\mathscr{D}_1(x) + \left(\tfrac{224}{27} - \tfrac{32}{3}\zeta(2)\right)\mathscr{D}_0(x)\Bigg]. \qquad \text{(B.8)}
\end{aligned}
$$

The hard gluon contributions from figs. 5 and 6 are denoted by $\Delta_{q\bar{q}}^{(2),C_A}$ and $\Delta_{q\bar{q}}^{(2),C_F}$, where the superscripts C_A and C_F refer to the two colour structures. The expressions for these quantities are

$$\Delta_{q\bar{q}}^{(2),C_A} = \left(\frac{\alpha_s}{4\pi}\right)^2 C_A C_F \left\{ \tfrac{22}{3}(1+x)\ln^2\left(\frac{Q^2}{M^2}\right) + \left[\frac{1+x^2}{1-x}\left[-8\,\mathrm{Li}_2(1-x) + \tfrac{70}{3}\ln x \right] \right.\right.$$

$$\left. + (1+x)\left[8\zeta(2) + \tfrac{88}{3}\ln(1-x) - 6\ln x \right] - \tfrac{4}{9}(19+124x) \right] \ln\left(\frac{Q^2}{M^2}\right)$$

$$+ \frac{1+x^2}{1-x}\left[-4\,\mathrm{S}_{1,2}(1-x) - 12\,\mathrm{Li}_3(1-x) + \tfrac{4}{3}\,\mathrm{Li}_2(1-x) \right.$$

$$+ 8\,\mathrm{Li}_2(1-x)\ln x - 8\,\mathrm{Li}_2(1-x)\ln(1-x) + 8\zeta(2)\ln x - \tfrac{29}{2}\ln^2 x - \tfrac{104}{3}\ln x$$

$$\left. + \tfrac{140}{3}\ln x \ln(1-x) \right] + (1+x)\left[16\,\mathrm{S}_{1,2}(1-x) - 12\,\mathrm{Li}_3(1-x) - 28\zeta(3) \right.$$

$$\left. + 8\,\mathrm{Li}_2(1-x)\ln(1-x) + 16\zeta(2)\ln(1-x) + \tfrac{88}{3}\ln^2(1-x) \right]$$

$$- \tfrac{4}{3}(7+x)\,\mathrm{Li}_2(1-x) - \tfrac{4}{3}(19+25x)\zeta(2) + \tfrac{1}{6}(23-25x)\ln^2 x$$

$$- 4(3-x)\ln x \ln(1-x) - \tfrac{2}{3}(26-57x)\ln x - \tfrac{4}{9}(38+239x)\ln(1-x)$$

$$\left. - \tfrac{446}{27} + \tfrac{2278}{27}x \right\}, \qquad \text{(B.9)}$$

$$\Delta_{q\bar{q}}^{(2),C_F} = \left(\frac{\alpha_s}{4\pi}\right)^2 C_F^2 \left\{ \left[-16\frac{1+x^2}{1-x}\ln x + 8(1+x)\left[\ln x - 4\ln(1-x) \right] \right.\right.$$

$$\left. - 8(5+x) \right] \ln^2\left(\frac{Q^2}{M^2}\right) + \left[\frac{1+x^2}{1-x}\left[16\,\mathrm{Li}_2(1-x) + 24\ln^2 x - 24\ln x \right.\right.$$

$$\left. - 112\ln x \ln(1-x) \right] + (1+x)\left[32\,\mathrm{Li}_2(1-x) + 32\zeta(2) - 12\ln^2 x \right.$$

$$\left. + 32\ln x \ln(1-x) - 96\ln^2(1-x) \right] + 8(15+2x) + 16(2-3x)\ln x$$

$$\left. - 16(7-x)\ln(1-x) \right] \ln\left(\frac{Q^2}{M^2}\right) + \frac{1+x^2}{1-x}\left[-32\,\mathrm{S}_{1,2}(1-x) \right.$$

$$- 8\,\mathrm{Li}_3(1-x) - 24\,\mathrm{Li}_2(1-x)\ln x + 24\,\mathrm{Li}_2(1-x)\ln(1-x) - 12\ln^3 x$$

$$+64\zeta(2)\ln x + 72\ln^2 x \ln(1-x) - 124\ln^2(1-x)\ln x + 56\ln x\Big]$$

$$+(1-x)\big[64\zeta(2) - 64\ln^2(1-x)\big] + (1+x)\big[\tfrac{14}{3}\ln^3 x - 64\ln^3(1-x)$$

$$-40\,\mathrm{Li}_3(1-x) + 48\,\mathrm{Li}_2(1-x)\ln(1-x) - 32\zeta(2)\ln x + 16\,\mathrm{S}_{1,2}(1-x)$$

$$+64\zeta(2)\ln(1-x) - 128\zeta(3) - 24\ln^2 x \ln(1-x) + 32\ln^2(1-x)\ln x\Big]$$

$$+8(3-2x)\mathrm{Li}_2(1-x) - 16(2-x)\ln^2 x + 16(7-6x)\ln x \ln(1-x)$$

$$-8(4-13x)\ln x + 4(64+3x)\ln(1-x) - 24(3-2x)\Big\}. \qquad \text{(B.10)}$$

The functions $\mathrm{Li}_n(x)$ and $\mathrm{S}_{n,p}(x)$ denote the polylogarithms and can be found in ref. [58].

The hard part of quark pair production due to the diagrams A in fig. 7 is equal to

$$\Delta^{(2)}_{\mathrm{q\bar{q}},\mathrm{A}^2} = \left(\frac{\alpha_s}{4\pi}\right)^2 n_f C_F\left\{-\tfrac{4}{3}(1+x)\ln^2\left(\frac{Q^2}{M^2}\right) + \left[-\frac{16}{3}\frac{1+x^2}{1-x}\ln x\right.\right.$$

$$\left.-\tfrac{16}{3}(1+x)\ln(1-x) - \tfrac{8}{9}(1-11x)\right]\ln\left(\frac{Q^2}{M^2}\right) + \frac{1+x^2}{1-x}\big[4\ln^2 x$$

$$-\tfrac{4}{3}\mathrm{Li}_2(1-x) + \tfrac{20}{3}\ln x - \tfrac{32}{3}\ln x \ln(1-x)\big] + (1+x)\big[\tfrac{4}{3}\mathrm{Li}_2(1-x)$$

$$+\tfrac{16}{3}\zeta(2) - \tfrac{16}{3}\ln^2(1-x) + \tfrac{2}{3}\ln^2 x\big] - \tfrac{16}{9}(1-11x)\ln(1-x)$$

$$\left.+\tfrac{8}{3}(2-3x)\ln x + \tfrac{4}{27}(47-103)\right\}. \qquad \text{(B.11)}$$

Finally we have the interference terms corresponding to the combinations AC and AD in figs. 7 and 8. For them we find

$$\Delta^{(2)}_{\mathrm{q\bar{q}},\mathrm{AC}} = \Delta^{(2)}_{\mathrm{q\bar{q}},\mathrm{AD}} = \left(\frac{\alpha_s}{4\pi}\right)^2 C_F\left(C_F - \tfrac{1}{2}C_A\right)\left\{\left[\frac{1+x^2}{1-x}\big[-8\,\mathrm{Li}_2(1-x)\right.\right.$$

$$\left.\left.-4\ln^2 x - 6\ln x\big] - 14(1+x)\ln x - 4(8-7x)\right]\ln\left(\frac{Q^2}{M^2}\right)\right.$$

$$+\frac{1+x^2}{1-x}\big[16\,\mathrm{Li}_3(1-x)-36\,\mathrm{S}_{1,2}(1-x)+\tfrac{8}{3}\ln^3 x-12\,\mathrm{Li}_2(1-x)\ln x$$

$$-16\,\mathrm{Li}_2(1-x)\ln(1-x)-6\,\mathrm{Li}_2(1-x)+\tfrac{15}{2}\ln^2 x-8\ln^2 x\ln(1-x)$$

$$+12\ln x-12\ln x\ln(1-x)\big]+(1+x)\big[-8\,\mathrm{Li}_3(1-x)-26\,\mathrm{Li}_2(1-x)$$

$$+4\,\mathrm{Li}_2(1-x)\ln x+\tfrac{2}{3}\ln^3 x+\tfrac{23}{2}\ln^2 x-28\ln x\ln(1-x)\big]$$

$$+2(22-9x)\ln x-8(8-7x)\ln(1-x)+2(47-39x)\Big\}. \qquad \text{(B.12)}$$

Notice that for $V=\gamma$ and Z both the AC and AD interference terms always contribute, whereas for W-production only one of the two gives a contribution. This is due to the fact that for W-production only one of the sets of diagrams, C or D, is possible for a fixed choice of the initial- and final-state quark flavours.

The remaining parts of $q\bar{q}$ scattering are free of mass singularities. Therefore they do not need mass factorization, which implies that their contributions are scheme and scale independent. The contributions originating from the diagrams B in fig. 7 and the interference terms BC and BD (see figs. 7 and 8) are

$$\Delta^{(2)}_{q\bar{q},B^2}=\left(\frac{\alpha_s}{4\pi}\right)^2 C_F\Big\{(1+x)^2\big[-\tfrac{32}{3}\,\mathrm{Li}_2(-x)-\tfrac{16}{3}\zeta(2)+\tfrac{8}{3}\ln^2 x$$

$$-\tfrac{32}{3}\ln x\ln(1+x)\big]+\tfrac{8}{3}(3+3x^2+4x)\ln x+\tfrac{40}{3}(1-x^2)\Big\}, \qquad \text{(B.13)}$$

$$\Delta^{(2)}_{q\bar{q},BC}=\Delta^{(2)}_{q\bar{q},BD}=\left(\frac{\alpha_s}{4\pi}\right)^2 C_F(C_F-\tfrac{1}{2}C_A)\Big\{(1+x^2+3x)\big[32\,\mathrm{S}_{1,2}(1-x)$$

$$+16\,\mathrm{Li}_2(1-x)\ln x\big]+(1+x)^2\big[-48\,\mathrm{S}_{1,2}(-x)-8\,\mathrm{Li}_3(-x)+24\,\mathrm{Li}_2(-x)$$

$$+24\,\mathrm{Li}_2(-x)\ln x-48\,\mathrm{Li}_2(-x)\ln(1+x)+12\zeta(2)-24\zeta(2)\ln(1+x)$$

$$+8\zeta(2)\ln x+20\ln^2 x\ln(1+x)-24\ln^2(1+x)\ln x+24\ln x\ln(1+x)\big]$$

$$+36(1-x^2)\mathrm{Li}_2(1-x)+\tfrac{4}{3}(1+x^2+4x)\ln^3 x+4(9+11x)\ln x$$

$$-2(-6+15x^2+8x)\ln^2 x-2(-27+13x^2+14x)\Big\}. \qquad \text{(B.14)}$$

The comment made for the interference terms AC and AD below eq. (B.12) also applies to BC and BD.

The matrix element corresponding to the interference term AB (fig. 7) involves the product of two fermion traces, each containing a vertex of the form $\gamma_\mu(v+a\gamma_5)$.

Therefore it is a type (3) matrix element, described below eq. (2.22) and we have to distinguish between the vector–vector and axial–axial parts, which we will denote by $\Delta^{(2),V}_{q\bar{q},AB}$ and $\Delta^{(2),A}_{q\bar{q},AB}$ respectively. The first part is zero due to Furry's theorem

$$\Delta^{(2),V}_{q\bar{q},AB} = 0, \tag{B.15}$$

whereas the axial–axial contribution is given by

$$\Delta^{(2),A}_{q\bar{q},AB} = \left(\frac{\alpha_s}{4\pi}\right)^2 C_F \left\{ 16\frac{1+x^2}{1-x}\ln x + 32x\ln x + 16(3-x) \right\}. \tag{B.16}$$

It is clear from eq. (B.15) that this interference term does not contribute for $V = \gamma$. It does not give a contribution to W-production either because the diagrams A and B can never have the same initial-state quarks due to charge conservation. For Z-production the contribution from eq. (B.15) vanishes by taking complete families of quarks into account.

With the correction terms mentioned above we have exhausted all contributions to $\Delta_{q\bar{q}}$ except those belonging to the singlet part. Since the latter are equal to the corrections Δ_{qq} calculated for the non-identical quark–quark scattering process, we will present them there.

B.2. THE (ANTI)QUARK–GLUON CONTRIBUTION

At $O(\alpha_s)$ the qg subprocess shows up for the first time. The Drell–Yan correction term for this reaction has been calculated in refs. [8, 12] and it is given by

$$\Delta^{(1)}_{qg} = \frac{\alpha_s}{4\pi} T_f \left\{ 2(1+2x^2-2x)\ln\left(\frac{(1-x)^2Q^2}{xM^2}\right) + 1 - 7x^2 + 6x \right\}. \tag{B.17}$$

The second order contribution to Δ_{qg} can be written as

$$\Delta^{(2)}_{qg} = \Delta^{(2)}_{\bar{q}g} = \Delta^{(2),C_A}_{qg} + \Delta^{(2),C_F}_{qg} + \frac{\alpha_s}{4\pi}\beta_0 \Delta^{(1)}_{qg} \ln\left(\frac{R^2}{M^2}\right). \tag{B.18}$$

The calculation of $\Delta^{(2)}_{qg}$ requires both mass factorization and renormalization. The latter gives rise to the β_0 term in eq. (B.18). The two parts $\Delta^{(2),C_A}_{qg}$ and $\Delta^{(2),C_F}_{qg}$ are equal to

$$\begin{aligned}
\Delta^{(2),C_A}_{qg} = \left(\frac{\alpha_s}{4\pi}\right)^2 C_A T_f \Bigg\{ & \Bigg[4(1+4x)\ln x + 4(1+2x^2-2x)\ln(1-x) \\
& + \tfrac{2}{3}\left(3 - 31x^2 + 24x + \frac{4}{x}\right) \Bigg] \ln^2\left(\frac{Q^2}{M^2}\right) + \Bigg[(1+2x^2+2x)\big[-8\,\mathrm{Li}_2(-x) \\
& - 8\ln x \ln(1+x)\big] - 8(1+3x)\ln^2 x + 8(3+2x^2+6x)\mathrm{Li}_2(1-x) \\
& - 16(1+2x^2-x)\zeta(2) + 8(1-2x^2+10x)\ln x \ln(1-x)
\end{aligned}$$

$$+12(1+2x^2-2x)\ln^2(1-x)+\tfrac{4}{3}\left(9-71x^2+54x+\frac{8}{x}\right)\ln(1-x)$$

$$+4(3+28x^2-2x)\ln x-\tfrac{58}{3}+\tfrac{146}{9}x^2-\tfrac{8}{3}x+\frac{88}{9x}\Bigg]\ln\left(\frac{Q^2}{M^2}\right)$$

$$+(1+4x^2+5x)[8\,\mathrm{Li}_2(-x)+8\ln x\ln(1+x)]$$

$$+(1+2x^2+2x)\Bigg[-8\,\mathrm{Li}_3(-x)+16\,\mathrm{Li}_3\left(\frac{1+x}{1-x}\right)-16\,\mathrm{Li}_3\left(-\frac{1+x}{1-x}\right)$$

$$+16\,\mathrm{Li}_2(-x)\ln x-16\,\mathrm{Li}_2(-x)\ln(1-x)+12\ln^2 x\ln(1+x)$$

$$-16\ln x\ln(1-x)\ln(1+x)\Bigg]+8(9+4x^2+16x)\mathrm{S}_{1,2}(1-x)$$

$$-4(15+12x^2+34x)\mathrm{Li}_3(1-x)-4(1+2x^2+4x)\zeta(3)$$

$$+8(7-2x)x\,\mathrm{Li}_2(1-x)\ln x+8(7+5x^2+10x)\mathrm{Li}_2(1-x)\ln(1-x)$$

$$+\tfrac{4}{3}\left(33+44x^2+90x+\frac{16}{x}\right)\mathrm{Li}_2(1-x)-16(5-2x)x\zeta(2)\ln x$$

$$-32(1+2x^2-x)\zeta(2)\ln(1-x)+\tfrac{4}{3}\left(15+107x^2-84x-\frac{8}{x}\right)\zeta(2)$$

$$+\tfrac{2}{3}(9+20x)\ln^3 x+\tfrac{26}{3}(1+2x^2-2x)\ln^3(1-x)-\left(5+\tfrac{346}{3}x^2\right)\ln^2 x$$

$$-4(3-2x^2+14x)\ln^2 x\ln(1-x)+4(1-6x^2+22x)\ln^2(1-x)\ln x$$

$$+\tfrac{4}{3}\left(6-77x^2+63x+\frac{8}{x}\right)\ln^2(1-x)-\tfrac{2}{9}(-354+457x^2+12x)\ln x$$

$$+20(1+13x^2-2x)\ln x\ln(1-x)+\tfrac{539}{9}+\tfrac{1837}{27}x^2-\tfrac{1226}{9}x+\frac{116}{27x}$$

$$+\tfrac{2}{9}\left(-210+74x^2+75x+\frac{88}{x}\right)\ln(1-x)\Bigg\}, \qquad \text{(B.19)}$$

$$\Delta_{qg}^{(2),C_F} = \left(\frac{\alpha_s}{4\pi}\right)^2 C_F T_f \Big\{ \Big[12(1+2x^2-2x)\ln(1-x) - 6(1+4x^2-2x)\ln x$$

$$-3(1-4x)\Big]\ln^2\left(\frac{Q^2}{M^2}\right) + \Big[(1+2x^2-2x)\big[-8\zeta(2)+36\ln^2(1-x)\big]$$

$$-48x^2\,\mathrm{Li}_2(1-x) + 8(1+4x^2-2x)\ln^2 x + 2(5+46x^2-40x)\ln x$$

$$-8(5+16x^2-10x)\ln x\ln(1-x) - 4(8+23x^2-34x)\ln(1-x)$$

$$+2(12+11x^2-34x)\Big]\ln\left(\frac{Q^2}{M^2}\right) + (-1+3x^2+2x)\big[-16\,\mathrm{Li}_2(-x)$$

$$-16\ln x\ln(1+x)\big] + (1+2x^2-2x)\big[32\,\mathrm{Li}_3(-x) + 100\zeta(3)$$

$$-16\,\mathrm{Li}_2(-x)\ln x - 16\zeta(2)\ln(1-x) + \tfrac{70}{3}\ln^3(1-x)\big]$$

$$-4(11+34x^2-22x)\mathrm{S}_{1,2}(1-x) + 4(-1+18x^2+2x)\mathrm{Li}_3(1-x)$$

$$+4(1-2x)\mathrm{Li}_2(1-x)\ln x - 4(3+26x^2-6x)\mathrm{Li}_2(1-x)\ln(1-x)$$

$$+2(3+40x^2-28x)\mathrm{Li}_2(1-x) + 24(1+4x^2-2x)\zeta(2)\ln x$$

$$+4(5-12x^2+2x)\zeta(2) - \tfrac{1}{3}(17+52x^2-34x)\ln^3 x$$

$$+8(3+10x^2-6x)\ln^2 x\ln(1-x) - \tfrac{1}{2}(35+4x^2-68x)\ln^2 x$$

$$-6(7+22x^2-14x)\ln^2(1-x)\ln x - 2(23+63x^2-80x)\ln^2(1-x)$$

$$+4(13+48x^2-50x)\ln x\ln(1-x) - (59+174x^2-245x)\ln x$$

$$+2(38+88x^2-147x)\ln(1-x) - \tfrac{181}{2} - \tfrac{305}{2}x^2 + 233x\Big\}. \qquad \text{(B.20)}$$

Notice the absence of the functions $\delta(1-x)$ and $\mathscr{D}_i(x)$ in Δ_{qg}, which were present in the expression for $\Delta_{q\bar{q}}$. Although the second-order contribution corresponds to graphs with a gluon in the final state, these singular functions do not show up since the lowest-order term $\Delta_{qg}^{(1)}$ is integrable in $x = 1$.

B.3. THE NON-IDENTICAL QUARK–QUARK CONTRIBUTIONS

The reaction represented by the diagrams in fig. 8 describes quark–antiquark as well as quark–quark scattering (without identical quarks). The contribution to the

DY correction term can be split into two parts. The first part, represented by the combinations C^2 and D^2, needs mass factorization. In this case the contributions for $q\bar{q}$, qq and $\bar{q}\bar{q}$ are all equal and are given by

$$\Delta^{(2)}_{q\bar{q},C^2} = \Delta^{(2)}_{q\bar{q},D^2} = \Delta^{(2)}_{qq,C^2} = \Delta^{(2)}_{qq,D^2} = \Delta^{(2)}_{\bar{q}\bar{q},C^2} = \Delta^{(2)}_{\bar{q}\bar{q},D^2}$$

$$= \left(\frac{\alpha_s}{4\pi}\right)^2 C_F T_f \left\{ \left[4(1+x)\ln x + \tfrac{2}{3}\left(3 - 4x^2 - 3x + \frac{4}{x}\right)\right] \ln^2\left(\frac{Q^2}{M^2}\right) \right.$$

$$+ \left[(1+x)\left[16\,\mathrm{Li}_2(1-x) - 8\ln^2 x + 16\ln x \ln(1-x)\right] + 4(3+4x^2+6x)\ln x \right.$$

$$+ \tfrac{8}{3}\left(3 - 4x^2 - 3x + \frac{4}{x}\right)\ln(1-x) - \tfrac{4}{9}\left(39 + 22x^2 - 39x - \frac{22}{x}\right)\Big] \ln\left(\frac{Q^2}{M^2}\right)$$

$$+ \left(3 - 4x^2 - 3x + \frac{4}{x}\right)\left[\tfrac{8}{3}\ln^2(1-x) - \tfrac{8}{3}\zeta(2)\right]$$

$$+ (1+x)\left[48\,S_{1,2}(1-x) - 32\,\mathrm{Li}_3(1-x) + 8\,\mathrm{Li}_2(1-x)\ln x\right.$$

$$+ 32\,\mathrm{Li}_2(1-x)\ln(1-x) - 16\zeta(2)\ln x + 6\ln^3 x - 16\ln^2 x \ln(1-x)$$

$$\left. + 16\ln^2(1-x)\ln x\right] + \tfrac{4}{3}\left(39 + 8x^2 + 15x + \frac{16}{x}\right)\mathrm{Li}_2(1-x)$$

$$- \tfrac{5}{3}(3 + 8x^2 + 15x)\ln^2 x + 8(3 + 4x^2 + 6x)\ln x \ln(1-x)$$

$$+ \tfrac{2}{9}(345 + 20x^2 - 48x)\ln x - \tfrac{8}{9}\left(39 + 22x^2 - 39x - \frac{22}{x}\right)\ln(1-x)$$

$$\left. + \tfrac{593}{9} + \tfrac{703}{27}x^2 - \tfrac{866}{9}x + \frac{116}{27x}\right\}. \qquad \text{(B.21)}$$

The second part, which is collinearly finite, consists of the interference between the graphs C and D in fig. 8. The matrix element is of type (3) (see below eq. (2.22)), therefore we have to distinguish between the vector–vector (V) and the axial vector–axial vector (A) terms which are represented by $\Delta^{(2),V}_{q\bar{q},CD}$ and $\Delta^{(2),A}_{q\bar{q},CD}$ respectively. The contributions to V and A are not equal to each other, like in the AB case (see eqs. (B.15) and (B.16)). Further notice the relative minus sign between the $q\bar{q}$ and the qq ($\bar{q}\bar{q}$) in the V-part. The expressions for these interfer-

ence terms are

$$\Delta^{(2),V}_{q\bar{q},CD} = -\Delta^{(2),V}_{qq,CD} = -\Delta^{(2),V}_{\bar{q}\bar{q},CD} = \left(\frac{\alpha_s}{4\pi}\right)^2 C_F T_f \left\{ \left(2+x+\frac{2}{x}\right)\left[32\,S_{1,2}(1-x)\right.\right.$$

$$-96\,S_{1,2}(-x) - 48\ln^2(1+x)\ln x - 48\zeta(2)\ln(1+x) + 40\ln^2 x\ln(1+x)$$

$$\left.-96\,\mathrm{Li}_2(-x)\ln(1+x)\right] + (1+x)\left[80\,\mathrm{Li}_2(-x) + 80\ln x\ln(1+x)\right.$$

$$\left.+40\zeta(2)\right] + 8\left(-6+3x+\frac{4}{x}\right)\mathrm{Li}_3(1-x) - 16\left(-10+3x+\frac{10}{x}\right)\mathrm{Li}_3(-x)$$

$$-24\left(-6+x+\frac{4}{x}\right)\zeta(3) + 8(10-x)\mathrm{Li}_2(1-x)\ln x - \tfrac{16}{3}x\ln^3 x$$

$$+32\left(2x+\frac{5}{x}\right)\mathrm{Li}_2(-x)\ln x + 8(10+x)\zeta(2)\ln x + 8(5-4x)\mathrm{Li}_2(1-x)$$

$$\left.-52x\ln^2 x - 16(5+4x)\ln x - 160(1-x)\right\}, \qquad \text{(B.22)}$$

$$\Delta^{(2),A}_{q\bar{q},CD} = \Delta^{(2),A}_{qq,CD} = \Delta^{(2),A}_{\bar{q}\bar{q},CD} = \left(\frac{\alpha_s}{4\pi}\right)^2 C_F T_f \left\{ (2+x)\left[32\,S_{1,2}(1-x)\right.\right.$$

$$-96\,S_{1,2}(-x) - 48\ln^2(1+x)\ln x - 48\zeta(2)\ln(1+x) + 40\ln^2 x\ln(1+x)$$

$$\left.-96\,\mathrm{Li}_2(-x)\ln(1+x)\right] + (1+x)\left[16\,\mathrm{Li}_2(-x) + 16\ln x\ln(1+x)\right.$$

$$\left.+8\zeta(2)\right] + 8(2-x)\mathrm{Li}_3(1-x) - 16(6-5x)\mathrm{Li}_3(-x) - 24(2-3x)\zeta(3)$$

$$+8\,\mathrm{Li}_2(1-x) + 8(2+3x)\mathrm{Li}_2(1-x)\ln x + 8(2+5x)\zeta(2)\ln x$$

$$\left.+128\,\mathrm{Li}_2(-x)\ln x - \tfrac{16}{3}x\ln^3 x - 4x\ln^2 x - 16\ln x - 32(1-x)\right\}. \qquad \text{(B.23)}$$

Finally we want to remark that in case of W-production only one of the two sets of diagrams contributes (C or D, depending on the quark flavours in the initial and final state). This implies that for W-production there is no contribution from the interference term CD.

B.4. THE IDENTICAL (ANTI)QUARK-(ANTI)QUARK CONTRIBUTIONS

In case there are identical quarks in the initial and/or final state, we have in addition to the graphs in fig. 8 also the ones in fig. 9. As the results for E^2, F^2 and

EF are equal to those for C^2, D^2 and CD (of course one has to implement the right statistical factors), we will not discuss them here (see the section on non-identical quark–quark scattering). The new contributions come from the interference terms CE, CF, DE and DF. Before giving the results let us explain in some detail how we have taken care of the statistical factors in our calculations.

In case of $V = \gamma$ or Z all four sets of diagrams C, D, E and F contribute and we have a statistical factor $\frac{1}{2}$. However, in the case of $V = W$ we have to distinguish between two cases (remember that for W-production the diagrams C and D cannot contribute simultaneously).

(i) Identical quarks in the initial state. In this case the contribution comes from either the graphs C and F or D and E and there is no statistical factor.

(ii) Identical quarks in the final state. Now only the combinations C and E or D and F give contributions. Moreover, in this case there is a statistical factor $\frac{1}{2}$.

For the expression of the hadronic structure function (see eq. (A.20)) it turned out to be convenient to use the statistical factors of the W-production case. Therefore a statistical factor $\frac{1}{2}$ is included in the results for CE and DF, but this is not the case for CF and DE.

Apart from the statistical factors there is another difference between CE (DF) and CF (DE). The first contains collinear divergences and needs mass factorization, whereas the latter is free of mass singularities.

The correction corresponding to the interferences CE and DF is equal to

$$\Delta^{(2)}_{qq,CE} = \Delta^{(2)}_{qq,DF} = \Delta^{(2)}_{\bar{q}\bar{q},CE} = \Delta^{(2)}_{\bar{q}\bar{q},DF}$$

$$= \left(\frac{\alpha_s}{4\pi}\right)^2 C_F(C_F - \tfrac{1}{2}C_A)\left\{\left[\frac{1+x^2}{1+x}\left[4\ln^2 x - 8\zeta(2)\right.\right.\right.$$

$$\left.\left.\left. - 16\,\mathrm{Li}_2(-x) - 16\ln x \ln(1+x)\right] + 8(1+x)\ln x + 16(1-x)\right]\ln\left(\frac{Q^2}{M^2}\right)$$

$$+ \frac{1+x^2}{1+x}\left[32\,S_{1,2}(1-x) - 16\,S_{1,2}(-x) - 32\,\mathrm{Li}_3(1-x) - 8\,\mathrm{Li}_3(-x)\right.$$

$$+ 32\,\mathrm{Li}_3\left(\frac{1+x}{1-x}\right) - 32\,\mathrm{Li}_3\left(-\frac{1+x}{1-x}\right) - 4\zeta(3) + 24\,\mathrm{Li}_2(1-x)\ln x$$

$$+ 32\,\mathrm{Li}_2(-x)\ln x - 32\,\mathrm{Li}_2(-x)\ln(1-x) - 16\,\mathrm{Li}_2(-x)\ln(1+x)$$

$$+ 12\zeta(2)\ln x - 16\zeta(2)\ln(1-x) - 8\zeta(2)\ln(1+x) - \tfrac{8}{3}\ln^3 x$$

$$+ 8\ln^2 x \ln(1-x) + 28\ln^2 x \ln(1+x) - 8\ln^2(1+x)\ln x$$

$$-32\ln x\ln(1-x)\ln(1+x)\Big]$$

$$+(1-x)\big[-16S_{1,2}(-x)+8\mathrm{Li}_3(-x)$$

$$+8\zeta(3)-16\mathrm{Li}_2(-x)\ln(1+x)+4\zeta(2)\ln x-8\zeta(2)\ln(1+x)-\tfrac{2}{3}\ln^3 x$$

$$+4\ln^2 x\ln(1+x)-8\ln^2(1+x)\ln x+32\ln(1-x)-34\big]$$

$$+(1+x)\big[8\mathrm{Li}_2(-x)+4\zeta(2)+16\ln x\ln(1-x)+8\ln x\ln(1+x)\big]$$

$$+8(3+x)\mathrm{Li}_2(1-x)-4(1+3x)\ln^2 x-2(9-7x)\ln x\Big\}. \tag{B.24}$$

The expression for the interference terms CF and DE is

$$\Delta^{(2)}_{qq,CF}=\Delta^{(2)}_{qq,DE}=\Delta^{(2)}_{\bar{q}\bar{q},CF}=\Delta^{(2)}_{\bar{q}\bar{q},DE}$$

$$=\left(\frac{\alpha_s}{4\pi}\right)^2 C_F(C_F-\tfrac{1}{2}C_A)\Big\{(1-x)^2\big[-16S_{1,2}(1-x)$$

$$+16\mathrm{Li}_3(1-x)-24\mathrm{Li}_2(1-x)-16\mathrm{Li}_2(1-x)\ln x-\tfrac{8}{3}\ln^3 x-12\ln^2 x\big]$$

$$-4(7-6x)\ln x-2(15+13x^2-28x)\Big\}. \tag{B.25}$$

Notice that the above expression is scheme and scale independent.

B.5. THE GLUON–GLUON CONTRIBUTION

The diagrams for the gluon–gluon subprocess can be obtained from the quark–antiquark annihilation graphs in fig. 6 via crossing. This subprocess shows up for the first time at $O(\alpha_s^2)$. We have divided its Drell–Yan correction term into two parts, viz.

$$\Delta^{(2)}_{gg}=\Delta^{(2),C_A}_{gg}+\Delta^{(2),C_F}_{gg}. \tag{B.26}$$

The C_A contribution is collinearly finite and is therefore scheme and scale independent. It is given by

$$\Delta^{(2),C_A}_{gg}=\left(\frac{\alpha_s}{4\pi}\right)^2\frac{N^2}{N^2-1}\Big\{(1+x)^2\big[16S_{1,2}(-x)+24\mathrm{Li}_3(-x)+16\zeta(3)$$

$$+\tfrac{16}{3}\mathrm{Li}_2(-x)-24\mathrm{Li}_2(-x)\ln x+16\mathrm{Li}_2(-x)\ln(1+x)+8\zeta(2)\ln(1+x)$$

$$+\tfrac{8}{3}\zeta(2)-12\ln^2 x\ln(1+x)+8\ln^2(1+x)\ln x+\tfrac{16}{3}\ln x\ln(1+x)\big]$$

$$-8(1-x)^2S_{1,2}(1-x)+\tfrac{2}{3}(-2+25x^2+2x)\ln^2 x$$

$$-\tfrac{2}{3}(6+75x^2+38x)\ln x-\tfrac{47}{3}+\tfrac{191}{3}x^2-48x\Big\}. \tag{B.27}$$

The C_F contribution contains collinear singularities. After mass factorization in the $\overline{\text{MS}}$ scheme we find

$$\Delta_{gg}^{(2),C_F} = \left(\frac{\alpha_s}{4\pi}\right)^2 \Bigg\{ \Big[-2(1+4x^2+4x)\ln x - 4(1-3x^2+2x)\Big]\ln^2\left(\frac{Q^2}{M^2}\right)$$

$$+\Big[(1+4x^2+4x)\big[-8\,\mathrm{Li}_2(1-x) + 2\ln^2 x - 8\ln x \ln(1-x)\big]$$

$$+2(1-4x^2+8x)\ln x - 16(1-3x^2+2x)\ln(1-x)$$

$$+7-67x^2+60x\Big]\ln\left(\frac{Q^2}{M^2}\right) + (1+4x^2+4x)\big[16\,\mathrm{Li}_3(1-x)$$

$$-4\,\mathrm{Li}_2(1-x)\ln x - 16\,\mathrm{Li}_2(1-x)\ln(1-x) + 4\ln^2 x \ln(1-x)$$

$$-8\ln^2(1-x)\ln x\big] + (1+x)\big[8\,\mathrm{Li}_2(-x) + 8\ln x \ln(1+x)\big]$$

$$+(1+x)^2\big[-16\,\mathrm{S}_{1,2}(-x) - 16\,\mathrm{Li}_2(-x)\ln(1+x) - 8\zeta(2)\ln(1+x)$$

$$+12\ln^2 x \ln(1+x) - 8\ln^2(1+x)\ln x\big] - 8(1+7x^2+10x)\mathrm{S}_{1,2}(1-x)$$

$$-8(1-x^2+2x)\mathrm{Li}_3(-x) - 4(1-2x^2+2x)\zeta(3)$$

$$-4(5-14x^2+4x)\mathrm{Li}_2(1-x) + 8(2+x^2+4x)\mathrm{Li}_2(-x)\ln x$$

$$+4(3+10x^2+10x)\zeta(2)\ln x + 4(5-12x^2+9x)\zeta(2)$$

$$-\tfrac{2}{3}(3+8x^2+8x)\ln^3 x - 2(3+4x^2+7x)\ln^2 x$$

$$-16(1-3x^2+2x)\ln^2(1-x) + 4(1-4x^2+8x)\ln x \ln(1-x)$$

$$-(23-105x^2+64x)\ln x + 2(7-67x^2+60x)\ln(1-x)$$

$$-2(16-49x^2+33x)\Big\}. \qquad \text{(B.28)}$$

B.6. THE DY CORRECTION TERMS IN THE LIMIT $x \to 1$

Before finishing this appendix it is also useful, in view of the discussion of eqs. (3.7)–(3.10), to present the behaviour of $\Delta_{ij}(x, Q^2, M^2)$ in the limit $x \to 1$. In this

limit the expressions in eqs. (B.2)–(B.28) become

$$\lim_{x\to 1} \Delta_{q\bar{q}}^{(1),H} = \left(\frac{\alpha_s}{4\pi}\right) C_F \left\{ -16\ln(1-x) - 8\ln\left(\frac{Q^2}{M^2}\right) + 8 \right\}, \tag{B.29}$$

$$\lim_{x\to 1} \Delta_{q\bar{q}}^{(2),C_A} = \left(\frac{\alpha_s}{4\pi}\right)^2 C_A C_F \left\{ \tfrac{176}{3}\ln^2(1-x) + \left[\tfrac{176}{3}\ln\left(\frac{Q^2}{M^2}\right) + 32\zeta(2) - \tfrac{2092}{9} \right] \ln(1-x) + \tfrac{44}{3}\ln^2\left(\frac{Q^2}{M^2}\right) + \left[16\zeta(2) - \tfrac{1136}{9}\right]\ln\left(\frac{Q^2}{M^2}\right) - 56\zeta(3) - \tfrac{224}{3}\zeta(2) + \tfrac{3128}{27} \right\}, \tag{B.30}$$

$$\lim_{x\to 1} \Delta_{q\bar{q}}^{(2),C_F} = \left(\frac{\alpha_s}{4\pi}\right)^2 C_F^2 \left\{ -128\ln^3(1-x) - \left[192\ln\left(\frac{Q^2}{M^2}\right) - 248\right]\ln^2(1-x) + \left[128\ln\left(\frac{Q^2}{M^2}\right) - 64\ln^2\left(\frac{Q^2}{M^2}\right) + 128\zeta(2) + 316\right]\ln(1-x) - 16\ln^2\left(\frac{Q^2}{M^2}\right) + \left[64\zeta(2) + 216\right]\ln\left(\frac{Q^2}{M^2}\right) - 256\zeta(3) - 128\zeta(2) - 152 \right\}, \tag{B.31}$$

$$\lim_{x\to 1} \Delta_{q\bar{q},A^2}^{(2)} = \left(\frac{\alpha_s}{4\pi}\right)^2 n_f C_F \left\{ -\tfrac{32}{3}\ln^2(1-x) - \left[\tfrac{32}{3}\ln\left(\frac{Q^2}{M^2}\right) - \tfrac{352}{9}\right]\ln(1-x) - \tfrac{8}{3}\ln^2\left(\frac{Q^2}{M^2}\right) + \tfrac{176}{9}\ln\left(\frac{Q^2}{M^2}\right) + \tfrac{32}{3}\zeta(2) - \tfrac{656}{27} \right\}, \tag{B.32}$$

$$\lim_{x\to 1} \Delta_{qq,AC}^{(2)} = \left(\frac{\alpha_s}{4\pi}\right)^2 C_F\left(C_F - \tfrac{1}{2}C_A\right)\left\{ -16\ln(1-x) - 8\ln\left(\frac{Q^2}{M^2}\right) + 12 \right\}, \tag{B.33}$$

$$\lim_{x\to 1}\Delta^{(2)}_{q\bar{q},B^2}=\left(\frac{\alpha_s}{4\pi}\right)^2 C_F\left[\tfrac{4}{15}(1-x)^5\right], \tag{B.34}$$

$$\lim_{x\to 1}\Delta^{(2)}_{q\bar{q},BC}=\left(\frac{\alpha_s}{4\pi}\right)^2 C_F\left(C_F-\tfrac{1}{2}C_A\right)\left[-\tfrac{2}{3}(1-x)^3\right], \tag{B.35}$$

$$\lim_{x\to 1}\Delta^{(2),A}_{q\bar{q},AB}=\left(\frac{\alpha_s}{4\pi}\right)^2 C_F\left[\tfrac{16}{3}(1-x)^2\right], \tag{B.36}$$

$$\lim_{x\to 1}\Delta^{(1)}_{qg}=\left(\frac{\alpha_s}{4\pi}\right)T_f\left\{4\ln(1-x)+2\ln\left(\frac{Q^2}{M^2}\right)\right\}, \tag{B.37}$$

$$\begin{aligned}\lim_{x\to 1}\Delta^{(2),C_A}_{qg}=\left(\frac{\alpha_s}{4\pi}\right)^2 C_A T_f\Bigg\{&\tfrac{26}{3}\ln^3(1-x)+12\ln\left(\frac{Q^2}{M^2}\right)\ln^2(1-x)\\&+\left[4\ln^2\left(\frac{Q^2}{M^2}\right)-24\zeta(2)+6\right]\ln(1-x)+\left[4-12\zeta(2)\right]\ln\left(\frac{Q^2}{M^2}\right)\\&+2\zeta(2)-4\Bigg\},\end{aligned} \tag{B.38}$$

$$\begin{aligned}\lim_{x\to 1}\Delta^{(2),C_F}_{qg}=\left(\frac{\alpha_s}{4\pi}\right)^2 C_F T_f\Bigg\{&\tfrac{70}{3}\ln^3(1-x)+\left[36\ln\left(\frac{Q^2}{M^2}\right)-12\right]\ln^2(1-x)\\&+\left[12\ln^2\left(\frac{Q^2}{M^2}\right)+12\ln\left(\frac{Q^2}{M^2}\right)-16\zeta(2)-42\right]\ln(1-x)+9\ln^2\left(\frac{Q^2}{M^2}\right)\\&-\left[8\zeta(2)+22\right]\ln\left(\frac{Q^2}{M^2}\right)+76\zeta(3)+12\zeta(2)-10\Bigg\},\end{aligned} \tag{B.39}$$

$$\begin{aligned}\lim_{x\to 1}\Delta^{(2)}_{q\bar{q},C^2}=\left(\frac{\alpha_s}{4\pi}\right)^2 C_F T_f\Bigg\{&8(1-x)\ln^2(1-x)+\left[8\ln\left(\frac{Q^2}{M^2}\right)-16\right](1-x)\ln(1-x)\\&+\left[2\ln^2\left(\frac{Q^2}{M^2}\right)-8\ln\left(\frac{Q^2}{M^2}\right)-8\zeta(2)+18\right](1-x)\Bigg\},\end{aligned} \tag{B.40}$$

$$\lim_{x\to 1}\Delta^{(2),V}_{q\bar{q},CD}=\left(\frac{\alpha_s}{4\pi}\right)^2 C_F T_f\left[7(1-x)^2\right], \tag{B.41}$$

$$\lim_{x\to 1} \Delta^{(2),A}_{q\bar{q},CD} = \left(\frac{\alpha_s}{4\pi}\right)^2 C_F T_f \left[7(1-x)^2\right], \tag{B.42}$$

$$\lim_{x\to 1} \Delta^{(2)}_{qq,CE} = \left(\frac{\alpha_s}{4\pi}\right)^2 C_F (C_F - \tfrac{1}{2}C_A)\Big\{2(1-x) + \tfrac{4}{5}(1-x)^5 \ln(1-x)$$

$$+ \tfrac{2}{5}\ln\left(\frac{Q^2}{M^2}\right)(1-x)^5\Big\}, \tag{B.43}$$

$$\lim_{x\to 1} \Delta^{(2)}_{q\bar{q},CF} = \left(\frac{\alpha_s}{4\pi}\right)^2 C_F (C_F - \tfrac{1}{2}C_A)\left[\tfrac{16}{3}(1-x)^3\right], \tag{B.44}$$

$$\lim_{x\to 1} \Delta^{(2),C_A}_{gg} = \left(\frac{\alpha_s}{4\pi}\right)^2 \frac{N^2}{N^2-1}\left[-\tfrac{2}{3}(1-x)^3\right], \tag{B.45}$$

$$\lim_{x\to 1} \Delta^{(2),C_F}_{gg} = \left(\frac{\alpha_s}{4\pi}\right)^2 \Big\{8(1-x)\ln^2(1-x) + \left[8\ln\left(\frac{Q^2}{M^2}\right) - 16\right](1-x)\ln(1-x)$$

$$+ \left[2\ln^2\left(\frac{Q^2}{M^2}\right) - 8\ln\left(\frac{Q^2}{M^2}\right) - 8\zeta(2) + 16\right](1-x)\Big\}. \tag{B.46}$$

From the list above we infer that all corrections $\Delta_{ij}(x, Q^2, M^2)$ get zero in the limit $x \to 1$ except for the non-singlet $q\bar{q}$ contribution in eqs. (B.2) and (B.7) and the qg correction terms in eqs. (B.17) and (B.18). This explains why the bulk of the K-factor can be attributed to these two contributions.

References

[1] H.D. Politzer, Nucl. Phys. B129 (1977) 301;
C.T. Sachrajda, Phys. Lett. B73 (1978) 185;
D. Amati, R. Petronzio and G. Veneziano, Nucl. Phys. B140 (1978) 54; B146 (1978) 29;
R.K. Ellis, H. Georgi, M. Machacek, H.D. Politzer and G.G. Ross, Phys. Lett. B78 (1978) 281; Nucl. Phys. B152 (1979) 285;
S.B. Libby and G. Sterman, Phys. Lett. B78 (1978) 618

[2] G. Altarelli, Phys. Rep. 81 (1982) 1; Ann. Rev. Nucl. Part. Sci. 39 (1989) 357

[3] P.M. Stevenson, Phys. Rev. D23 (1981) 2916; Nucl. Phys. B203 (1982) 472

[4] G. Grunberg, Phys. Lett. B95 (1980) 70; [Erratum: B110 (1982) 501]; Phys. Rev. D29 (1984) 2315

[5] J.H. Christenson et al., Phys. Rev. Lett. 25 (1970) 1523

[6] S.D. Drell and T.M. Yan, Phys. Rev. Lett. 25 (1970) 316; Ann. Phys. (N.Y.) 66 (1971) 578

[7] J.C. Collins, D.E. Soper and G. Sterman, Nucl. Phys. B261 (1985) 104; B308 (1988) 833;
G.T. Bodwin, Phys. Rev. D31 (1985) 2616; [Erratum: D34 (1986) 3932]

[8] G. Altarelli, R.K. Ellis and G. Martinelli, Nucl. Phys. B143 (1978) 521; [Erratum: B146 (1978) 544]; B157 (1979) 461

[9] J. Abad and B. Humpert, Phys. Lett. B77 (1978) 105; B78 (1978) 627; [Erratum: B80 (1979) 433]; B80 (1978) 115; B80 (1979) 286

[10] J. Kubar-André and F.E. Paige, Phys. Rev. D19 (1979) 221
[11] K. Harada, T. Kaneko and N. Sakai, Nucl. Phys. B155 (1979) 169; [Erratum: B165 (1980) 545]
[12] B. Humpert and W.L. van Neerven, Phys. Lett. B84 (1979) 327; [Erratum: B85 (1979) 471]; B89 (1979) 69; Nucl. Phys. B184 (1981) 225
[13] J. Kubar, M. le Bellac, J.L. Meunier and G. Plaut, Nucl. Phys. B175 (1980) 251
[14] J. Badier et al., Phys. Lett. B89 (1979) 145;
R. Barate et al., Phys. Rev. Lett. 43 (1979) 1541
[15] K. Freudenreich, Int. J. Mod. Phys. A5 (1990) 3643
[16] L. Fayard, $W^{\pm}$ and Z^0 production at hadron colliders, LAL 90-48
[17] K.G. Chetyrkin, A.L. Kataev and F.V. Tkachev, Phys. Lett. B85 (1979) 277;
M. Dine and J. Sapirstein, Phys. Rev. Lett. 43 (1979) 668;
W. Celmaster and R.J. Gonsalves, Phys. Rev. Lett. 44 (1980) 560; Phys. Rev. D21 (1980) 3112;
S.G. Gorishny, A.L. Kataev and S.A. Larin, Phys. Lett. B212 (1988) 238
[18] G. Kramer and B. Lampe, Z. Phys. C34 (1987) 497; [Erratum: C42 (1989) 504]
[19] V.N. Gribov and L.N. Lipatov, Sov. J. Nucl. Phys. 15 (1972) 438; 675;
G. Altarelli and G. Parisi, Nucl. Phys. B126 (1977) 298
[20] A.P. Contogouris and J. Kripfganz, Phys. Rev. D20 (1979) 2295;
A.N. Schellekens and W.L. van Neerven, Phys. Rev. D21 (1980) 2619; D22 (1980) 1623;
A.N. Schellekens, thesis Nijmegen University 1981
[21] T. Matsuura and W.L. van Neerven, Z. Phys. C38 (1988) 623
[22] T. Matsuura and W.L. van Neerven, Contribution to the Proc. Int. Europhys. Conf. on High Energy Physics, Vol. 1 (Uppsala, Sweden, 25 June–1 July, 1987), ed. O. Botner (Uppsala University) p. 198
[23] T. Matsuura, S.C. van der Marck and W.L. van Neerven, Phys. Lett. B211 (1988) 171; Nucl. Phys. B319 (1989) 570
[24] T. Matsuura, thesis Leiden University 1989
[25] T. Matsuura, R. Hamberg and W.L. van Neerven, Nucl. Phys. B345 (1990) 331
[26] F. Bloch and A. Nordsieck, Phys. Rev. 52 (1937) 54;
D.R. Yennie, S.C. Frautschi and H. Suura, Ann. Phys. (N.Y.) 13 (1961) 379
[27] R. Doria, J. Frenkel and J.C. Taylor, Nucl. Phys. B168 (1980) 93;
A. Andrasi, M. Day, R. Doria, J. Frenkel and J.C. Taylor, Nucl. Phys. B182 (1981) 104;
C. Di'lieto, S. Gendron, I.G. Halliday and C.T. Sachrajda, Nucl. Phys. B183 (1981) 223
[28] T. Kinoshita, J. Math. Phys. 3 (1962) 650;
T.D. Lee and M. Nauenberg, Phys. Rev. 133 (1964) B1549;
N. Nakanishi, Prog. Theor. Phys. 19 (1958) 159
[29] A.C. Hearn, Reduce User's Manual, The Rand Corporation, Santa Monica, CA, 1985
[30] H. Strubbe, Comput. Phys. Comm. 8 (1974) 1
[31] R.J. Gonsalves, J. Pawłowski and C.F. Wai, Phys. Rev. D40 (1989) 2245 and references therein;
J. Pawłowski, Phys. Lett. B246 (1990) 477
[32] W.L. van Neerven, Nucl. Phys. B268 (1986) 453
[33] R.J. Gonsalves, Phys. Rev. D28 (1983) 1542
[34] R.K. Ellis, M.A. Furman, H.E. Haber and I. Hinchliffe, Nucl. Phys. B173 (1980) 397
[35] J. Smith, D. Thomas and W.L. van Neerven, Z. Phys. C44 (1989) 267
[36] W. Beenakker, H. Kuijf, W.L. van Neerven and J. Smith, Phys. Rev. D40 (1989) 54
[37] E.G. Floratos, P. Lacaze and C. Kounnas, Phys. Lett. B98 (1981) 285
[38] E.G. Floratos, D.A. Ross and C.T. Sachrajda, Nucl. Phys. B129 (1977) 66; [Erratum B139 (1978) 545]; Nucl. Phys. B152 (1979) 493
[39] A. Gonzalez-Arroyo, C. Lopez and F.J. Yndurain, Nucl. Phys. B153 (1979) 161;
A. Gonzalez-Arroyo and C. Lopez, Nucl. Phys. B166 (1980) 429
[40] E.G. Floratos, P. Lacaze and C. Kounnas, Phys. Lett. B98 (1981) 89, 285
[41] W. Furmanski and R. Petronzio, Phys. Lett. B97 (1980) 437;
G. Curci, W. Furmanski and R. Petronzio, Nucl. Phys. B175 (1980) 27
[42] A.N. Schellekens, Nuovo Cimento Lett. 24 (1979) 513

[43] D.A. Dicus and S.C. Willenbrock, Phys. Rev. D34 (1986) 148
[44] G. Altarelli, M. Diemoz, G. Martinelli and P. Nason, Nucl. Phys. B308 (1988) 724
[45] A.D. Martin, R.G. Roberts and W.J. Stirling, Phys. Rev. D37 (1988) 1161; Mod. Phys. Lett. A4 (1989) 1135;
P.N. Harriman, A.D. Martin, W.J. Stirling and R.G. Roberts, Phys. Rev. D42 (1990) 798
[46] P.N. Harriman, A.D. Martin, W.J. Stirling and R.G. Roberts, Phys. Lett. B243 (1990) 421
[47] J.G. Morfín and Wu-Ki Tung, Parton distributions from a global QCD analysis of deep inelastic scattering and lepton-pair production, Fermilab-Pub-90/74
[48] P. Nason, S. Dawson and R.K. Ellis, Nucl. Phys. B303 (1988) 607; B327 (1989) 49
[49] W. Beenakker, W.L. van Neerven, R. Meng, G.A. Schuler and J. Smith, DESY 90-064, to be published in Nucl. Phys. B.
[50] P. Aurenche, R. Baier, M. Fontannaz and P. Schiff, Nucl. Phys. B286 (1987) 509; B297 (1988) 661
[51] F. Aversa, P. Chiappetta, M. Greco and J.P. Guillet, Phys. Lett. B210 (1988) 225; B211 (1988) 465; Nucl. Phys. B327 (1989) 105
[52] A.D. Martin and W.J. Stirling, W and Z hadroproduction as a probe of very small x, DTP/90/34
[53] J. Kwiecinski, A.D. Martin, W.J. Stirling and R.G. Roberts, Parton distributions at small x, DTP/90/46 and references therein
[54] C. Albajar et al., UA1 Collaboration, Measurement of the ratio $R \equiv \sigma_W \mathrm{BR}(W \to \mu\nu)/\sigma_Z \mathrm{BR}(Z \to \mu\mu)$ and Γ_W^{tot} at the CERN proton-antiproton collider, CERN-PPE/90-141
[55] J. Alitti et al., UA2 Collaboration, Z. Phys. C47 (1990) 11
[56] P.F. Derwent, CDF Collaboration, Production properties of W, Z bosons, talk presented at the 25th Recontres de Moriond, Les Arcs, Savoie, France, March 1990
[57] F. Abe et al., CDF Collaboration, Phys. Rev. Lett. 64 (1990) 152
[58] L. Lewin, Polylogarithms and associated functions (North-Holland, Amsterdam, 1983);
R. Barbieri, J.A. Mignaco and E. Remiddi, Nuovo Cimento 11A (1972) 824;
A. Devoto and D.W. Duke, Riv. Nuovo Cimento 7 (1984) 1